DESIGN AND EVALUATION OF SCAFFOLDS FOR ARTERIAL GRAFTS USING EXTRACELLULAR MATRIX BASED MATERIALS

A Dissertation
Presented to
The Academic Faculty

by

Vivek A. Kumar

In Partial Fulfillment
of the Requirements for the Degree
Doctor of Philosopy in Bioengineering in the
School of Biomedical Engineering

Georgia Institute of Technology
December, 2011

DESIGN AND EVALUATION OF SCAFFOLDS FOR ARTERIAL GRAFTS

USING EXTRACELLULAR MATRIX BASED MATERIALS

Approved by:

Dr. Elliot L. Chaikof, Advisor
Department of Surgery
Harvard Medical School
Beth Israel Deaconess Medical Center
Harvard University

Dr. Mark G. Allen
Department of Electrical and
Computer Engineering
Georgia Institute of Technology

Dr. Rudolph L. Gleason
The Wallace H. Coulter Department of
Biomedical Engineering
Georgia Institute of Technology

Dr. Robert M. Nerem
Department of Mechanical
Engineering
Georgia Institute of Technology

Dr. Steve L. Stice
Department of Biomedical Engineering
University of Georgia

Date Approved: October, 21, 2011

ACKNOWLEDGEMENTS

My sincere gratitude is extended to my research advisor, mentor and friend, Dr Elliot Chaikof, who has given me endless opportunities to be creative, explore science, provided invaluable guidance and worked tirelessly to help me succeed. Moreover, it is without the help and collaborative efforts of my thesis committee members that this work could not have been done. I would also like to extend my thanks to all the members of our laboratory who have assisted in guiding me through my work and have been instrumental in providing help both inside and outside of lab. Further, I am most appreciative of the work by all of our collaborators at the Georgia Institute of Technology, Emory University, University of Georgia, Harvard University, Massachusetts Institute of Technology and Beth Israel Deaconess Medical Center who have helped in one way or another.

I would like to thank my parents and sister who have always lent a helping hand in times of need, and have supported my dreams every step of the way.

The work presented herein has been financially supported by the American Heart Association.

TABLE OF CONTENTS

	Page
ACKNOWLEDGEMENTS	iii
LIST OF TABLES	vi
LIST OF FIGURES	vii
SUMMARY	xii
CHAPTER	
1 Introduction	1
1.1 Objective, Hypothesis and Specific Aims	1
1.2 Background and significance	4
2 Fabrication and Characterization of Large Scale Structurally and Mechanically Anisotropic Nanofibrous Collagen Matrices for Soft Tissue Engineering	25
2.1 Introduction	25
2.2 Materials and Methods	29
2.3 Results	33
2.4 Discussion	45
2.5 Conclusions	50
3 Strong Collagen-Based Substrates with Tunable Microarchitectures for Soft Tissue Engineering	51
3.1 Introduction	51
3.2 Materials and Methods	55
3.3 Results	61
3.4 Discussion	78
3.5 Conclusions	89

4 Design of Tissue-Mimetic Arterial Grafts 90

4.1 Introduction 90

4.2 Materials and Methods 94

4.3 Results 101

4.4 Discussion 120

4.5 Conclusions 126

5 Summary and Future Directions 128

REFERENCES 138

LIST OF TABLES

Page

Table 1.1: Mechanical properties of common blood vessels and current synthetic replacements. Ranges represent average values from cited studies 10

Table 2.1: Consolidated mechanical and structural properties of collagen lamellae cast at different initial concentrations and aligned to different amounts 44

Table 3.1: Thermal properties of collagen matrices 69

Table 3.2: Design variations for ablated collagen mats 71

Table 3.3: Mechanical properties of unablated and ablated collagen matrices 86

Table 4.1: Mechanical characterization of uncrosslinked 2.5 mg/ml collagen, 2.5 mg/ml elastin CEM and grafts, compared to native tissue and prosthetic grafts 108

LIST OF FIGURES

Page

Figure 2.1: **Schematic of the mechanical setup used to induce strain alignment of collagen gels.** Collagen gels were cast in a rectangular mold (Length x Width x Thickness: 100 x 80 x 4 mm) at 4°C (A), incubated in a fibril incubation buffer for 48 h at 37°C (B), mounted on a motorized stretcher (C), and stretched to a strain of 0%, 10% or 20% stretch, at 3 μm/s or 300 μm/s (D). 34

Figure 2.2: **Ultrastructure of collagen matrices.** Scanning electron micrographs showing (A) isotropic microstructure (scale bar: 1 μm), (B) with 83.1 ± 9.44 nm fibrils (scale bar: 200 nm). Transmission electron micrographs showing (C) a dense fibrillar matrix (scale bar: 1 μm) and (D) native collagen banding showing preservation of the native D-periodic banding pattern (scale bar: 200 nm). 35

Figure 2.3: **Stretching rate, strain amount and concentration dependence on alignment of collagen matrices.** Top panel shows SEM images, and bottom panel shows histograms of FFT analyses of SEM images of 9 regions of 4 independent samples of (A & D) 2.5 mg/mL matrix aligned at 300 μm/s to 10% strain, (B & E) 2.5 mg/mL matrix aligned at 3 μm/s to 10% strain and (C & F) 2.5 mg/mL matrix aligned to 20% strain. Scale bar: 500 nm. 37

Figure 2.4: **Alignment of collagen fibrils based on Gaussian fit of alignment data derived from FFT of SEM images at 10kX magnification.** (A) Maximum relative frequency of fibrils, (B) Full width at half maximum, FWHM (where majority of fibrils reside). *$p<0.05$ 39

Figure 2.5: **Mechanical properties of 20% stretch aligned, 20% stretch aligned tested perpendicular to alignment, 10% stretch aligned and (0%) unaligned 2.5 mg/mL collagen mats**. (A) Tensile strength, (B) Strain at failure, (C) Young's modulus, (D) Fibril diameter and (E) Lamella thickness. (A) Tensile strength and (C) Young's moduli depend on percent alignment of matrices. (B) Strain to failure, (D) Fibril diameter and (E) Lamella thicknesses are similar for all constructs. Data presented as mean ± s.d. *$p < 0.05$ 40

Figure 2.6: **Representative stress-strain plot of collagen matrices.** Matrices were stretch-aligned to different amounts at a rate of 3 μm/s (—: 20%, ··· : 10%, ---:0%). Samples were cut into 20 mm long x 5 mm wide strips and mechanically tested. Samples were pre-conditioned 15 times to 66% of failure strain, and then tested to failure. 43

Figure 3.1: **Schematic of fabrication strategy for layered collagen elastin nanocomposites.** Collagen gels were cast at 4 mm thickness. (A) Collagen lamellae are dried to a thickness of approximately 10 μm, (D) and layered into *multi-layer* collagen mats. (B) Single layer collagen lamellae are embedded in elastin into a single ply, in a sandwich molding technique, (E) multi-layer lamellae are embedded into a multi-layer single ply composite. (C) single layer single ply composites are stacked into single layer multi-ply composites, (F) multi-layer single ply composites are stacked into multi-layer multi-ply composites. 62

Figure 3.2: **Mechanical properties of genipin crosslinked collagen mats.** Increasing concentration of initial gels results in improved strength and stiffness with a commensurate increase in thickness (A,B,G,H). Increasing the number of layers shows an increase in strength and stiffness (C,D,I,J). Increasing initial thickness of 2.5 mg/mL collagen gels in 4 layer lamellae systems resulted in significantly stronger matrices (E,F,K,L). (*$p<0.05$) 64

Figure 3.3: **Ablation schemes of collagen matrices.** (A) Schematic of collagen lamella ablated using an excimer laser to create a defined "wavy" collagen lamella with linear supports, inset shows additional nomenclature. (B) Uniformity and transfer of wavy ablated pattern with high fidelity onto collagen mats, scale bar 500 μm. (C-D) Ablated collagen lamella displayed clear excimer laser cuts with no apparent material damage, scale bar 100 μm. 67

Figure 3.4: **Endothermic heat transitions of collagen matrices.** Microdifferential scanning calorimetry of lyophilized collagen (solid), collagen lamella (dotted), excimer ablated collagen film (dash), genipin crosslinked collagen lamella (dash-dot). (n=3) 68

Figure 3.5: **Meso- and ultra-structure of collagen matrices of varying vertical strip width.** (A-E) Optical micrographs of stainless steel (B) and aluminum-on-quartz masks (A,C,D,E) for Designs 1-5 (A-E), respectively, scale bar 500 μm. (F-J) Optical micrographs of genipin crosslinked collagen lamellae for Designs 1-5, respectively, scale bar 500 μm. SEM of wavy collagen matrices (K) 200 X, wave edge (L) 5 kX, and magnified view of fibrillar structure (M) 50 kX, scale bars 300 μm, 10 μm, 1 μm respectively. TEM images of wavy collagen mats, (N) 10 kX bulk and (O) 10 kX wave edge, scale bar 1 μm. 72

Figure 3.6: **Mechanical strength of ablated collagen mats, Designs 1-5.** (A) Ultimate tensile strength of ablated crosslinked collagen mats. (B) Strain at failure of ablated collagen mats. (C) Young's modulus of ablated collagen samples. 74

Figure 3.7: **Cellularization of unablated and ablated scaffolds.** (A) Unablated scaffold seeded with rMSCs at 100,000 cells/cm^2, for 24 h Live (green)/Dead (red) stained. (B) Ablated scaffold seeded with rMSCs at 100,000 cells/cm^2, for 24 h (Design 2). (C) Actin cytoskeletal staining and DAPI nuclei staining showing alignment of cells on ablated scaffolds. 76

Figure 4.1: **Schematic of fabrication scheme for acellular and cellularized grafts.** (A) Collagen-elastin CEM lamellae are dried from collagen-elastin gels into defined thicknesses. (B) Lamellae can be cellularized with rMSCs at 100,000 cells/cm^2. (C) Acellular and cellularized lamellae are embedded in elastin at defined thicknesses dictated by plastic shims (purple). (D) Acellular and cellularized composite sheets are rolled on a mandrel to create vascular grafts. 102

Figure 4.2: **Mechanical properties of genipin crosslinked CEMs.** Introducing elastin into collagen gels resulted in an improvement in strength and stiffness (A,B,G,H). Increasing collagen concentration while maintaining elastin concentration resulted in weaker matrices (C,D I,J). Increasing the number of layers of a 1.25 mg/ml collagen, 1.25 mg/ml elastin CEM shows an unexpected improvement in strength and stiffness, indicating interpenetration of matrices and reinforcement (E,F,K,L). (*$p<0.05$) 103

Figure 4.3: **Representative stress-strain plots showing mechanical characterization of uncrosslinked 2.5 mg/ml collagen, 2.5 mg/ml elastin CEM.** (A) Preconditioning curves of 2.5 mg/ml collagen - 2.5 mg/ml elastin CEM, ●: first cycle, ○: 15th cycle. (B) Characteristic mechanical response of CEM (—), LysB10 (**---**) and 2.5 mg/ml collagen only matrix (●●●), showing increase in stiffness and strain to failure with incorporation of elastin. 106

Figure 4.4: **Meso- and Ultrastructure of CEM grafts.** (A) Photo of unimplanted graft segment, (B) long graft segment showing kink resistance, (C) Van Geison stained cross-section of graft wall clearly delineating layers: collagen in CEM stained red, elastin yellow, scale bar 100 μm, (D) SEM of graft cross-section, scale bar 500 μm, (E) SEM of graft wall showing contiguous elastin layer and site of rolling initiation, scale bar 100 μm, (F) SEM of elastin structure on lumen of graft, scale bar 1 μm, (G) SEM of fibrous structure of 2.5 mg/ml collagen only lamella showing fibrillar collagen, 50 kX, scale bar 1 μm, 10 kX inset showing global nanofibrous morphology, scale bar 2 μm, (H) SEM of fibrous structure of 2.5 mg/ml collagen, 2.5 mg/ml elastin CEM lamella showing fibrillar collagen "decorated" with elastin, 50 kX, scale bar 1 μm, 10kX inset showing global nanofibrous morphology, scale bar 2 μm, (I) SEM of nanofibrous region of graft impregnated with elastin, scale bar 1 μm. (J) TEM of CEM lamella showing characteristic collagen banding, scale bar 1 μm. (K) and (L) TEM of cross-section of elastin (top) embedded CEM showing preservation of native structure, scale bar 10 μm and 0.5 μm respectively. 110

Figure 4.5: **Cellularization of CEM.** (A-I) Planar CEM seeded with rMSCs at 50 000, 100 000 and 200 000 cells/cm^2, showing cell adhesion (4 h – 12 h) and spreading (12 h - 24 h). 113

Figure 4.6: **Live/Dead staining for cell viability on graft surfaces.** (A) Planar CEM seed with rMSCs at 100 000 cells/cm^2 for 24 h embedded in elastin. (B) Cellularized composite imaged after 3 days. A series of 0.9 mm grafts rolled either with infused superficial elastin facing the lumen (C-D) or infused CEM facing the lumen (E-F) were constructed. (C) rMSCs were seeded on adventitial side (CEM exposed) of rolled grafts at 100 000 cells/cm^2 for 24 h. (D) No cells present on luminal elastin side. (E) rMSCs were seeded on luminal side (CEM exposed) of rolled grafts at 100 000 cells/cm^2 for 24 h, (F) murine dermal microvascular ECs were seeded on luminal side (CEM exposed) of rolled grafts at 100 000 cells/cm^2 for 24 h, Scale bar is 300 μm. 114

Figure 4.7: **Implantation of a 1 cm long 1.3 mm ID aortic interposition graft in the infrarenal suprailiac position.** Gross morphology of the graft was noted: (A) Photo of graft at implant showing reddish color of blood flow, (B) Photo of graft at explant after exsanguination and perfusion fixation. (C) Evaluation of patency of lumen using contrast based angiographic computed tomography.* delineates graft 117

Figure 4.8: **Evaluation of graft morphology and cellular infiltrate.** (A) Masson's Trichrome staining of ECM of graft sections showing CEM layers in blue (Lys-B10 does not stain positively), and neointima, scale bar 100 μm, (B) magnified image showing trapped red blood cells and blue staining of neo-collagen matrix in neointima, (C) thin layer of mononuclear cells adherent on adventitial CEM surface. * indicates luminal side. 119

SUMMARY

For small diameter (<6 mm) blood vessel replacements, lack of collaterals and vascular disease preclude homografts; while synthetic analogs, ePTFE, expanded polytetrafluoroethylene, and PET, polyethyleneterephathalate, are prone to acute thrombosis and restenosis. It is postulated that the hierarchical assembly of cell populated matrices fabricated from protein analogs provides a new design strategy for generating a structurally viable tissue engineered vascular graft. To this end, synthetic elastin and collagen fiber analogs offer a novel strategy for creating tissue engineered vascular grafts with mechanical and biological properties that match or exceed those of native vessels. **The objective** of this work is to develop techniques for the fabrication of prosthetic vascular grafts from a series of extracellular matrix analogs composed of nanofibrous collagen matrices and elastin-mimetic proteins, with and without cells, and subsequently evaluate their biocompatibility and mechanical properties. The first aim relates to the fabrication and mechanical analysis of vascular grafts made from aforementioned protein analogs. The second aim relates to the seeding and proliferation of rodent mesenchymal stem cells on protein-based composites to recapitulate the media of native vasculature. The third aim relates to assessing the *in vivo* biocompatibility and stability of tissue engineered vascular grafts.

CHAPTER 1

INTRODUCTION

1.1 Objective, Hypothesis, and Specific Aims

The objective of this project is to develop techniques for the fabrication of prosthetic vascular grafts from a series of extracellular matrix analogs composed of nanofibrous collagen matrices and elastin-mimetic proteins, with and without cells, and subsequently evaluate their biocompatibility and mechanical properties *in vitro* and *in vivo*. **The central hypothesis** is that by utilizing nanofibrous collagen matrices, recombinant elastin mimetic polypeptides and mesenchymal stem cells, the microstructure of blood vessels can be recapitulated, resulting in a vascular prosthesis that is mechanically and biologically similar to native vasculature and biocompatible. The specific aims of this project were:

Specific Aim I: Develop a strategy for the fabrication of mechanically robust collagen nanofiber-elastin vascular conduits. Synthetic elastin and collagen nanofiber analogs provide a new framework for creating tissue engineered vascular grafts with mechanical characteristics that match or exceed those of native vessels. Aligned nanofibrous collagen lamellae (25 – 30 μm thick, 60-90 nm fibril diameter) will be manufactured by constant strain alignment of collagen gels and subsequent drying, detailed in Chapter 2. Chapter 3 details the development of nanofibrous collagen sheets and strategies to tune their mechanical properties by generating structural anisotropy within the matrices utilizing microfabrication strategies. Nanofibrous lamellae will be embedded in a recombinant elastin matrix, or co-cast from mixtures of collagen and

recombinant elastin, to form protein composite sheets. These sheets will be rolled on a 4mm mandrel, and individual layers will be reconstituted by thermal cooling and reheating, as detailed in Chapter 4. The use of biomimetic protein based polymers, collagen nanofibrous matrices and recombinant elastin mimetics attempts to address the critical need for small diameter vascular grafts that are mechanically and structurally similar to native vasculature over current synthetic substitutes.

Specific Aim II: Develop and optimize a strategy for the modification of collagen-elastin protein composites to support mesenchymal stem cell growth and proliferation. Mechanically robust protein composite sheets will be constructed in a fashion to enhance cell adhesive capabilities of matrices afforded by collagen, which can act as a suitable substrate for the adhesion and proliferation of mesenchymal stem cells, which can be rolled to form cellularized vascular graft composites. Collagen-elastin composite sheets will be seeded with rodent bone marrow derived mesenchymal stem cells (rodent BM-MSCs), cultured to confluence, and rolled on a 4mm mandrel to form a cellularized vascular graft. BM-MSC seeded tubular conduits will be evaluated for cell seeding density, proliferation and cell survival. Protein composites, with the addition of mesenchymal stem cells, presents a strategy for the fabrication of cellularized vascular grafts that have helically oriented cells and collagen fibers, similar to native blood vessels. Further, in Chapter 4 the development of an optimal cell seeding protocol and fabrication strategies employed to create tubular media equivalents with other cells types is explored.

Specific Aim III: Determine the capacity of acellular and cell-populated vascular bioprostheses to resist stenosis, thrombus formation and aneurysm formation *in vivo*. Cell populated compliance matched media equivalents will display enhanced resistance to fatigue related mechanical damage, thrombus formation and aneurysm formation *in vivo*. Cellularized and acellular collagen nanofiber – elastin tubular composites will be fabricated and implanted in a rodent aortic interposition model. Implanted grafts will be analyzed for patency, acute thrombosis and chronic pathologies including arteriosclerosis, thrombosis and stenosis. Further, vascular graft remodeling, seeded cell morphology and phenotype, ability to resist tissue inflammation and graft mechanics will be evaluated upon explant. Acute thrombosis and chronic restenosis are two of the most common routes for synthetic graft failure, along with acute and chronic inflammation. The ability to generate biomimetic and biocompatible small diameter vascular prostheses, with or without mesenchymal stem cell based media equivalents, which remain patent *in vivo*, is a tremendous step in the development of treatment modalities for small diameter (<6 mm) blood vessel tissue engineering, and is further discussed in Chapter 4. Finally, the future of the project, eventual goals that we hope to achieve in the long-term and development of a platform for studies into higher level constructs for the advancement of vascular tissue engineering is discussed in Chapter 5.

1.2 Background and Significance★

Cardiovascular disease (CVD) affects over 71 million people in the United States of America alone and costs exceed 500 billion dollars annually. Specific to cardiovascular disease in America, the number of annual inpatient visits totaled over 7 million with over 450,000 in-patient bypass surgeries, caused in part by diet and inherited factors [1]. Despite improvements in the medical therapy of CVD, the number of vascular interventions, including bypass grafting and angioplasty with or without stenting has increased in recent years. Vascular bypass grafting and balloon angioplasty with stent placement account for a large number of procedures and are more prevalent in patients over the age of 65 years, who are less likely to have sufficient vein for use as a conduit for revascularization [2; 3]. Although autologus veins or arteries provide the best patency rates for cardiac and peripheral vascular bypass grafting, many patients do not have suitable vessels, and autograft suitability may be difficult to define in advance of the bypass operation.

The replacement of large diameter vessels (>6 mm), such as the aorta, has been performed successfully with synthetic polymer prosthetics with long-term patency. However, most blood vessels within the peripheral, cerebral and cardiac vasculature display diameters of less than 6 mm.

★ Reproduced in part from Kumar, VA, Brewster, LP, Caves, JM and Chaikof EL. Tissue Engineering of Blood Vessels: Functional Requirements, Progress, and Future Challenges. Cardiovascular Engineering and Technology,2,3: 137-148, 2011[4].

Several studies have shown that small-diameter synthetic polymer grafts have rapid thrombus formation and intimal hyperplasia subsequent to bypass surgery, limiting their utility [3; 5; 6]. These acute and chronic phenomena were localized not only to the regions of graft anastomoses but also to the mid-graft region, and these findings may also extend to larger diameter grafts [7; 8]. Synthetic vascular grafts also present a continued risk of bacterial colonization and subsequent graft infection and, in addition, are capable of promoting a low-level, chronic inflammatory response that may contribute to the development of neointimal hyperplasia. Mechanically, the compliance mismatch between a prosthetic graft (0.5-1.5%/100 mmHg) and the host artery (5-15%/100 mmHg) may also lead to neointimal hyperplasia and late graft failure. Finally, the inability of synthetic grafts to grow and adapt decreases the utility of prosthetic grafts in pediatric patients.

Motivated by these limitations, the development of a tissue-engineered blood vessel (TEBV) has progressed significantly over the past two decades. In concept, the TEBV will closely match the biomechanical aspects of healthy artery and be capable of growth, remodeling, and vasoactive responses. An endothelial cell (EC) layer will provide anti-platelet, anti-coagulant and pro-fibrinolytic properties that would decrease thrombogenesis and restenosis [9].

Functional requirements in blood vessel tissue engineering

Requirements for TEBV design may be conceptually divided into the linked areas of mechanical and biological performance. Biological-mechanical interconnectivity is often desirable, such as the contractile responses achieved with some TEBV [10], or an observed increase in compliance, from 2 to 9 %/100 mmHg, after 6 months *in vivo* remodeling [11]. However, maladaptive biological responses leading to premature biodegradation and mechanical failure are a common consideration for all degradable-scaffold grafts.

Mechanical requirements.

International standards for Dacron™ and ePTFE prostheses provide a foundation for these requirements, although the complexity of tissue-engineering requires developers to look much further [12]. Mechanical considerations include burst pressure, fatigue-resistance, suture retention, kinking radius, and compliance. Designers must also consider homogeneity over the length of the prosthesis, which may be tens of centimeters [13], variations as the implant remodels, and lot-to-lot variability inherent to cell-based products. Despite broad and prolonged interest in this area, standardized mechanical targets and protocols are still evolving [14].

Testing of burst pressure and mechanical resistance to catastrophic rupture/ tearing of the vascular prosthesis is required to ensure the graft can withstand physiologic variations in pressure. For example, the average pressure in the arterial circulation close to the heart is 100 mmHg, but in the femoral or popliteal artery, while standing, is about 250 mmHg, owing to the contribution of hydrostatic pressure. Conversely, pressures in

the cerebral vasculature are generally lower; 60-100 mmHg [15]. However, a significantly challenging vessel to replace is the common carotid. This is due not only to high flowrates (approximating 200mL/min) but turbulent and recirculating flows at the internal/external carotid bifurcation and carotid sinus [15; 16; 17; 18]. Thus there is still much debate as to the best approach to treat carotid atherosclerotic disease; stenting, endarterectomy, with or without a patch material or bypass grafting [19; 20; 21; 22]. High burst pressures are clearly desirable. However, whether TEBV must match native vein, artery, or simply be at a level above maximum physiologic pressure remains debated. In pigs, investigators have suggested that TEBV with burst pressures as low as 600-700 mm Hg can be implanted in the arterial circulation without observed dilatation [23]. Typical burst pressure testing involves the steady inflation of a blood vessel/ tissue engineered construct to a pressure at which the construct starts to rupture. Porous constructs are tested by inflating either a flexible elastomer, with a stiffness negligible to that of the material being tested, in the tubular construct, or sealing the pores of the construct with a material of negligible mechanical strength. Burst pressures are measured with systems that apply increasing internal pressure loads, and record outer diameter and internal pressure. Specimens are typically maintained in physiologic buffer (37°C PBS) during testing. Of particular note is the inflation rate to bursting of tissue engineered constructs: typical inflation rates that compensate for potential creep and stress relaxation of materials in a physiologic setting have been established to be around 0.2 mL/s [24]. However, faster inflation rates have been shown to drastically increase the expected burst pressure, as the material rapidly inflates with little to no deformation. Further, it is important for grafts to remain fatigue resistant, ensuring their structural components and

mechanical properties do not alter with repeated cycling in a pulsatile flow setting [25; 26]. Notably, extrapolation of burst pressure from the ultimate tensile stress of flat strips or ring specimens may over-estimate direct burst pressure measurements [14]. Interestingly, for specific TEBV systems non-invasive prediction of burst pressure from stiffness measurements at low pressures has been demonstrated [27]. Typical burst pressures of native vasculature and synthetic alternatives are shown in Table 1.1.

Compliance and fatigue may be evaluated with similar test fixtures. Compliance is calculated from the percent change in internal radius over a physiologic range of pressure (80-120 mmHg) and is often expressed in units of %/100 mmHg. The pressurized inner radius must often be calculated from images of the pressurized outer diameter, the inner diameter at rest, and the assumption of incompressibility of the graft wall. Typical compliances are dependent on the locale of the vessel, arterial, venous or synthetic, detailed in Table 1.1 [2; 28; 29; 30; 31]. Similar to burst pressure, the mechanical response of constructs is dependent on the rate at which scaffold inflation is performed due to time-dependent phenomena such as stress relaxation [24; 32; 33]. Further, it is critical to evaluate the compliance of tissue constructs in physiologically relevant conditions that simulate the native environment: flowrates, flow medium, pulsatile flow, pressure gradients and temperature. The reader is directed to the following references for further vessel specific mechanical properties [2; 28; 29; 30; 31]. Fatigue testing may consist of sustained static, cyclic, or stepwise pressures profiles, followed by an assessment of the burst pressure or compliance to monitor any change from initial strength. Although the importance of short-term fatigue tests is clear, when

significant biodegradation and remodeling is anticipated the predictive value of long-term *in vitro* fatigue tests may be limited.

Suture retention strength is measured by placing a suture 2 mm from the end of a vessel specimen and measuring the force required to dislodge the suture in a physiologically relevant condition and rate: 1 mm/s, 37˚C [12]. Typical suture retention strengths of native vasculature range widely depending on vessel type (Table 1) [31; 32; 34; 35; 36; 37].

Table 1.1: Mechanical properties of common blood vessels and current synthetic replacements. Ranges represent average values from cited studies.

	Compliance (%/100 mmHg)	Suture Retention Strength (grams-Force)	Burst Pressure (mmHg)
Artery	Coronary: 8.0-17.0 [38; 39], Carotid: 5.0-14.7 [40; 41], Femoral: 6.0-14.1 [42; 43], Popliteal: 4.7-8.5 [42], Internal thoracic artery:6.5-12.0 [14; 44]	88-200 [14; 34]	2200-4225 [44; 45]
Vein	Saphenous: 0.7-2.6 [34; 40; 44], Umbilical: 1.5-3.7 [40; 46]	180-250 [34; 45; 47]	1600-2500 [34; 44; 45; 47]
Synthetic grafts	PTFE: 0.2-0.9 [40; 48], Dacron™: 0.76-1.9 [40; 48]	250-1200 [49; 50]	2580-8270 [51]

Biological requirements.

Biological failure occurs due to different modes depending on whether it occurs acutely, over the first weeks/months, or longer-term over months to years. The acute response is usually characterized by blood material interactions that lead to non-specific protein adsorption and subsequent blood clotting or thrombosis on the graft luminal surface. The chronic response to vascular graft implantation is determined in part by the remodeling of the implant, as pannus tissue grows in from the anastamotic regions or transmurally, and long term material interactions with the host, such as biodegradation and scar tissue formation [52; 53; 54].

Of note is the small population of patients that have infection during implantation (eg.*Staphylococcus epidermidis*) which typically populates the anastamotic regions of a graft and is estimated to be as high as 1-6% [55].

The generation of a luminal layer that prevents non-specific protein adsorption and a subsequent immune response is a significant problem that has challenged the field till present, especially with the current synthetic standard of care which uses hydrophobic materials that present surfaces that are entropically more favorable for blood protein adsorption than hydrophilic surfaces. However, to circumvent the potential for thrombus formation, novel biomaterials strive to combine hydrophilicity and resistance to protein adsorption through surface modifications or the use of a luminal layer of endothelial cells. A quiescent EC layer has been shown to be vital to promoting an (i) anti-platelet, (ii) anti-coagulant and (iii)pro-fibrinolytic surface [56; 57; 58; 59; 60; 61]. Conversely, occlusion due to activation of the present or neo-endothelial cells is of major concern [6; 61; 62; 63; 64].

Biochemical and chemical modifications, including homing of cells using CD34 antibody conjugated to graft surfaces, stromal derived factor-1 (SDF-1) an inducer of endothelial progenitor cell migration from the bone marrow, and plasma treatment of surfaces facilitate neo-endothelialization of vascular grafts. Although the source of the repopulating EC is still debated (bone marrow endothelial progenitor cells/circulating progenitor cells/ECs from the nascent vasculature), endothelial cells play a pivotal role in the biocompatibility of blood-contacting materials. Moreover, the former strategies of creating a homing-like environment for cell adhesion and localization is preferred for an "off-the-shelf" product that does not require pre-seeding with ECs that often have limited proliferative potential due to the age of the patient and the time required for EC isolation, culture, seeding and preconditioning to ensure seeded cells do not slough off in a hemodynamic environment [65; 66]. Recent canine and baboon studies have suggested that immediate recapitulation of the EC layer *in vitro* or soon after *in vivo* implantation may not be required for short term (6month) graft performance [45], but is still thought to be essential for long term graft survival [67; 68; 69].

Smooth muscle cells (SMC) represent another important cellular component of the vascular wall. In normal pulsatile blood flow, the SMC layer contributes to the vascular tone and medial compliance of the vessel. However, in a variety of specific disease states, they are indicated in the progression of atherosclerosis through myointimal hyperplasia [70]. Although much work has focused on the use of luminal EC seeded grafts, SMC seeded grafts have shown the potential for improved host integration, increased medial contractility, and medial cellularization [71]. Additionally, several groups have shown the importance of SMC to aid in the development of the vascular

media which is essential for biomechanical function of the vessel. Specifically, they have shown SMC secretion and rearrangement of the matrix into helical or circumferential orientations, more closely mimicking native structure [10; 72; 73]. Similar to the need to maintain a quiescent state for endothelial cells, the phenotypic expression of smooth muscle cells is critical to recapitulation of medial function. When SMCs are expanded in culture prior to seeding, they frequently adopt a non-contractile, proliferative, synthetic phenotype due to the loss of actin filaments [74; 75]. Development of a contractile SMC phenotype depends on a milieu of factors including local stress/strains, growth factors, and paracrine/ autocrine signaling [76; 77]. Correct phenotype is essential in preventing medial thickening and intimal hyperplasia from proliferative SMCs. The reader is referred to a review by Chan-Park et al for more details [78]. A variety of other cell types, both native and non-native to vasculature have been used for repopulation of tissue engineering vascular grafts. Of note, work with stem cells, including endothelial progenitor cells and mesenchymal stem cells, umbilical cord cells and peritoneal cells is discussed in detail herein.

Mediation of the immune response due to surgical trauma and foreign body reaction is critical to graft performance. Several groups have attempted to create functional tissue replacements that serve to passively prevent acute and chronic rejection. This has been done through the incorporation of bioactive materials, tailoring of degradation of biodegradable polymers to leach minimally cytotoxic degradation products, and incorporation of biomimetic moieties, such as collagen, elastin, and glycosaminoglycans [2; 3; 79; 80; 81; 82; 83; 84; 85]. However, there has been a recent trend to actively modulate the inflammatory response of tissue replacements by

incorporation of moieties that strive to curtail adverse inflammatory responses such as neutrophil invasion, macrophage polarization and modulation of the adaptive immune response, notwithstanding the use of immunocompromised animal models [86; 87; 88]. Further, recent studies have demonstrated the importance of ensuring that the local environment of the graft is maintained to be non-inflammatory. Specific to macrophage polarization, Ariganello and colleagues have shown the utility of decellularized matrices to direct macrophage polarization to a non-inflammatory phenotype that would promote healing and resolution, instead of inflammation [89; 90]. The incorporation of bone marrow mesenchymal stem cells (BM-MSCs) within tissue engineered and biodegradable scaffolds has been widely reported. Specific to vascular grafts, bone marrow derived stem cells have been shown to differentiate into endothelial progenitor like-cells [91; 92; 93; 94], as well as other vascular wall cellular constituents, smooth muscle cells [95; 96]. In addition to repopulating ECM-based scaffolds, MSC have also been shown to attenuate the inflammatory and immune responses associated with surgical trauma and implants. MSC have the ability to direct macrophage polarization toward an M2 phenotype (healing/ resolution) over an M1 phenotype (inflammatory), down-regulate MHC, major histocompatibility complex, and co-stimulatory molecule expression, decrease inflammatory cytokine expression (TNF-α, IL-12, IFN-γ), increase anti-inflammatory cytokine expression (IL-10), promote T-regulatory cell proliferation and interfere with lymphocyte replication [97; 98; 99; 100; 101; 102].

In vitro tests for TEBV include standard biocompatibility assays and, depending upon the design concept, may extend to consideration of cell supportive properties, hemocompatibility, and vasoactivity. Cytocompatibility is usually established with

seeding of human EC, SMC and fibroblasts. To simulate features of the innate immune response, groups have used bio-similar environments with the addition of secretion products from inflammatory cells, such as macrophages and neutrophils, to simulate degradation *in vivo* and *in vitro* [6; 30; 54; 103; 104; 105]. *In vitro* hemocompatibility is typically determined with the use of whole blood clotting times, platelet adhesion and morphology, and activation states of inflammatory cells on vascular biomaterials in a variety of systems: static clotting time / platelet adhesion and morphology assays, flow loops and AV shunt models, preceding *in vivo* implants [6; 31; 106; 107; 108; 109].

In vivo studies typically commence in rodents. Despite small vessels (< 1 mm), murine systems provide the potential to test constructs with human cells in nude [110] or severe combined immunodeficiency (SCID) mice [111]. Mouse models have been developed to incorporate intravital molecular imaging to track labeled cells and protease activity [110]. Rat models allow the assessment of human-cell constructs in (immune compromised) athymic animals [34], using slightly larger 1-2 mm inner diameter test vessels. A recent review highlights pitfalls to anticipate as investigators proceed to large animal models [13].

Evolving concepts and current status of TEBV technology

Collagen and other biopolymers. Traditional "cell-plus-scaffold" tissue engineering was first applied to blood vessel constructs by Weinberg and Bell in 1986 [112]. Employing a collagen gel cultured with SMC and EC, they observed a near-confluent and biologically active EC luminal surface. However, maximum burst pressures in the range of 400 mmHg necessitated the additional support of a Dacron™ mesh. Several other studies have used collagen or other biologically derived blood vessel constituents to recapitulate the features of a blood vessel in scaffolds, with limited success, given the weak nature of collagen gels [8; 113; 114]. Strategies incorporating cells, matrix components and intracellular biomolecules have been shown to improve the mechanical strength of collagen-based constructs by compaction and re-organization of collagen fibril architecture [115; 116; 117; 118; 119]. In particular, Seliktar et al. have demonstrated the ability of seeded cells and mechanical conditioning to rearrange collagen fibrils circumferentially, leading to increased strength [120]. Our research group has observed high burst pressures using a biomaterial composite consisting of crosslinked, oriented collagen microfibers reinforcing a matrix comprised of a recombinant elastin analogue [83].

Fibrin is of interest as an alternative biopolymer scaffold due to advantages including its natural role in wound healing, widespread clinical acceptance as a tissue sealant and the potential for generating an autologous biomaterial from the patients' own blood [121]. Cummings et al. found that while fibrin vascular constructs were weaker and more extensible than collagen, fibrin-collagen composites displayed higher strength and gel compaction than collagen alone [122]. Fibrin gels have also been shown to stimulate

SMC to synthesize elastin, an important component of the artery wall, which is neglected in many collagen-based TEBV [123]. Short segments (1.5 - 2.0 cm) of TEBV from fibrin cultured with either bone-marrow derived progenitor cells or SMC and seeded with EC demonstrated vasoactivity and have been implanted as interpositional grafts in the lamb external jugular vein [124; 125]. Recently, a bioreactor design capable of simultaneously processing six TEBV from fibrin with human dermal fibroblasts resulted in burst pressures of 1400 – 1600 mmHg after 5 to 7 weeks of culture [27]. The resulting compliance was 2-5 %/ mmHg and low suture retention strengths were compensated by the addition of polymeric cuffs from poly(lactic acid). Fibrin-based approaches have also been augmented through the addition of growth factors via sustained delivery systems in order to enhance and sustain cellular in-growth [126].

Biodegradable and bioresorbable synthetic polymers. In addition to biopolymers, biodegradable synthetic polymer scaffolds, such as polylactic acid (PLA), polyglycolic acid (PGA), polycaprolactone (PCL), polyurethanes (PU), and related copolymers or composites have been extensively studied [10; 73; 127; 128; 129; 130; 131; 132]. Typically these scaffolds are pre-seeded with cells using a variety of techniques, including static seeding, dynamic seeding, vacuum aided seeding, or electrostatic seeding and conditioned in a bioreactor to ensure the cells can withstand physiologic blood flow [133; 134; 135]. In a well-studied example of the biodegradable polymer approach, Niklason et al fabricated TEBV using PGA seeded with SMC and cultured at 1-2% cyclic mechanical strain in a bioreactor for 7 to 8 weeks, followed by EC seeding [10]. Further, Dahl et al report TEBV scaffolds generated from PGA seeded with allogeneic SMCs, conditioned in a bioreactor, and subsequently decellularized.

Acellular specimens were studied in a baboon AV shunt model, and scaffolds with a luminal EC coating were investigated in a canine peripheral and coronary bypass model. A potential disadvantage of this strategy is the relatively low levels of endothelialization (14±8%) [45]. Further, in a challenging model of porcine carotid grafting, Niklason and colleagues showed that decellularized, engineered grafts resisted both thrombosis and intimal hyperplasia. Head-to-head comparisons with autologous vein grafts showed that decellularized, engineered grafts had less neointima formation and superior patency rates after 30 days. The etiology of this advantage may be related to decreased activation of the mTOR pathway in engineered grafts as compared to vein, though this result remains to be confirmed in other studies *(personal communication)*.

With respect to the proliferative capacity of the cells used in tissue engineered constructs, aging is associated with decreasing telomere length and directly related to decreased doubling capacity. To overcome this limitation, Poh et al. have demonstrated an increase in the population doublings of adult VSMCs through retroviral infection with the telomerase reverse transcriptase subunit (hTERT) [65]. Despite improvement, mechanical strength remained too low, potentially due to reduced collagen synthesis [136; 137]. To circumvent the challenges of SMCs, human mesenchymal stem cells (MSC) were used in an 8 week protocol involving proliferation and differentiation phases [81]. Collagen matrix synthesis and substantial conversion to an SMC phenotype were demonstrated, but burst pressures remained at approximately 400 mmHg. These biodegradable systems have confirmed that: (i) non-degraded polymer fragments can amplify stresses and dramatically compromise strength; (ii) collagen organization, as well as quantity, is required for strength; (iii) low compliance may be due to the absence of

organized extracellular elastin sheets, as well as sub-physiologic SMC contractility [138; 139].

The vascular tissue engineering system developed by Shin'oka and colleagues uses similar biodegradable polymers. Employing porous ε-caprolactone and L-lactide copolymer reinforced with a PGA fabric, seeded with cultured autologous venous cells, they reported the first clinically effective TEBV implants [140]. By substituting autologous bone-marrow mononuclear cells (BMC), the cell culture step was avoided in subsequent implants [132]. Given the cost, delay, contamination potential, as well as dependence on xenogenic serums in culture medium, avoidance of prolonged *in vitro* culture represented a significant advantage. Notably, in these reports the TEBV implants repaired congenital defects in the pulmonary circulation of a pediatric population, while most TEBV applications must address more demanding mechanics of the arterial circulation, as well as the limitations of autologous cells obtained from elderly donors. Early efforts to adapt the technology to arterial implants have been reported [141]. Despite initial suggestions that BMCs differentiate and proliferate as the TEBV is incorporated [132; 142], recent analysis in SCID/beige mice found no evidence that the implanted cells persist longer than about one week [87]. BMCs appear to accelerate *in vivo* remodeling by paracrine recruitment of host monocytes. The authors also suggest that, in turn, accelerated monocyte infiltration triggered enhanced repopulation by host SMC and EC. Regardless of technique employed, the persistence of seeded cells and the ability to withstand hemodynamic forces (shear in the lumen or compressive in the vascular wall), remaining a desired phenotype, or differentiation along specific lineages

(for stem cells), and maintenance of viable cytokine/chemokine expression, is critical to graft success [86; 135; 143].

Bioresorbable vascular grafts are incorporated into the recipient through host mediated degradation systems that include enzymolysis, oxidation and hydrolysis, while allowing for concomitant repopulation of the scaffold with native cells. Wolfe et al have shown that bioresorbable electrospun polydioxane (PDO) or PCL scaffolds elicited varying tissue factor expression when exposed to monocytes; demonstrating no greater risk of thrombotic occlusion than ePTFE [144]. Other groups have used a variety of bioresorbable polymeric constructs showing mechanical and biological utility [2; 145; 146; 147]. Campbell et al have developed an interesting technique wherein the host's peritoneal cavity is used as a bioreactor to construct hierarchical tissue. They implanted silastic tubing in the peritoneal cavity of rats and rabbits for 2 weeks, which resulted in scaffolds that had developed layers of ECM, and were populated with myofibroblasts and mesothelium. 10-20 mm long grafts were subsequently implanted in the host animal, with greater than 4month patency. Their technique has been extended to the development of a variety of soft tissues including vas deferens, bladder and uterus [148; 149]. Vito's group has developed a method for the *in vivo* or *ex vivo* stretching of arterial segments in suitable media conditions for generation of blood vessels. They have studied several aspects of the biomechanical regimes that effect remodeling and growth of vessels [150; 151; 152; 153]. These studies were further carried into collagen based gels which have been seeded with cells and show morphological changes in ultrastructure and cellular behavior as a function of mechanical conditioning [120].

Cell-sheet tissue engineering. TEBV fabricated from cell sheet-based tissue engineering consist entirely of autologous cells and secreted matrix proteins. Initially, sheet-based TEBV consisted of SMC or fibroblasts cultured with ascorbic acid for approximately 30 days to form cohesive sheets [9]. The SMC sheet was wrapped about a tubular support to create the vessel media, matured for one week, wrapped with a fibroblast-sheet "adventitia," matured for 7 weeks, and then seeded with EC. This process was replaced with a scheme consisting of a decellularized internal membrane fabricated from a fibroblast sheet, a living adventitial layer, and a seeded endothelial layer, requiring a total of 28 weeks of culture [34]. This design demonstrated favorable mechanics for implantation in the arterial circulation, and these TEBV have been successfully implanted as arteriovenous fistulas in high-risk patients [154]. This groundbreaking progress with a sheet-based tissue engineering system has been encouraging, although long culture times remain an important factor in keeping costs high and limiting application to non-urgent indications. Similar work has been done by other groups that have developed rolling techniques with localized regions of specific cell types or synthetic/biosynthetic materials such as PLLA, collagen and elastin [83; 86; 155].

Decellularized tissue scaffolds. This technique maintains the native extracellular matrix proteins that provide both structural integrity and instructive cues for cellular ingrowth. By incubating bone marrow derived cells in decellularized canine carotid arteries, Cho et al. demonstrated cellular incorporation into the scaffold and subsequent differentiation of these cells into endothelial and vascular smooth muscle cells and subsequently into 3 distinct vessel layers [95]. Zhou et al have shown that heparin and VEGF modified decellularized canine carotids grafts have higher 6 month patency rates

than unmodified grafts [156]. In a similar study, Zhou et al showed that heparin immobilized on decellularized grafts implanted in rats supplemented with 14days of granulocyte-colony stimulating factor had higher patency and lower neointima formation compared to controls; due to homing of circulating EPCs to the graft surface, demonstrating the potential for cytokine treatment post surgical intervention [157]. Further, potential changes in the long term mechanical response associated with decellularization protocols, specifically the shape of the pressure-diameter curves, and how they relate to compliance is of concern [158]. Other decellularized tubular conduits have been investigated for vascular tissue engineering. Specifically, aorta [159; 160], umbilical arteries [5], saphenous vein [47], ureter [161; 162], and small intestinal submucosa (SIS) [163; 164] to name a few. Clarke et al report vascular grafts from decellularized bovine tissue that show high patency in a canine model, with host cell repopulation of the prosthesis [165]. Further, decellularized bovine ureter, has shown the potential to be used in humans as a blood vessel replacement. However, early results show the potential for aneurysm formation [166], poor long term patency as hemodialysis access shunts, (14% at 1year) [167], similar to ePTFE access grafts [168]; and infection and inflammation due to potential residual xenoantigen [169].

Translational challenges

At present, TEBV use in humans has required at least a bone marrow aspiration and brief cell seeding for pediatric pulmonary artery replacement and up to 28 weeks of maturation of rolled fibroblast sheets to withstand arterial pressures for use as arteriovenous conduits in patients requiring dialysis. Advanced cell or biomaterial technologies may drive the next generation of solutions. In particular, the recent recognition that BMC are likely to survive only transiently and cellular repopulation is driven by monocyte infiltration may suggest new cell and biomaterial strategies for TEBV researchers [87]. In addition, early results translating biodegradable polymer scaffold systems to the arterial circulation in mice suggest that protocols requiring as little as 1 week maturation in culture may be attainable [141].

Research timeline, regulatory, and economic issues. McAllister et al. have argued that the unique challenges inherent to translating cell-based therapies, including tissue-engineering, will benefit from the application of several distinct strategies [170]. In particular, the authors note that researchers should include an early focus on proof-of-principle with human cells and anticipate an extended (20 year) R&D timeline. A focus on modeling the cost-effectiveness of the technology is emphasized, but not until later in this timeline, as clinical trials are planned. Regulatory approval pathways for tissue-engineered products are still evolving, and the cost of quality assurance is expected to be a challenge given the small lot sizes of tissue-engineered products [171].

Summary and future directions

The design of a tissue engineered vascular graft to supplant the diseased arteries' function requires consideration of mechanical, biological and clinical factors that influence behavior *in vitro* and *in vivo*. To date, tissue engineered products have yet to replace the current "gold standard" of an autologous artery or vein. Mechanical considerations include (i) a sufficient burst pressure to prevent catastrophic failure of the vessel and long-term fatigue resistance, (ii) a suitable compliance that approximates that of the vessel to prevent mechanical mismatch, and (iii) a strong enough suture retention strength to permit implantation and tolerate hydrodynamic and mechanical forces at the anastomoses. Biological and clinical considerations include (i) generation of a non-fouling luminal surface to prevent thrombosis, (ii) mediation of the immune response due to surgical trauma and potential graft rejection and regeneration, and (iii) evaluation in an *in vivo* environment.

Several groups have demonstrated the efficacies of various strategies that range from modification of existing ePTFE/Dacron™ grafts to acellular/cellularized constructs to de novo engineering of tissue substitutes that mimic native vessels. TEBV derived from cell-sheet tissue engineering and degradable synthetic polymer scaffolding have demonstrated early clinical success and continued progress with several additional systems suggests that these technologies will continue to evolve. Clinical success will be determined by utilizing a "bottom-up" approach wherein recapitulation of the fundamental features of the vascular wall, incorporation of key elements that obviate thrombosis and acute graft failure, and potentially a cellular component that will direct the unavoidable inflammatory response towards healing.

CHAPTER 2

Fabrication and Characterization of Large Scale Structurally and Mechanically Anisotropic Nanofibrous Collagen Matrices for Soft Tissue Engineering

2.1 Introduction:

Collagen based scaffolds have been widely used in tissue engineering due to their versatility and ease of production [172; 173]. Collagen, typically isolated from an animal source (for example: rat tail tendon, calf skin and others) can be solubilized and purified by acid extraction from tissue, which preserves the monomeric protein structure; or by enzymatic digestion of collagen, which leads to removal of telopeptides vital to reorganization of the collagen molecule [174; 175; 176]. Alone or in combination with other biomolecules, collagen matrices have been processed into a wide variety of tissue substitutes used widely in cardiovascular, musculoskeletal, neural and dermal tissue engineering [173; 177; 178]. The ability to modulate the mechanical and physical properties of collagen based scaffolds is critical to its utility. Further it is critical to mimic tissue structure to ensure that regeneration of native tissue is guided and supported during implant healing.

Although of significantly less tensile strength and stiffness as compared to many synthetic non-degradable and biodegradable polymers such as PE (polyethylene), PTFE (polytetrafluroethylene), or PLGA (poly-lactic-co-glycolic acid), collagen and other biologically derived polymers offer significant advantages related to decreased

immunogenicity, increased homology to native structures, and "in-built" cell recognition regions [172; 175]. Additionally, several groups, and this report, have shown the ability to tailor the mechanical response of collagen, based on the requirements of the tissue to be replaced, depending on choice of processing techniques, crosslinker and fabrication schemes [179; 180; 181; 182; 183].

Being the most abundant protein in mammalian systems, collagen is the primary protein constituent of many tissues, from blood vessels to bone and skin. The Type I collagen molecule, part of the fibril forming collagen family, is comprised of a tripeptide repeat of the amino acids Glycine-Proline-Hydroxyproline, although the latter two have some heterogeneity. Type I collagen further forms a coiled coil structure that leads to the formation of fibrils approximately 300nm in length and 5nm in diameter. Further, staggered linear stacking of collagen molecules with characteristic 67nm gaps allows for native collagen structure staining and identification [174; 176]. Owing to the complex nature of the molecular and supramolecular arrangement of collagen, fibrillar collagens are able to withstand high tensile/compressive stresses [184; 185]. The higher order supramolecular arrangement of collagen structures *in vivo*, for example in blood vessels, confers support and resistance to bursting, while providing little stiffness in the physiologic regime due to crimping of collagen fibers [139; 182; 186].

Fibril alignment, density and microstructure affect mechanical properties by directing load and distribution of stress, as well as by providing compliance and resilience to engineered constructs and native tissue. Several investigators have commented on the

need for aligned collagen matrices [187; 188; 189; 190; 191; 192]. Specifically, quoting Guo & Kaufman, *"an easy and effective way to make highly oriented collagen gels with no specialized equipment has not yet been demonstrated,"* further underscoring the importance and need for aligned collagen matrices [187]. To this end, several groups have attempted a variety of techniques to align collagen matrices. Given the negative diamagnetic anisotropy of collagen molecules, one of the earliest reports of alignment of collagen was performed using a magnetic field. Studies by Chen et al [193], Torbet and Ronziere [189] and Tranquillo's group [194; 195; 196; 197] have reported collagen alignment using magnetic fields. The primary disadvantage is that the strength of the magnetic field required for collagen alignment is on the order of 1-10 Tesla, higher than that required for MRI, and thus proving to be prohibitively costly. To circumvent the need for such high magnetic fields, other groups have used additives to collagen to assist in alignment of collagen fibrils. Cheng and Kaufman used magnetic beads with modified surface functionalities in a weaker magnetic field (10^{-4}T) to align thin (order of μm) collagen gels. However, the potential for leaching of the additives, and concomitant cytotoxicity may be prohibitive *in vivo* [187]. Another method to align collagen molecules is through the use of microfluidics. Lee et al have reported the production of aligned collagen molecules in microfluidic channels. Since the collagen was gelled prior to flow into microchannels, there is the likelihood of a fibril density gradient forming during collagen gelation in the channels during flow, notwithstanding concerns including removal of the collagen from the channels, as well as scaled up manufacturing of larger constructs [198], similar to work by Guo et al [187]. Cheng and colleagues have been able to use an electrochemical field to align collagen molecules. This technique,

however, has shown only modest alignment with lack of characteristic collagen D-periodicity in fibers that are 50-400 μm in diameter and inches in length. However, interestingly, they and other groups have reported aligned matrices were significantly stronger than unaligned matrices, demonstrating the increase in strength in aligned fibrillar collagen matrices [185; 199]. Deitch et al report a novel method to make aligned collagen matrices using conventional printing technology, whereby collagen is loaded into an ink cartridge and *printed* onto a glass substrate. Although novel, this technique has yielded thin films, which lack consistency and precise molecular alignment. Further, of concern is that the heat generated by the inkjet printer may denature the collagen [200]. Vader et al report a novel methodology that employs strain induced alignment of small regions of collagen gels that are of approximately 1mm thickness, by pulling apart glass pipets [201]. However, we have developed a novel large-scale alignment technique that allows for the rapid generation of aligned collagen constructs, suitable for tissue engineering. Further, through the variation of concentration, buffers, temperature of gelation, thickness of constructs and fabrication schemes; high density nanofibrous collagen matrices that have strengths that approximate and supersede that of most collagen-gel based constructs, tissue engineered matrices, and native tissue have been created.

2.2 Materials and methods

All chemicals were purchased from Sigma-Aldrich, unless otherwise stated.

Isolation and purification of monomeric collagen. Monomeric Type I rat tail tendon collagen was obtained by acid extraction from Sprague-Dawley rats (Pel-Freez Biologicals, Rogers, AR) following a procedure adapted from Silver and Trelstad [202]. Briefly, rat tail tendons were extracted with the aid of autoclaved pliers and dissolved in 10mM HCl for 4 h at 25˚C to dissolve the proteinaceous components. Insoluble tissue and other contaminants were removed by centrifugation at 30,000g at 4˚C for 30 min with subsequent vacuum filtration through 20 μm, 0.45 μm and 0.2 μm filters. The sterile filtered collagen in HCl was precipitated from solution by adding NaCl to a final concentration of 0.7M. The precipitated collagen was pelleted by centrifugation, redissolved in 10mM HCl and dialyzed first against 20mM phosphate buffer at room temperature, then at 4˚C, second against 10mM HCl at 4˚C and finally against deionized water at 4˚C. The collagen was lyophilized and stored at 4˚C until use.

Production of collagen mats. Monomeric rat tail tendon collagen dissolved in 10mM HCl, at concentrations of 0.3125 mg/mL - 2.5 mg/mL, was neutralized using a gelation buffer (4.14 mg/mL monobasic sodium phosphate, 12.1 mg/mL dibasic sodium phosphate, 6.86 mg/mL TES (N-tris (hydroxymethyl) methyl-2-aminoethane sulfonic acid sodium salt, 7.89 mg/mL sodium chloride, pH 8.0) at 4˚C for 24 h. Gels were subsequently placed in a fiber incubation buffer (7.89 mg/mL sodium chloride, 4.26

mg/mL dibasic sodium phosphate,10 mM Tris, pH 7.4) at 37°C for 48 h to promote fibrillogenesis [203]. Gels were then dried at room temperature under a steady air stream.

Generation of structural anisotropy. Collagen gels (100 x 80 x 4 mm) were adhered onto 125 μm thick plastic frames, and mounted onto a motorized vertical stretching device (Figure 2.1). The stretcher was expanded uniaxially at 3 μm/s and 300 μm/s to strains of 0, 10, 20% in deionized water, 25°C. Strains larger than 20% resulted in tearing of the collagen gels. Aligned gels were then air dried under constant tension for 24 h at 25˚C, resulting in a dense collagen mat.

Imaging of collagen fibril orientation, morphology and ultrastructure. Dry collagen lamellae were hydrated in water for 24 h and subsequently processed for SEM imaging. Briefly, samples were dehydrated in serial exchanges of acetone-water mixtures from 30%-100%. The samples were then critical point dried, sputter coated with gold and imaged at an accelerating voltage of 10 keV using a field emission scanning electron microscope (Joel DS 150, Tokyo, Japan). Scanning electron microscopy, SEM, images were taken at 10,000X magnification for alignment and 50,000X magnification for fibril diameter measurements. To determine the ultrastructure and presence of D-periodicity in the fibrils, hydrated samples were prepared for transmission electron microscopy (TEM). Briefly, samples in PBS were washed in 0.1M cacodylate buffer and fixed in glutaraldehyde. After washing in water, samples were partially dehydrated in ethanol and stained with uranyl acetate. Samples were then fully dehydrated in ethanol, embedded in resin and polymerized. 60-80 nm sections were then cut using a RMC MT-7000

ultramicrotome (Boeckeler, Tucson, AZ). Sections were then post stained with uranyl acetate and lead citrate and imaged using a JOEL JEM 1210 TEM (JOEL, Tokyo, Japan) at 90 kV.

Quantification of alignment. Alignment was determined using Fast Fourier Transforms of 10,000X SEM images in ImageJ®. Uniformity of alignment was determined by analysis of various parts of each sample, and amongst various sections of the sample. The relative frequency of fibrils in any given angle was determined,divided into 5˚ bins of angles and plotted. The plots were then fitted with a Gaussian distribution to determine the peak relative frequency of fibril alignment, and full width at half maximum (FWHM), corresponding to the angles between which most of the fibrils are distributed.

Crosslinking and mechanical testing of constructs. Anisotropic and isotropic collagen lamellae were crosslinked in a biocompatible crosslinker, genipin-PBS (Fisher Scientific) at 6 mg/mL for 24hours at 37˚C. Samples were then cut into 20mm long x 5mm wide rectangles that were mounted onto a Dynamic Mechanical Thermal Analyzer V (DMTA V, Rheometric Scientific, Piscataway, NJ) with a gauge length of 10 mm, immersed in PBS at 37˚C and preconditioned 15 times to 66% of the average maximum failure strain for the sample, and then tested to failure at 5 mm/min. A total of 8 samples were tested for each group. Thickness of hydrated sample was measured using optical microscopy and then correlated to mechanical data to determine the ultimate tensile strength and strain at failure. Young's modulus was determined from the slope of the last 4% of the stress-strain curve.

Statistical Analysis. Means and S.D. were obtained for all measurements, image analyses and mechanical data. Comparisons will be made using the Student's *t* test for paired data, ANOVA for multiple comparisons, with Tukey post hoc analysis for parametric data. Nonparametric tests will be carried out using the Kruskal-Wallis ANOVA, with Dunn's post hoc analysis as indicated. Values of $P < 0.05$ were considered statistically significant.

2.3 Results:

Rapid generation of high density collagen mats. We have shown the ability generate large (centimeter scale) collagen matrices that can be mechanically tuned and anisotropically defined. Type I collagen was isolated from rat tail tendon and confirmed for purity by PAGE gel analysis. Collagen gels were structurally aligned, analyzed for native ultrastructure and tested for mechanical strength. Gels were synthesized at a variety of concentrations (0.3125 mg/mL, 0.625 mg/mL, 1.25 mg/mL and 2.5 mg/mL) by neutralization in a phosphate buffer for 24 hours at 4˚C. Gel thickness was determined by the volume of total solution in 10 cm x 8 cm rectangular molds, Figure 2.1 A. Fibrillogenesis within collagen gels was enhanced by incubation in a fiber incubation buffer for 48 hours at 37˚C, Figure 2.1 B. For alignment of collagen matrices, gels were mounted on a axial stretcher and stretched to 0, 10, 20% strain at 3 or 300 μm/s, Figure 2.1 C & D. Collagen gels were subsequently air dried to less than 1% of their initial thickness under a constant air stream, generating collagen mats. We have thus demonstrated a technique for the development of collagen matrices with structural anisotropy in a scalable method, generating large centimeter scale non-denatured matrices suitable for tissue engineering.

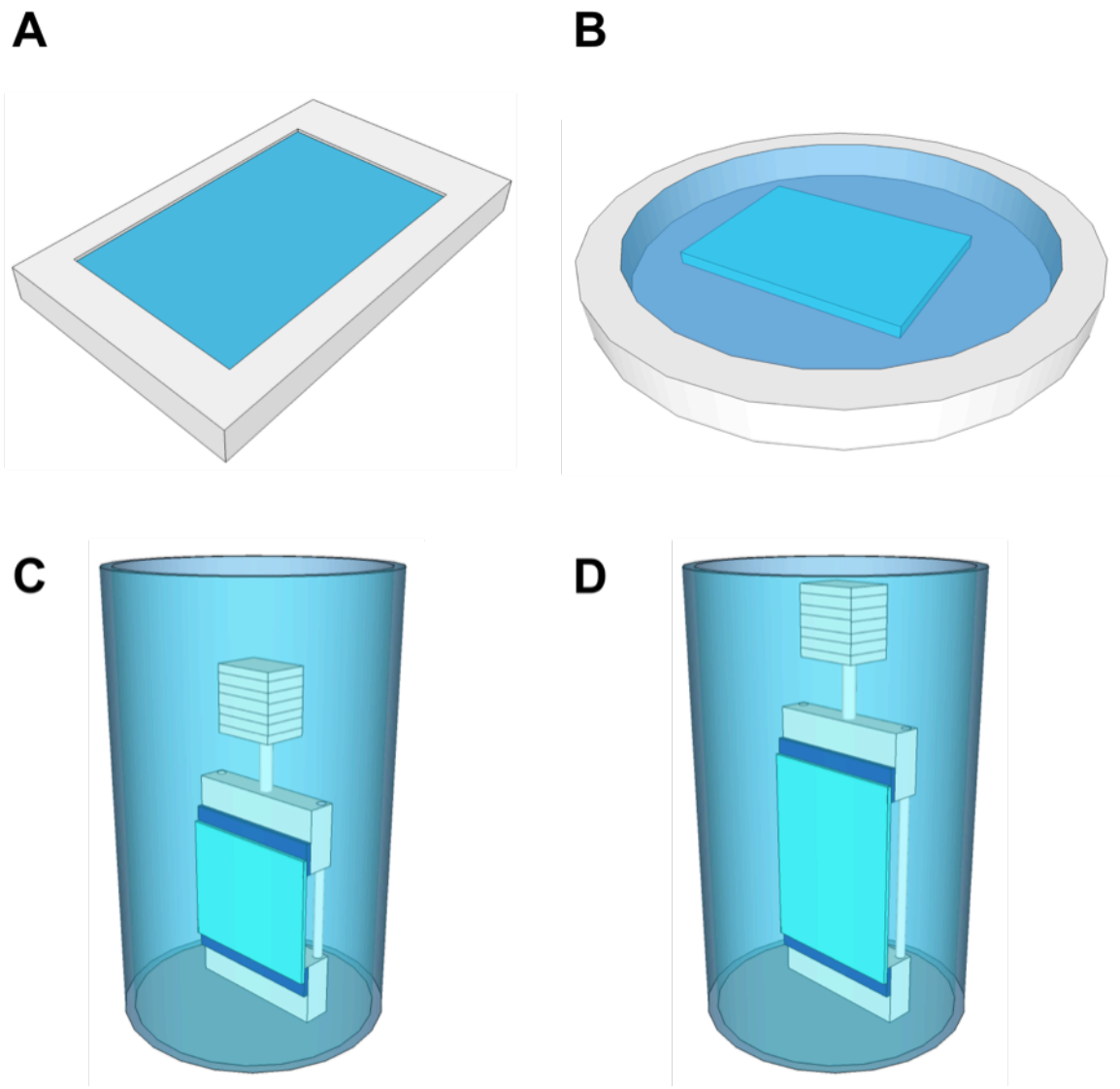

Figure 2.1: **Schematic of the mechanical setup used to induce strain alignment of collagen gels.** Collagen gels were cast in a rectangular mold (Length x Width x Thickness: 100 x 80 x 4 mm) at 4°C (A), incubated in a fibril incubation buffer for 48 h at 37°C (B), mounted on a motorized stretcher (C), and stretched to a strain of 0%, 10% or 20% stretch, at 3 μm/s or 300 μm/s (D).

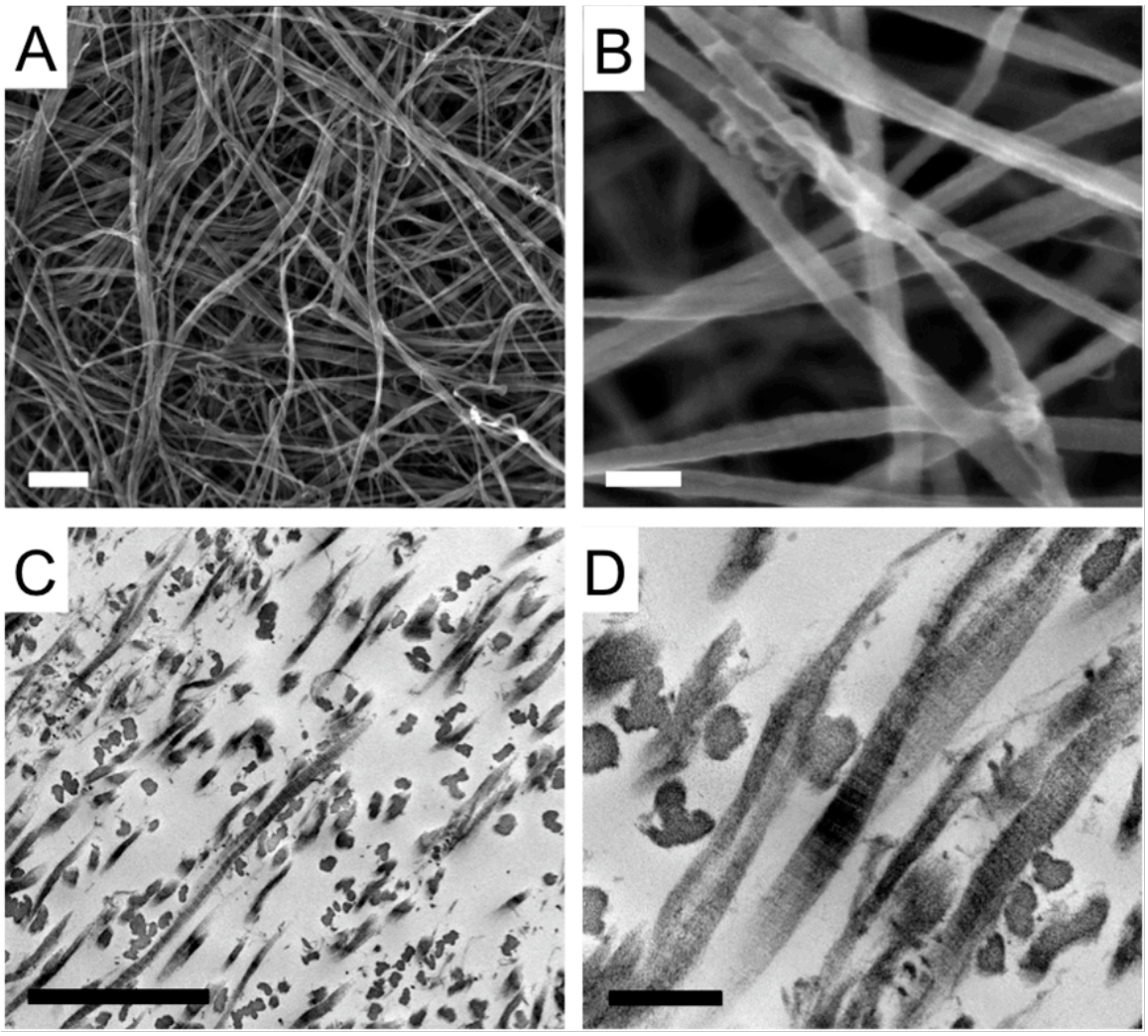

Figure 2.2: Ultrastructure of collagen matrices. Scanning electron micrographs showing (A) isotropic microstructure (scale bar: 1 μm), (B) with 83.1 ± 9.44 nm fibrils (scale bar: 200 nm). Transmission electron micrographs showing (C) a dense fibrillar matrix (scale bar: 1 μm) and (D) native collagen banding showing preservation of the native D-periodic banding pattern (scale bar: 200 nm).

Fibrillar microstructure and preservation of native collagen structure.

Ultrastructural analysis of collagen lamellae showed uniformity of collagen fibril diameter for unaligned and aligned gels. 10kX SEM images of critical point dried collagen matrices show uniformity and isotropy of unaligned matrices (Figure 2.2 A). 50kX magnification SEM images of critical point dried collagen matrices were used to measure collagen fibril diameter, Figure 2.2 B. Fibril diameter for unaligned 2.5 mg/mL gels was 83.1 ± 9.44 nm, for 1.25 mg/mL gels was 75.7 ± 14.8 nm and for 0.625 mg/mL gels was 74.3 ± 11.4 nm. Fibril diameter for 20% aligned 2.5 mg/mL gels was 78.2 ± 17.0 nm, for 10% aligned 2.5 mg/mL gels was 81.7 ± 14.8 nm and for 20% aligned 0.3125 mg/mL gels was 88.52 ± 11.7 nm, which showed no significant difference with alignment, stretch amount, stretch rate or concentration. TEM images of uranyl acetate stained collagen lamellae showed characteristic D-periodicity, 67 nm collagen banding patterns (Figures 2.2 C & D). Concentration variation did not significantly affect the fibril diameter or the ultrastructure of the collagen gels (Table 2.1). Through the neutralization of collagen gels using a phosphate based buffer, subsequent incubation with fibril incubation buffer to promote fibrillogensis of collagen fibrils, and drying into dense matrices, collagen lamellae which resemble native matrix in macro- and ultra-structure have been created.

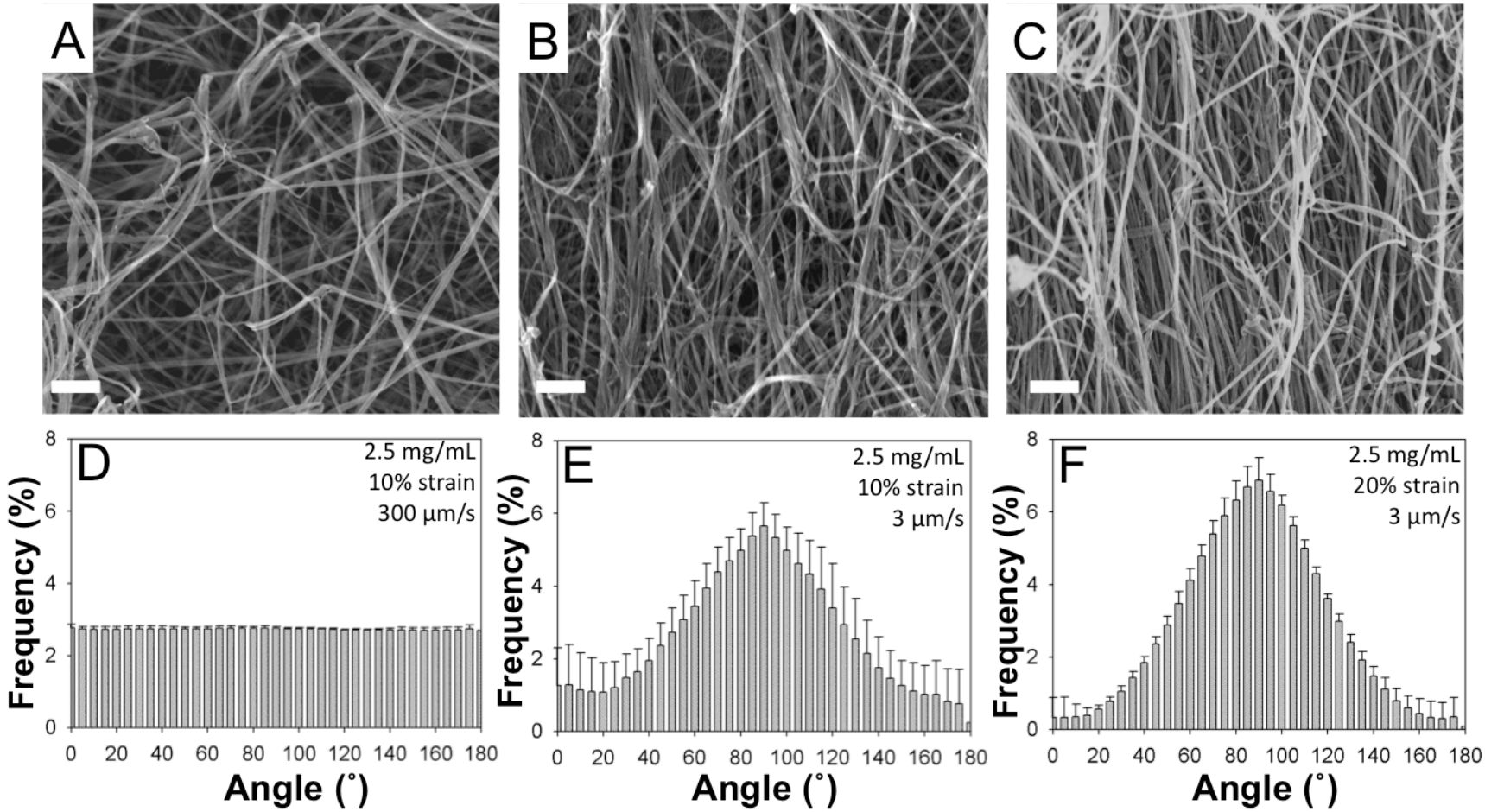

Figure 2.3: Stretching rate, strain amount and concentration dependence on alignment of collagen matrices. Top panel shows SEM images, and bottom panel shows histograms of FFT analyses of SEM images of 9 regions of 4 independent samples, of (A & D) 2.5 mg/mL matrix aligned at 300 μm/s to 10% strain, (B & E) 2.5mg/mL matrix aligned at 3 μm/s to 10% strain and (C & F) 2.5 mg/mL matrix aligned to 20% strain. Scale bar: 500 nm

Generation of structural anisotropy within collagen matrices. To enhance tissue mimetic architecture, it is required that matrices exhibit mechanical anisotropy to ensure matching of tissue based replacements. Subsequent to treatment in fiber incubation buffer gels were adhered onto plastic frames and mounted on an automated motorized stretching device (Figure 2.1 C). Higher stretching rates (300 μm/s) resulted in an inability to generate structural anisotropy (Figure 2.3 A and Table 2.1). Lower stretching rates (3 μm/s) resulted in distinct fibril reorganization into defined structures (Figures 2.3 B & C, Table 2.1). FFT analysis of 10kX SEM images of collagen lamellae yield relative frequencies of fibrils from the horizontal axis. Fibril relative frequencies were summed in 5 degree increments and histograms were plotted as a function of angle, Figures 2.3 D-F. Histogram plots were then fitted with a Gaussian curve and FWHM was subsequently determined. FFT analysis of 10kX magnification images of 300 μm/s strained samples to 10% or 20% showed no preferential alignment of collagen fibrils, Figure 2.3 D. Depending on the strain amount, 10% or 20%, the degree of alignment varied at a lower strain rate of 3 μm/s, Figure 2.3 E & F. Maximum alignment was achieved with 20% strain at a rate of 3 μm/s. Concentration variation did not significantly affect the amount of alignment, or the maximum alignment, Table 2.1. Alignment for 2.5mg/mL gels strained to 10% at a rate of 3 μm/s had a maximum of 5.64% with a FWHM of ± 37.5˚. Alignment for 2.5 mg/mL gels strained to 20% at a rate of 3 μm/s had a significantly higher maximum of 6.86% with a FWHM of ± 35.2˚, Figure 2.4. We have thus shown the ability to modulate the alignment of collagen matrices as a function of strain rate and strain amount.

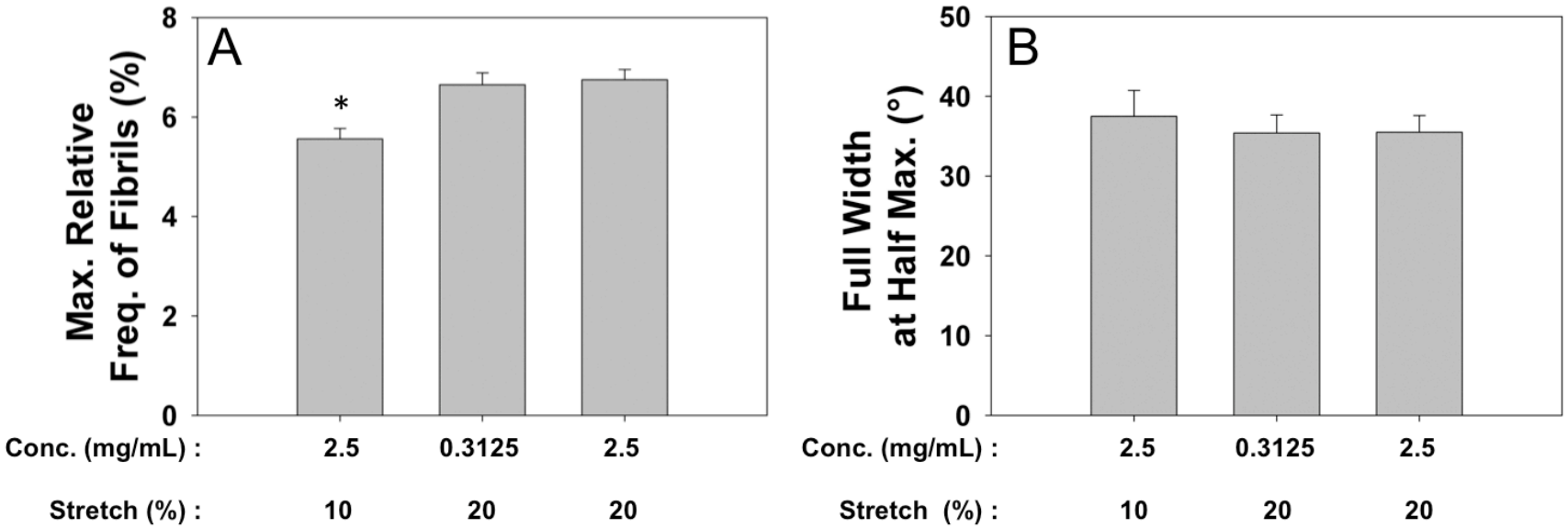

Figure 2.4: Alignment of collagen fibrils based on Gaussian fit of alignment data derived from FFT of SEM images at 10kX magnification. (A) Maximum relative frequency of fibrils, (B) Full width at half maximum, FWHM (where majority of fibrils reside). *p<0.05

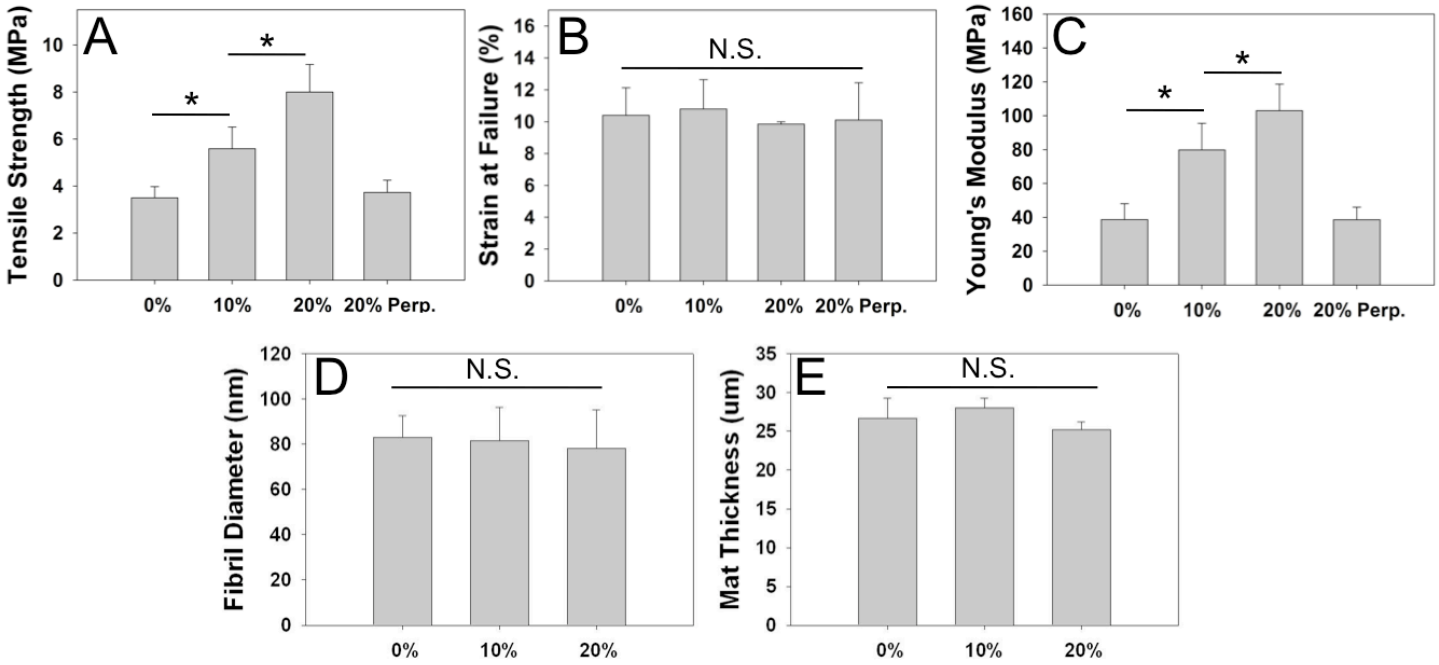

Figure 2.5: Mechanical properties of 20% stretch aligned, 20% stretch aligned tested perpendicular to alignment, 10% stretch aligned and (0%) unaligned 2.5 mg/mL collagen mats. (A)Tensile strength, (B) Strain at failure and (C) Young's modulus, (D) Fibril diameter and (E) Lamella thickness. (A) Tensile strength and (C) Young's moduli depend on percent alignment of matrices. (B) Strain to failure, (D) Fibril diameter and (E) Lamella thicknesses are similar for all constructs. Data presented as mean ± s.d. *$p < 0.05$

Mechanical strength of collagen matrices with and without alignment. In order to determine utility in a variety of soft tissue engineering applications, we determined the strength of collagen matrices as a function of alignment. Collagen gels of various concentrations from 0.3125 mg/mL - 2.5 mg/mL we aligned, dried and crosslinked with genepin. Uniaxial stress-strain testing collagen lamellae were performed using a DMTA V mechanical tester. Rectangular strips, 20 mm x 5 mm were cut from sheets of unaligned and aligned matrices in the direction of alignment, and perpendicular to alignment. Sheets were mounted vertically on the testing platform and immersed in PBS at 37°C. Samples were preconditioned and tested to failure. Samples that failed at the mounting points and those that slipped were discounted from analyses. Mechanical anisotropy was noted correlating to structural anisotropy. The mechanical strength, ultimate tensile strength (UTS), and stiffness, Young's modulus (Mod.), of aligned collagen matrices were significantly higher than that of unaligned samples, irrespective of concentration, Table 2.1. Aligned matrices showed an approximate doubling in mechanical strength independent of concentration, for 2.5 mg/mL gels from ~3.50 MPa to 8.00 MPa, Table 2.1. Further, stiffening of matrices occurred, resulting in Young's Moduli increases for 2.5 mg/mL gels from 38.7 MPa to 103 MPa, Table 2.1. Mechanical strength was a function of alignment with 10% aligned matrices having significantly lower UTS and Young's Moduli than 20% aligned matrices, Figures 2.5 A & C, Table 2.1. The mechanical strength in the direction perpendicular to that of alignment in anisotropic samples was not significantly different than unaligned samples, Figure 2.5. Increase in stretch amount of 2.5 mg/mL matrices from 10% to 20% resulted in a greater amount of alignment, and consequently in significantly higher strength and stiffness

($p<0.05$), Table 2.1. Further, this correlated with maximum relative frequency of fibrils, which was significantly different for unaligned, 10% aligned and 20% aligned matrices, although the distribution of fibrils from the peak, FWHM, was not, Table 2.1. Strain to failure of collagen matrices did not change significantly as a function of alignment, Figure 2.5 B. Collagen matrices did not show a significant difference in fibril diameter as concentration or alignment varied, ranging from 74.3 ± 11.4 nm to 88.5 ± 11.7 nm, Table 2.1. Further, concentration of initial gels did not significantly affect dried lamella thickness, Figures 2.5 D & E and Table 2.1. We have thus demonstrated the ability to modulate mechanical strength as a function of strain amount and strain rate. Further, microstructural alignment of collagen fibrils provides structural and mechanical buttressing during mechanical testing.

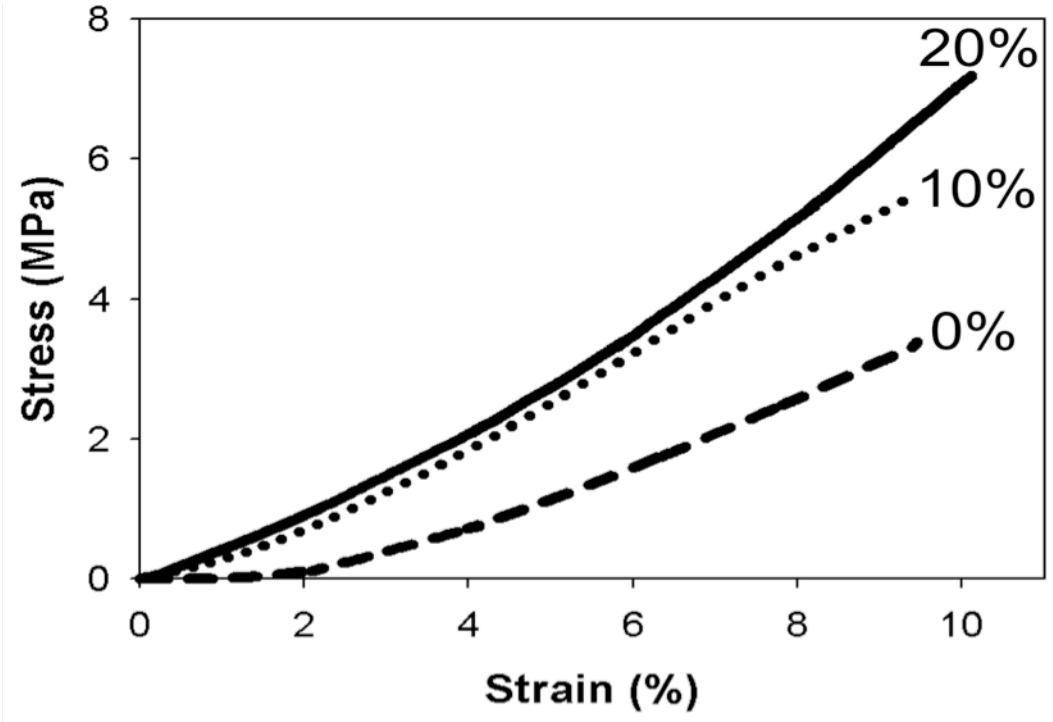

Figure 2.6: **Representative stress-strain plot of collagen matrices.** Matrices were stretch-aligned to different amounts at a rate of 3 μm/s (—: 20%, ··· : 10%, ---:0%). Samples were cut into 20 mm long x 5 mm wide strips and mechanically tested. Samples were pre-conditioned 15 times to 66% of failure strain, and then tested to failure.

Table 2.1: Consolidated mechanical and structural properties of collagen lamellae cast at different initial concentrations and aligned to different amounts.

Initial gel conc. (mg/mL)	Fibril diameter (nm)	Mat thickness	UTS (MPa)	Strain at failure (%)	Young's modulus	Maximum relative frequency of fibrils	FWHM	% Stretch Alignment
0.3125	88.4 ± 12.5	26.4 ± 1.42	3.71 ± 0.716	10.0 ± 1.19	43.1 ± 7.80	NA	NA	0
0.625	74.3 ± 11.4	27.6 ± 1.04	3.25 ± 0.31	10.5 ± 1.25	44.7 ± 8.21	NA	NA	0
1.25	75.7 ± 14.8	28.5 ± 2.68	3.27 ± 0.400	11.2 ± 1.60	42.7 ± 3.51	NA	NA	0
2.5	83.1 ± 9.44	26.7 ± 2.58	3.50 ± 0.478	10.4 ± 1.73	38.7 ± 9.37	NA	NA	0
0.3125	88.5 ± 11.7	24.9 ± 2.03	7.57 ± 0.682	11.2 ± 1.04	98.3 ± 15.2	6.65 ± 0.237	35.4 ± 2.26	20
0.625	85.4 ± 12.2	25.7 ± 2.06	7.43 ± 0.564	10.2 ± 1.24	91.4 ± 10.7	6.69 ± 0.206	35.1 ± 1.31	20
1.25	83.4 ± 9.26	26.3 ± 1.86	7.49 ± 0.639	10.7 ± 1.55	92.7 ± 6.23	6.63 ± 0.180	36.3 ± 1.36	20
2.5	81.7 ± 14.8	28.0 ± 1.28	6.20 ± 1.04	10.8 ± 1.83	79.8 ± 15.7	5.56 ± 0.213	37.5 ± 3.25	10
2.5	78.2 ± 17.0	25.2 ± 1.03	8.00 ± 1.17	9.85 ± 1.46	103 ± 15.6	6.75 ± 0.209	35.5 ± 2.10	20

Discussion:

Collagen based fabrics can be aligned by stretching to generate structural and mechanical anisotropy. Collagen gels are generated by the neutralization of acidified Type I monomeric rat tail tendon collagen in a phosphate based buffer. Gel dimensions are dependent on the volume of collagen solution and buffer used, and allow for large (centimeter scale) structures to be fabricated. Fibrillogenesis within gels is further enhanced by incubation in a fiber incubation buffer. Gels are subsequently dried to less than 1% of their original thickness to create high density collagen mats, 4 mm cast gel dried to 28 μm. Structural anisotropy was generated by adhering gels onto mechanical supports and stretching at rates of 3 μm/s and 300 μm/s to strains of 10% and 20%. Previous reports of gelation systems and fabrication of smaller-scale anisotropic collagen matrices have been limited in size (sub-micron to millimeter scale) which have shown lack of scalability or utility for regeneration of large tissue replacements [187].

Dependence of gelation conditions on ultrastructure of collagen gels. Collagen gelation kinetics is highly dependent on collagen isolation method, initial collagen concentration, temperature of gelation, pH and presence of ions. Several groups have shown the effects of the aforementioned parameters on fibrillar size and microarchitecture of collagen matrices [203; 204; 205; 206; 207; 208]. Pepsin digested collagen structures are devoid of telopeptide sequences that are critical to fibril formation with recapitulation of native collagen D-periodic structure, unlike acid solubilized collagen which still retains telopeptide sequences. The literature is replete with

conflicting reports on fibril diameter and parameters that influence gelation. Reports have noted the effect of longer gelation times, and lower initial concentrations of collagen allow more time for fibrillogenesis without spatial restrictions from adjacent fibrils; our studies indicate little difference in fibril diameter as a function of concentration (0.3125 mg/mL – 2.5 mg/mL) in our gelation conditions, buffers used, stretch rate or stretch amount, Table 2.1 [209; 210; 211; 212; 213; 214]. These small nanoscale differences do not directly translate to larger scale mechanical differences in ultimate tensile strength or strain at failure of centimeter scale constructs. Rather, there is a dependence on processing conditions and architectural arrangement of collagen fibrils in terms of alignment and packing density [184; 185; 215; 216; 217]. Further the importance of D-periodicity is exemplified by the characteristic 67 nm banding pattern of collagen (Figure 2.2 C-D), which helps maintain the native structure of the collagen; this is critical in higher order architectures that involve fibrillar collagen formation and preservation of cell binding moieties (ex. GFOGER which mediates binding with cell surface integrins). Further, integrin-mediated binding to collagen is dependent, on 3 dimensional structural motifs that are generated by the triple helix, and is dependent on the denaturation state of collagen [218; 219; 220].

Modulation of mechanical properties of collagen gels. Generation of structural anisotropy within fiber matrices has been known to significantly improve their strength. Specific to collagen, our group and others have shown that anisotropic collagen structures can withstand greater mechanical load bearing applied in the direction of fibrils [185; 188; 201]. Stretching of collagen gels has been shown not only to yield structural

anisotropy and linear alignment of collagen fibrils in the direction of applied strain, Figure 2.3, but also mechanical strengthening and reinforcement, Table 2.1 and Figure 2.4. Although of significant strength, uncrosslinked collagen constructs may degrade more quickly and are of lower strength than crosslinked constructs [217]. Therefore, we chose to employ a crosslinking scheme to strengthen our collagen matrices and modulate potential degradation. Genipin, a naturally occurring crosslinker, known specifically for its ability to conjugate lysine residues and impart significant strength onto bioengineered matrices, has also been established to be biocompatible [221; 222; 223]. Genipin crosslinked matrices exhibit an increase in ultimate tensile strength and stiffness, Young's modulus, with little to no change in strain at failure. Ultimately, uncrosslinked and crosslinked collagen constructs allow for the generation of a variety of mechanically tunable structures which can be adapted to several tissue engineering applications, including the development of blood vessels, cartilage, tendon, abdominal wall defect replacements or artificial skin, to name a few.

Dissimilitude and advantages compared to alternative alignment techniques. The importance of alignment and structural anisotropy in tissue engineered constructs is critical to recapitulation of native tissue mechano-biological behavior. Several groups have attempted to align collagen matrices that have resulted in monolayers of aligned collagen, matrices of varying collagen densities, thin collagen gels, weak matrices unable to support physiologically relevant loads and matrices with isolated regional alignment. The methods of these attempts include electrical gradients,[199] magnetic fields,[188; 189] microfluidics,[187; 198; 224] patterned substrates[113; 225] and mechanical

stresses [201]. Cheng et al used an electric field to align collagen molecules into a thick strand, 50-400 μm. However, their technique destroys the native collagen structure and denatures the molecule, as demonstrated by the lack of D-periodicity in their collagen fibers [199]. The use of large scale magnetic fields, 1-10 Tesla, to orient diamagnetic collagen molecules is prohibitive in cost, safety and efficiency in the rapid generation of collagen matrices, as described by Torbet and Ronziere[189] and Tranquillo's group [194; 195; 196; 197]. Although Cheng and Kaufman have described a methodology wherein magnetic beads with modified surface functionalities help align collagen molecules in a weaker magnetic field (10^{-4}T), the gels made were an order of magnitude smaller than in this study, and included a proxy material that could potentially be deleterious depending on the application of the material [187]. Lee et al and Lanfer et al have employed the use of microfluidics to align collagen molecules [198; 224; 226; 227]. In addition to the significantly thinner and small constructs that they have synthesized, the potential for the formation of a density gradients across the sample due to viscous flow shear lamellae, and along the sample due to fibril polymerization prior to fully traversing the length of the channel, can create inhomogeneities within samples. Further removal of aligned collagen constructs from channels restricts these methods to much smaller scales, unsuitable for large scale tissue engineering. Moreover, their studies require longer processing times and layer-by-layer deposition of multiple aligned collagen matrices in order to gain utility. This study however employs large (10 x 8 cm) collagen gels with gel thicknesses of 4 mm. Further, these constructs are freely moving, unadhered to a surface and can be easily manipulated into larger tissue based constructs. Deitch et al have employed inkjet printer technology to print collagen solutions onto

glass substrates. The thin films they have produced lack consistency and have not demonstrated precise molecular alignment [200]. Vader et al have used a similar technique of strain alignment for the formation of structural anisotropy with collagen gels. Their study used controlled actuation of glass rods which perforated small 1 mm thick collagen gels. The imposed strain between the glass rods yielded localized regions of alignment within the sample. They reported plastically deforming uncrosslinked gels into aligned states, but noted that glutaraldehyde crosslinked gels were structurally elastic [201]. Although an elegant strategy, their alignment technique lacked versatility and scalability – localized regions of alignment, small size of the collagen gels, and low mechanical strength. Herein we have described a novel technique to create large constructs with global tunable alignment and a strategy for the development of high-density collagen matrices which have suitable mechanical strengths for a variety of tissue engineering applications.

2.5 Conclusion

Collagen is a critical building block of the extracellular matrix. The present study has demonstrated the ability to generate large collagen matrices with suitable mechanical and structural properties to native tissue structures with preservation of native fibrillar structure and characteristic D-periodicity. Further we have circumvented the problem of weakness in collagen gels, which are usually too weak to be used in many tissue engineering applications, by drying and crosslinking them into high density lamellae that have mechanical strengths on the order of several soft tissues, 1-10MPa. Further, large lamellae can be fabricated with structural anisotropy. The amount of collagen fibril alignment is dependent on the amount of strain induced on the matrix and on the stretching rate, with a maximum alignment of 6.86%, with greater than 95% of fibrils within ±35.2˚ of the direction of alignment. The utility of this fabrication scheme allows for the rapid fabrication of large, aligned collagen matrices which can be further investigated for use to mimic native tissue structures.

CHAPTER 3

Strong collagen-based substrates with tunable microarchitectures for soft tissue engineering

3.1 Introduction:

The generation of scalable mechanically matching and biocompatible materials comprising completely natural biopolymers for soft tissue engineering has been a challenge the biomaterials field has been attempting to address for over a half century [228]. Coupled with the immense cost of disease specific morbidity and mortality, many efforts, and multi-billion dollar federal funding, have been devoted to the development and fabrication of tissue-mimetic constructs [229]. However, most materials have been fabricated for only one or a few tissue specific applications. Additionally, significant efforts have been made to engineer *in vitro* living tissue systems and organs; however, most of these approaches have utilized weak synthetic hydrogels that lack mechanical strength for ultimate *in vivo* utility given their poor mechanical strength, cell adhesive properties, and the lack of a native extracellular matrix environment to physically and biologically recapitulate native tissue growth/responses.

Several groups have attempted to use synthetic non-degradable and biodegradable polymers to recapitulate the ECM environment by generating nanofibrous architectures. Common techniques include porogen leaching [230], gas foaming [231], freeze drying [232], electrospinning,[233] 3D printing, sterolithography, solid free form fabrication and a variety of other technologies summarized well by Sachlos and Czernuszka [234]. While

these techniques have shown reasonable promise, concerns over immune rejection, macrophage/neutrophil mediated degradation, inflammation, mechanical failure, and ultimately integration into the host system have limited large-scale utilization.

Another widely studied alternative to the generation of ECM-mimetic scaffolds is the decellularization of native tissue matrices. After devitalization and removal of potentially immunogenic antigens, tissues are often crosslinked to maintain stability and mechanical integrity. Further, the complex 3D structure of tissue is retained in decellularized scaffolds; this in turn aids the infiltration of scaffolds and presents a conducive niche for regeneration. The resulting scaffolds have found many uses in the engineering of a variety of tissue replacements [235; 236; 237]. However, decellularized matrices lack defined architecture and can often become irreversibly damaged during processing. Consequently, there is a diminished ability to mechanically tune such matrices without the addition of dopants, which may in turn elicit a host tissue response. Further, given that most decellularized tissues are harvested from xenogenic sources, there is the potential for residual xeno-antigen presentation and residual cells/ cell fragments, which may result in an immune response, even if the ultimate building blocks of the scaffold (collagen, elastin, proteoglycans) have high interspecies homology. Conversely, allogeneic matrices may lack availability and harbor a potential for viral or bacterial transmission. Thus, there exists a large demand for the generation of engineered matrices that provide a 3D niche for tissue infiltration and integration, which can be mechanically tailored for a variety of applications, and that structurally mimics the native tissue environment.

Noting these considerations, we have identified 5 critical criteria for tissue engineered scaffolds: (1) require minimal processing and allow for scalable manufacture, (2) have a hierarchical structure that can be tailored both structurally and mechanically to match native tissue, (3) provide a conducive environment for cellular adhesion, growth and proliferation, (4) degrade to yield non-toxic products, and (5) cause minimal inflammatory response. Capitalizing on the natural abundance of collagen in native tissues, we have designed a bottom-up approach for the creation of bioartificial matrices. Coupled with a recently described recombinant elastin-like protein polymer (ELP) [238; 239], we have generated collagen fiber-elastin reinforced nanocomposites for utility in soft tissue applications. To mimic the crimped form of fibrous collagen which supports tensile loading in native tissue (10 – 200 μm wavelengths) [240; 241], we have applied excimer laser ablation to create "wavy" collagen structures that enhance tissue engineered matrix compliance (<10 – 90 % elongation at break) with no appreciable protein denaturation. By systematically controlling collagen gel hydration and global micro- and macro- structure, a series of strong (1-15 MPa strength) collagen sheets embedded with elastin have been developed with mechanical and biological properties that mimic native tissue. Cytocompatibility was established by culture of bone marrow derived mesenchymal stem cells, showing confluence within hours and conformal scaffold based cell morphology. Through the development and utilization of layer-reinforced collagen networks and novel microfabrication techniques, we have developed a natural biopolymer matrix with tunable mechanical properties that have potential for

use as biosynthetic blood vessels, tendon replacements, hernia patches, muscle tissue, nerve guidance conduits, artificial skin and other soft tissue applications.

3.2 Materials and Methods:

All chemicals were purchased from Sigma-Aldrich, unless otherwise stated.

Isolation and purification of monomeric collagen. Monomeric Type I rat tail tendon collagen was obtained by acid extraction from Sprague-Dawley rats (Pel-Freez Biologicals, Rogers, AR) following a procedure adapted from Silver and Trelstad [202]. Briefly, rat tail tendons were extracted with the aid of autoclaved pliers and dissolved in 10 mM HCl for 4 h at 25°C to dissolve the proteinaceous components. Insoluble tissue and other contaminants were removed by centrifugation at 30,000g at 4˚C for 30 mins with subsequent vacuum filtration through 20 μm, 0.45 μm and 0.2 μm filters. The sterile filtered collagen in HCl was precipitated from solution by adding NaCl to a final concentration of 0.7 M. The precipitated collagen was pelleted by centrifugation, redissolved in 10 mM HCl and dialyzed first against 20 mM phosphate buffer at room temperature, then at 4°C, second against 10 mM HCl at 4°C and finally against deionized water at 4°C. The collagen was then frozen and lyophilized till use.

Production of collagen mats. Monomeric rat tail tendon collagen dissolved in 10mM HCl, at concentrations of 0.3125 mg/mL-2.5 mg/mL, was neutralized using a gelation buffer (4.14 mg/mL monobasic sodium phosphate,12.1 mg/mL dibasic sodium phosphate, 6.86 mg/mL TES (N-tris (hydroxymethyl) methyl-2-aminoethane sulfonic acid sodium salt, 7.89 mg/mL sodium chloride, pH 8.0) at 4˚C, in rectangular molds (10 x 8 cm) for 24 h. Gel thicknesses were 2, 3, or 4 mm. Gels were subsequently placed in a

fiber incubation buffer (7.89 mg/mL sodium chloride, 4.26 mg/mL dibasic sodium phosphate,10 mM Tris, pH 7.4) at 37°C for 48 h to promote fibrillogenesis [203]. Gels were then dried at room temperature under a steady air stream to create collagen mats. Stacked lamellae consisting of 2 to 8 layers were generated by serially drying additional gels on top of dried mats. Some specimens were crosslinked in genipin at 6 mg/mL in 1x PBS at 37°C for 24 h.

Excimer ablation of collagen mats. Two different mask types were used in this study: stainless steel masks and quartz masks. Stainless steel masks were constructed by infrared laser ablation of 50 μm thick stainless steel sheet stock. Quartz contact masks (Advance Reproductions, MA) were fabricated using photolithography and wet etching of 5 μm thick aluminum coated quartz. Five designs consisting of linear or sawtooth ablation patterns were investigated with geometric design variables consisting of strip length, strip width, interstrip gap and vertical strip width. These variables ultimately dictated the frequency and amplitude of the resultant waveform, Figure 3.2. The mask was placed over collagen matrices and ablated with an excimer laser with parameters adjusted to yield a fluence of 26.7 J/cm^2 (Microelectronics Research Center at Georgia Tech, Atlanta, GA).

Microdifferential scanning calorimetry of collagen mats. To determine the effect of lamella fabrication and excimer laser ablation on collagen triple helical structure, thermal denaturation temperature and enthalpy of denaturation were measured using a differential scanning calorimeter (μDSC, SETARAM, Pleasanton, CA). Briefly, 5-10 mg segments

of lyophilized collagen, dried collagen lamellae pre or post excimer ablation, and post crosslinking in genipin were hydrated in 0.5 mL of PBS for 10 h at 5˚C. Lamellae were then heated from 5°C to 90°C and back to 5°C at 0.5°C/min. The enthalpy of phase changes relating to denaturation, H_D, was measured, as well as the denaturation temperature, T_D. Complete denaturation was confirmed by the lack of a denaturation peak upon a repeated heating (to 90°C) and cooling cycle.

Synthesis of a recombinant elastin-like protein polymer (ELP). Development and production of the ELP, LysB10, has been described elsewhere [239]. Briefly, a triblock amphiphilic copolymer was designed to contain hydrophobic endblocks and a hydrophilic midblock. The 75kDa polypeptide comprised 33 repeats of the pentapeptide sequence $[IPAVG]_5$, and the 58 kDa midblock comprised 28 repeats of the sequence [(VPGAG)2VPGEG(VPGAG)2]. Flanking both the hydrophobic plastic endblocks and the hydrophilic elastic midblock were the crosslinkable amino acid sequences: [KAAK] which allow for amine-based crosslinking. Subsequent to expression in *E. coli* protein was extracted and purified using hot/cold centrifugation cycles and nucleic acid removal. Protein solutions were then dialyzed against water and lyophilized.

Fabrication of planar nanofibrous collagen-elastin composites. LysB10, dissolved in molecular grade water (10 mg/mL, 4˚C) was used to embed single layer and multi-layer collagen lamellae in a sandwich molding setup. The setup was warmed to 25˚C to allow the LysB10 solution to gel, creating single ply composites. Single ply were stacked, cooled and reheated to create multi-ply structures [242].

Imaging of composite architecture. Optical microscopy, fluorescence microscopy, scanning electron microscopy (SEM), and transmission electron microscopy (TEM) were used to analyze the collagen structure pre and post embedment in elastin. For SEM studies, briefly, dry collagen lamellae were hydrated in water for 24 h and dehydrated in serial exchanges of ethanol-water mixtures from 30%-100%. The samples were then critical point dried (Auto Samdri 815 Series A, Tousimis, Rockville, MD), sputter coated with 8nm of gold (208HR Cressington, Watford, England) and imaged at an accelerating voltage of 10keV using a field emission scanning electron microscope (Zeiss Supra 55 FE-SEM, Peabody, MA). To determine the ultrastructure and presence of D-periodicity in the fibrils, showing maintenance of native collagen structure, hydrated samples were prepared for TEM. Samples in PBS were washed in 0.1M cacodylate buffer and fixed in glutaraldehyde. After washing in water, samples were partially dehydrated in ethanol and stained with uranyl acetate. Samples were then fully dehydrated in ethanol, embedded in resin and polymerized. Ultrathin (60 - 80 nm) were cut using a RMC MT-7000 ultramicrotome (Boeckeler, Tucson, AZ). Post-staining with uranyl acetate and lead citrate was followed by imaging using a JOEL JEM-1400 TEM (JOEL, Tokyo, Japan) at 90 kV.

Rat mesenchymal stem cell (rMSC) cell culture. Bone marrow-derived rMSCs (Stice lab, University of Georgia, GA) were seeded onto collagen constructs to establish cytocompatibility. Collagen scaffolds with and without microablation were sterilized in 70% ethanol for 30 min, washed several times in 1X PBS, and incubated in media for 30

min prior to cell seeding. Cells were cultured in Alpha MEM, supplemented with 10% fetal bovine serum, 1% L-glutamine and 1% penicillin-streptomycin. Cells were removed from tissue culture-treated polystyrene flasks using 0.25% trypsin-EDTA, suspended in media, and seeded at a concentrations of 100 000 cells/cm^2 for 24 h.

Assessment of cellular viability and alignment. Cell adhesion and morphology was probed using Live/Dead staining (Invitrogen, Carlsbad, CA), and Alexa Fluor® 568 phalloidin (Invitrogen, Carlsbad, CA), as per manufacturer's protocol. For Live/Dead staining, scaffolds were washed 3 times in PBS without divalent salts, and incubated with 2 mL of Live/Dead stain (2μM calcein AM and 4μM Ethidium homodimer-1 solution in PBS) for 1 hour. Scaffolds were then placed on glass slides with the addition of 20μL of Live/Dead stain and coverslipped. Stained cells were imaged using a Lecia SP5 confocal coupled with a white light laser and adjustable emission collectors (Leica, Buffalo Grove, IL). Calcein AM was imaged using excitation of 488 nm and emission of 518 nm, and Ethidium homodimer-1 was imaged at an excitation of 528 nm and emission of 617 nm. For cellular alignment, actin filament organization was probed. Briefly, scaffolds were washed with PBS, fixed in 4% buffered paraformaldehyde, washed in 0.5% Triton X in PBS, washed in 100mM glycine in PBS, blocked with 1% BSA in PBS, and stained with Alexa Fluor 568 phalloidin dissolved in methanol. Excess stain was washed in PBS. Scaffolds were mounted onto glass slides, 20 μL of DAPI Prolong Gold® (Invitrogen, Carlsbad, CA) was added and coverslipped. Scaffolds were imaged after 24 h using a Leica SP5XMP inverted confocal microscope (Leica, Buffalo Grove, IL) coupled with a white light laser and 405 nm diode laser. DAPI was imaged using excitation of 405 nm

and emission of 461 nm, and phalloidin was imaged using excitation of 578 nm and emission of 600 nm.

Mechanical testing of composites. To simulate application in planar soft tissues, collagen sheets (with and without microablation) were cut into 20mm x 5mm strips and mounted onto a Dynamic Mechanical Thermal Analyzer V (DMTA V, Rheometric Scientific, Piscataway, NJ) with a gauge length of 10mm, immersed in PBS at 37°C. Samples were preconditioned 15 times to 66% of the average maximum failure strain determined from pilot samples, and then tested to failure at 5 mm/min (n=8 for each group). Hydrated thickness was measured using optical microscopy for calculation of cross-sectional area. Young's modulus was determined from the slope of the last 4% of the stress-strain curve. Suture retention strength of planar constructs was determined by cutting 4mm x 4mm square inserting 4-0 FS-2 prolene suture (Ethicon) through the center of the segment, and pulling out the suture with force measured on the DMTA (n=4 for each design).

Statistical Analysis. Means and S.D. was obtained for all measurements, image analyses and mechanical data. Comparisons will be made using the Student's *t* test for paired data, ANOVA for multiple comparisons, and Tukey post hoc analysis for parametric data. Nonparametric tests were carried out using the Kruskal-Wallis ANOVA, with Dunn's post hoc analysis as indicated. Values of $P < 0.05$ were considered statistically significant.

3.3 Results:

Generation of collagen lamellae and nanofibrous composites. Collagen materials with high strength and tunable mechanical properties were generated in single and multiple layers, Figure 3.1. Multi-layer mats, generated by the serial drying process, were well-integrated with no distinguishable interface between layers. Mechanical peeling of lamellae resulted in whole tears, without the ability to tweeze out individual layers of multi-layer mats.

Collagen mats, due to their fibrillar nature, allow for impregnation with alternative matrices that can modulate mechanical or biological behavior. The sandwich molding technique permited the infusion of ELP into collagen matrices, leading to nanofibrous composite matrices, schematically shown in Figures 3.1 B, C, E, & F [182; 183; 242]. Dry matrices before and after the addition of ELP had spatial densities of 0.772 ± 0.0626 mg/cm^2 or 0.983 ± 0.0558 mg/cm^2, respectively, suggesting the composite matrices are 78.5% collagen and 21.5% ELP by dry weight. In addition to the single- and multi-*layer lamellae* described above, the ELP molding process allowed the formation of single- and multi-*ply* structures, Figure 3.1.

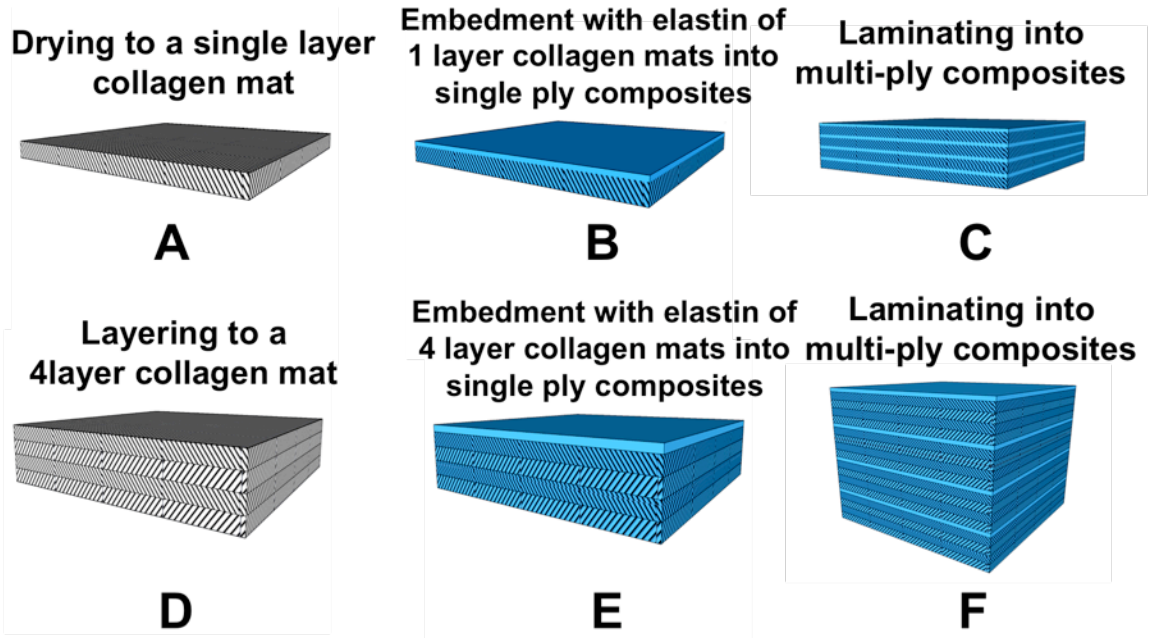

Figure 3.1: Schematic of fabrication strategy for layered collagen elastin nanocomposites. Collagen gels were cast at 4mm thickness. (A) Collagen lamellae are dried to a dry thickness of approximately 10 μm, (D) and layered into *multi-layer* collagen mats. (B) Single layer collagen lamellae are embedded in elastin into a single ply, in a sandwich molding technique, (E) multi-layer lamellae are embedded into a multi-layer single ply composite. (C) single layer single ply composites are stacked into single layer multi-ply composites, (F) multi-layer single ply composites are stacked into multi-layer multi-ply composites.

Mechanically tunable collagen lamellae as a function of concentration, thickness and layering. Initial collagen constructs showed a significant increase in strength and stiffness of matrices as a function of concentration, but not a significant difference in strain at failure, Figures 3.2 A, B & G. When compared to single layer matrices, multi-layer matrices showed an increase in strength (4-14 MPa), strain at failure (10-17 %) and stiffness (40-100 MPa), Figure 3.2 C, D & I. Increasing gel thickness from 2 to 4 mm prior to drying resulted in collagen lamellae of increasing strength and stiffness, with no significant effect on strain-at-failure, Figures 3.2 E, F & K. Individual collagen lamellae had a nominal thickness of 14.9 - 40.8 μm depending on initial collagen concentration in the gels, Figure 3.2 H. Layering of collagen gels showed a commensurate near-linear increase of thickness, Figure 3.2 J.

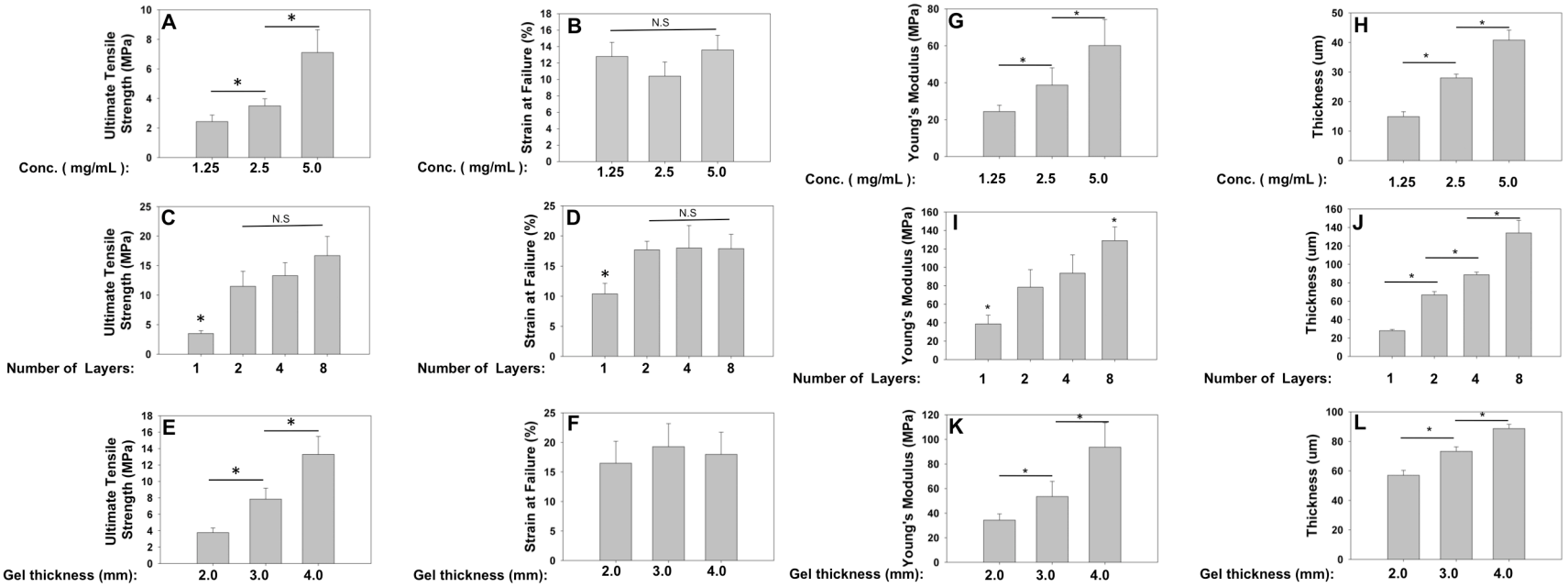

Figure 3.2: Mechanical properties of genipin crosslinked collagen mats. Increasing concentration of initial gels results in improved strength and stiffness with a commensurate increase in thickness (A,B,G,H). Increasing the number of layers shows an increase in strength and stiffness (C,D,I,J). Increasing initial thickness of 2.5 mg/mL collagen gels in 4 layer lamellae systems resulted in significantly stronger matrices (E,F,K,L). (*$p<0.05$)

Development of structurally and mechanically anisotropic collagen microarchitectures. Excimer laser ablation permits the use of a variety of masking techniques to ablate almost any design onto collagen substrates. Critical features of the triangular waves designs, described herein, included wave height, strip width, inter-strip width, wave width, and vertical strip width, Figure 3.3 A and Table 3.2. The fidelity and resolution of the excimer laser allows for exact cuts to be made into the collagen mats, Figure 3.3 B, C, D. Although the theoretical resolution of the excimer laser is 248 nm, the practical resolution is typically higher. Consequently minimum feature sizes were 10 μm, Table 3.2.

Preservation of collagen macromolecular structure. Thermal analysis showed that the denaturation temperature of lyophilized collagen was lower than uncrosslinked and crosslinked collagen mats, 46.0 ± 0.5°C, 52.9 ± 0.4°C and 73.2 ± 2.1°C, respectively, Table 3.1. Lyophilized collagen consisted of monomeric collagen prior to higher order assembly, thus exhibiting a lower T_D than collagen mats, which were treated with phosphate buffer. Further the ion concentrations, pH and heating rate (in addition to buffer type) contribute to collagen monomer organization into larger fibrils. Additionally, changes in ultrastructure conferred during phosphate buffer treatment and densification of the matrix during lamella fabrication contribute to a higher T_D for collagen mats. Lyophilized collagen and collagen lamellae exhibited similar H_D. Crosslinking of matrices results in a greater stabilization of the collagen structure and consequently raises the T_D, but lowers H_D. There was no significant difference in the thermal transitions or

enthalpy between collagen lamellae with and without ablation, Figure 3.4 and Table 3.1, suggesting no measurable loss in triple helical structure.

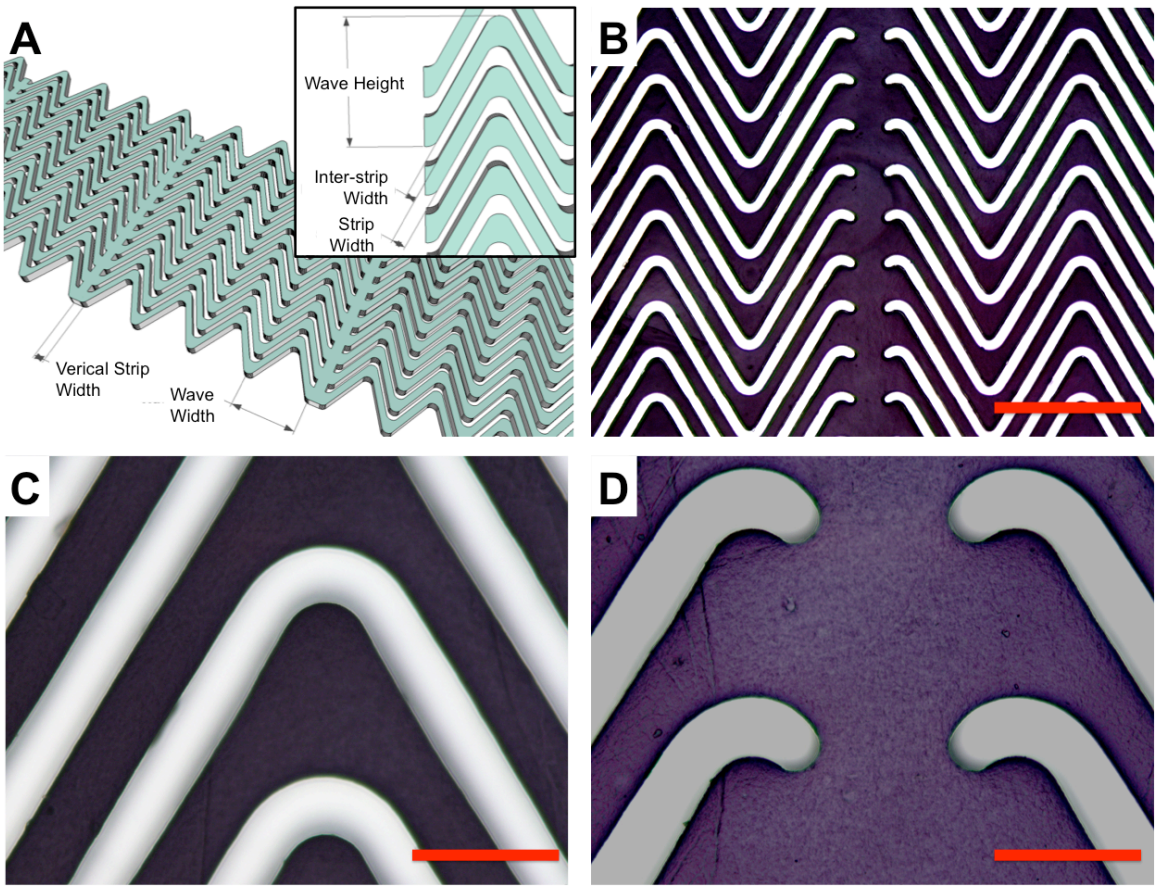

Figure 3.3: Ablation schemes of collagen matrices. (A) Schematic of collagen lamella ablated using an excimer laser to create a defined "wavy" collagen lamella with linear supports, inset shows additional nomenclature. (B) Uniformity and transfer of wavy ablated pattern with high fidelity onto collagen mats, scale bar 500 μm. (C-D) Ablated collagen lamella displayed clear excimer laser cuts with no apparent material damage, scale bar 100 μm.

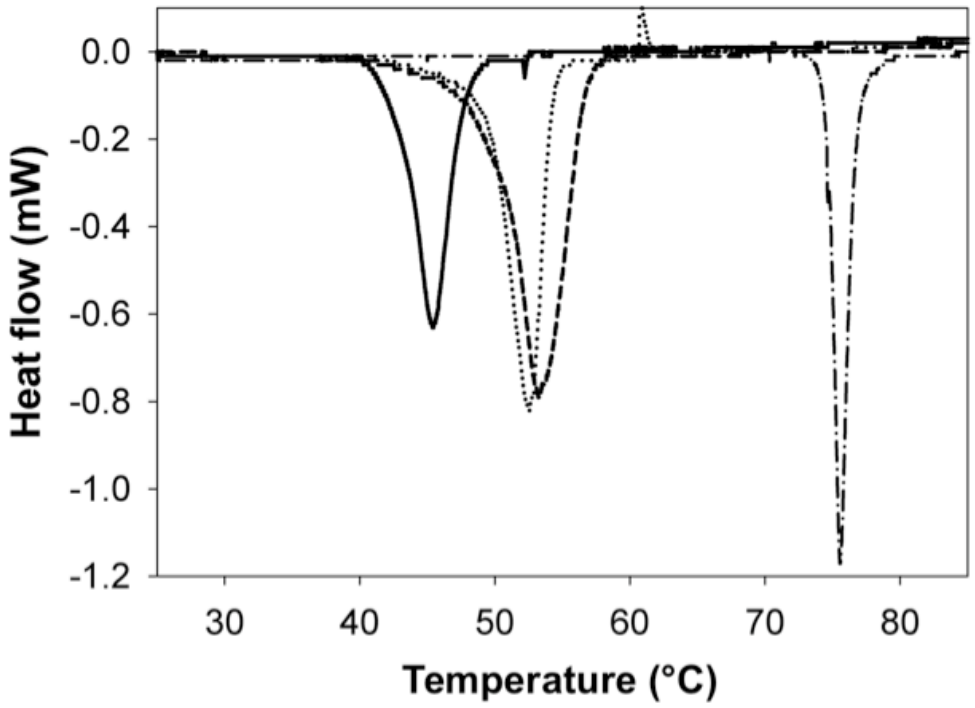

Figure 3.4: Endothermic heat transitions of collagen matrices. Microdifferential scanning calorimetry of lyophilized collagen (solid), collagen lamella (dotted), excimer ablated collagen film (dash), genipin crosslinked collagen lamella (dash-dot). (n=3)

Table 3.1: Thermal properties of collagen matrices

	Monomeric collagen*	Collagen lyophilized	Collagen mat	Excimer-treated collagen lamella	Genipin crosslinked collagen mat
T_D (°C)	36.2 ± 0.6	46.0 ± 0.521	52.9 ±0.396	53.1±0.203	73.2±2.11
ΔH (J/g)	49.4 ± 0.8	47.8 ± 4.77	44.0±3.21	48.2±1.32	27.3±1.89

Monomeric rat tail tendon collagen (MRTC), lyophilized collagen (Col. lyophilized), collagen lamella (Col. mat), collagen lamella excimer ablated (Col. lamella excimer), collagen lamella crosslinked in 6 mg/mL genipin, 37°C, 24 h (Col. lamella X-link). *[185]

Design of mechanically variant structures for optimized mechanical compliance. Pilot designs ablated into collagen lamellae to show proof of principle and to benchmark ablation techniques involved ablation of holes 10-100 μm in diameter, direct write of lines and waves, and variations of the designs listed in Table 3.2. However, it was realized that the strip width to height (film thickness) ratio needs to be approximately < 1 to ensure features are stable and do not laterally collapse during subsequent processing. Further, it was determined that thick wave strips (> 180 μm) resulted in out of plane bending of wave features, data not shown. Consequently, the subset of designs that resulted in improvements of mechanical properties is shown, Table 3.1. Linear ablation patterns were also generated to determine the altered mechanical response as a function of excimer laser ablation pattern. Wave patterns with varied vertical strip thickness 60-600 μm and interstrip thickness with variation from 10-30 μm demonstrate the modulation of mechanical strength and suture retention strength as detailed below.

Table 3.2: Design variations for ablated collagen mats.

Design	Wave strip length (μm)	Wave strip width (μm)	Interstrip width (μm)	Angle of wave crest (˚)	Strip aspect ratio (Height : Width)	Vertical Strip thickness (μm)
1	2000	120	10	0	0.5	100
2	500	60	30	60	1	60
3	500	60	10	60	1	100
4	500	60	10	60	1	300
5	500	60	10	60	1	600

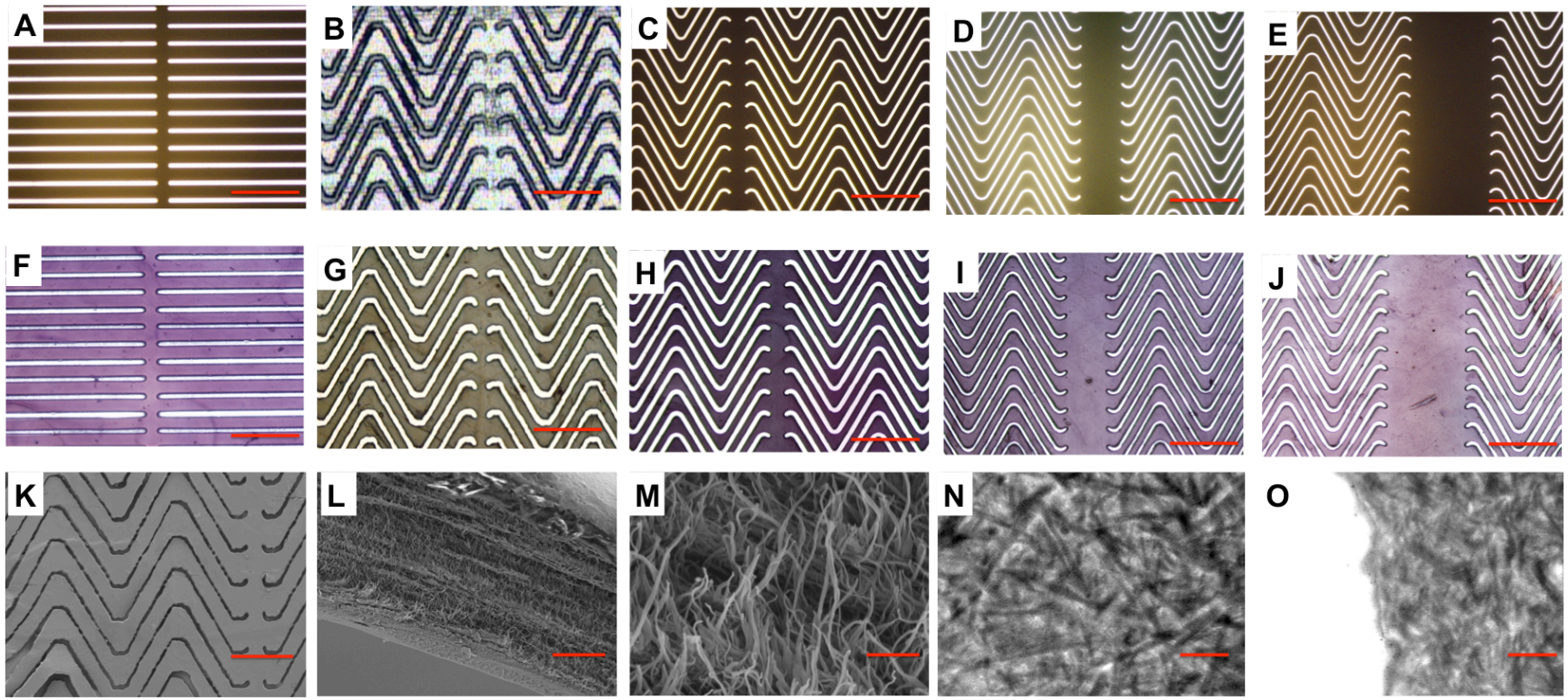

Figure 3.5: Meso- and ultra-structure of collagen matrices of varying vertical strip width. (A-E) Optical micrographs of stainless steel (B) and aluminum-on-quartz masks (A, C, D, E) for Designs 1-5 (A-E), respectively, scale bar 500 μm. (F-J) Optical micrographs of genipin crosslinked collagen lamellae for Designs 1-5, respectively, scale bar 500 μm. SEM of wavy collagen matrices (K) 200 X, wave edge (L) 5 kX, and magnified view of fibrillar structure (M) 50 kX, scale bars 300 μm, 10 μm, 1 μm respectively. TEM images of wavy collagen mats, (N) 10 kX bulk and (O) 10 kX wave edge, scale bar 1μm.

Collagen lamella ablation closely mimics mask features with no protein denaturation. Metal masks (stainless steel shim stock, 50 μm), Figure 3.5 B, or aluminum coated quartz, Figures 3.5 A, C-E, allow laser transmission through 10-30 μm gaps, showing high ablation fidelity, allowing patterns on the centimeter scale to be completely ablated over a period of less than 1 h, Table 3.2 and Figures A-E and F-J. Collagen wave ablation shows high precision and uniformity under SEM, Figure 3.5 K, which is composed of a nanofibrous (80μm) fibrillar matrix, Figure 3.5 L & M. To demonstrate regeneration and reconstitution of native collagen structure, in addition to the differential scanning calorimetry described above, native collagen banding structure is noted in the matrix bulk, Figure 3.5 N, and edge of waves, Figure 3.5 O.

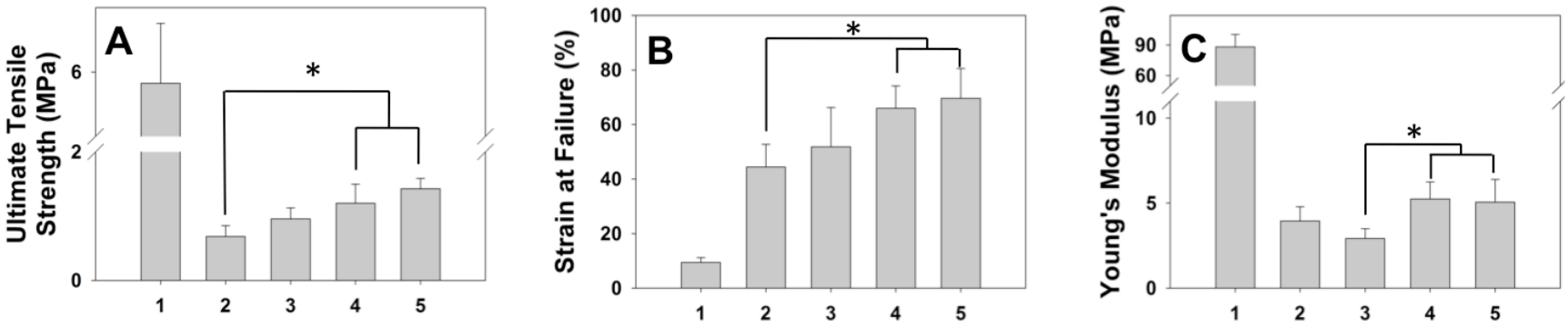

Figure 3.6: Mechanical strength of ablated collagen mats, Designs 1-5. (A) Ultimate tensile strength of ablated crosslinked collagen mats. (B) Strain at failure of ablated collagen mats. (C) Young's modulus of ablated collagen samples.

Mechanical properties of ablated composites. The utility of excimer laser ablation to modulate stiffness and extensibility is shown, Figure 3.6. Linear ablation patterns result in a slightly greater than 50% reduction in tensile strength from unablated matrices, 5.82 ± 0.93 MPa vs 13.3 ± 2.19 MPa, Figure 3.2 C vs Figure 3.6 A. In the triangular wave designs, increasing vertical strip width enhanced ultimate tensile strength. With other features constant, vertical strip width ranging from 100 μm, 300 μm and 600 μm (designs 3-5), had UTS of 0.958 ± 0.172 MPa, 1.20 ± 0.296 MPa, 1.43 ± 0.162 MPa, respectively. This trend is maintained with collagen waves in Design 2 which had a significantly lower UTS of 0.683 ± 0.168 MPa, a thinner vertical strip thickness, 60 μm, and waves spaced further apart, 30 μm. Triangular patterning tended to increase strain at failure, from 9.43 ± 1.76 % for linear ablation patterns (Design 1) to 44.5 ± 8.27 %, 51.8 ± 14.4 %, 65.9 ± 8.19%, and 69.6 ± 10.9 % for Designs 2-5, respectively. Further, there is a significant increase in the strain at failure for Designs 4 and 5 over Design 2. The Young's modulus of linear ablated constructs is significantly higher than that of triangular wave patterned collagen, 88.1 ± 12.9 MPa, compared to 3.95 ± 0.839 MPa, 2.92± 0.579 MPa, 5.24 ± 1.00 MPa, 5.06 ± 1.34 MPa for Designs 2-5, respectively. Suture retention strengths for 4 layer composites, stacked into 4 ply systems with ELP, showed a suture retention strength of 52.4 ± 9.18 gF. However, ablated constructs, which have less collagen, had suture retention strengths of 51.2 ± 7.43 gF, 37.7 ± 12.1 gF, 40.1 ± 5.88 gF, 36.36 ± 6.23 gF and 37.3 ± 5.48 gF for Designs 1-5 above, respectively.

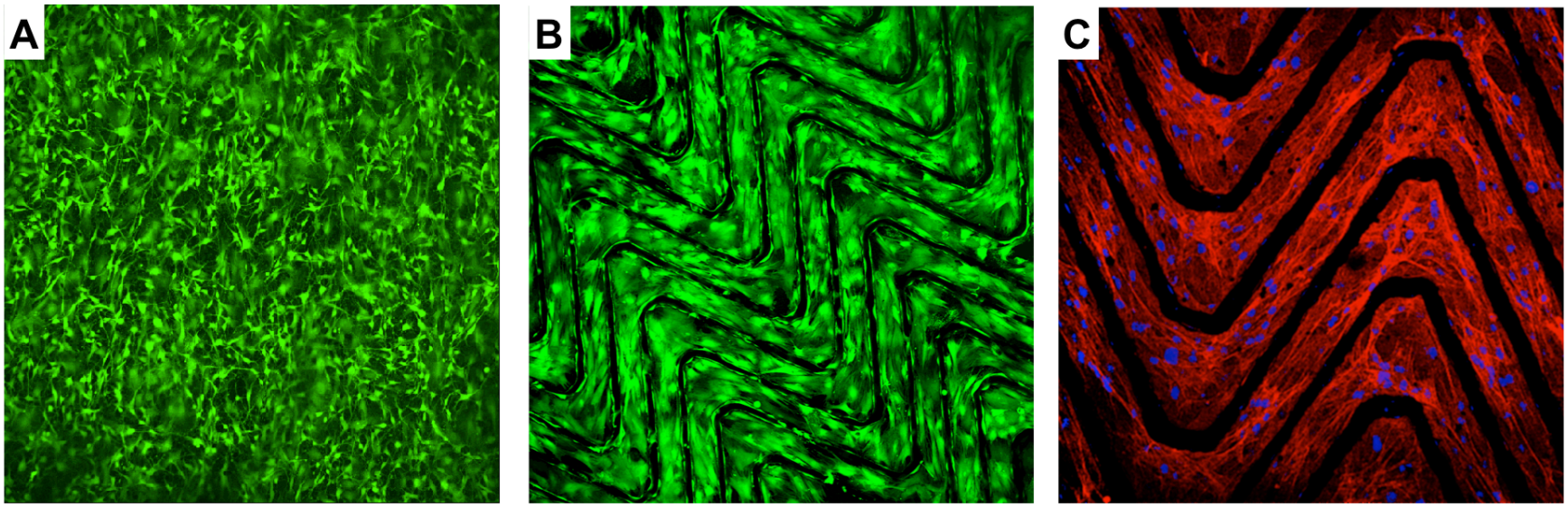

Figure 3.7: Cellularization of unablated and ablated scaffolds. (A)Unablated scaffold seeded with rMSCs at 100,000 cells/cm^2, for 24 h Live (green)/Dead(red) stained. (B) Ablated scaffold seeded with rMSCs at 100,000 cells/cm^2, for 24 h (Design 2). (C) Actin cytoskeletal staining and DAPI nuclei staining showing cells conforming to ablated scaffolds.

Structural features dictate cellular adhesion. Adhesion and spreading of rMSCs on microablated collagen matrices was observed within 4 h and proliferation in 24 h, Figure 3.7 A, at low seeding densities, 100,000 cells/cm^2. Further through the use of microfabrication techniques, we have established a novel method to enhance adhesion and conforming of cells discretely to microablated matrices, as seen in Live/Dead staining and staining of cytoskeletal actin filaments, Figure 3.7 B & C.

3.4 Discussion

Use of purified collagen and recombinantly expressed elastin to mimic the extracellular matrix. The extracellular matrix is composed of several components that provide strength (collagen, mineral phosphates), structural support and anisotropy (collagen, elastin and proteoglycans), and cell adhesion (collagen, glycoproteins, fibronectin, laminin). Recapitulation of the nanofibrous ECM milieu has been attempted using a variety of technologies – electrospinning,[243; 244] nanofibrous scaffolds[245] and use of biological (naturally derived/ reconstituted) matrices [246]. However several drawbacks limit the use of synthetic materials – immuno-rejection, degradation products, denaturation of electrospun protein based polymers, and lack of tunability of mechanical properties to match that of native tissue. The choice of collagen as a biomaterial is supported by the fact that it naturally forms a fibrillar nanofibrous structure, is naturally capable of cell adhesion, has high species homology, and is FDA approved for several collagen based products. However to date one of the primary limitations of collagen based tissue engineering is the inability to modulate the mechanics, strength, and suturability of relatively weak collagen scaffolds.

Noting the abundance and importance of collagen, we have developed a facile method for the production of cell adhesive matrices that can be generated with structural anisotropy while maintaining modulatable tissue-like strength. For applications in soft tissue engineering, the stiffness and compliance of matrices is of critical importance. Further, the ability to modulate these features allows for the generation of a class of novel

biopolymers that can architecturally and physiologically replicate native tissue. Collagen matrices currently used in tissue engineering have primarily been in hydrogel form which are often weak and lack clinical utility in mechanically demanding applications. Further, hydrogels have the potential to collapse by elimination of water, shrink by degradation or cell-matrix interactions, and fail due to repeated mechanical conditioning. To obviate these limitations, we have developed and characterized a novel fabrication strategy that harnesses the cell adhesive properties of collagen matrices, coupled with drying techniques that enhance the structural strength and novel laser ablation technology to generate structural anisotropy.

Collagen matrices neutralized from acid solutions of collagen created gels. Fibrillogenesis was enhanced through the use of fibril incubation buffer. Resultant gels were dried to less than 1% of their initial thickness. With the ability to create gels of any size, we have fabricated large-scale constructs that can be used for tissue engineering. To further enhance mechanical strength, we have developed a novel layering technique that structurally reinforces collagen matrices, resulting in a non-linear increase in strength and stiffness of matrices.

While collagen has excellent cell adhesive properties, for applications that involve contact with blood, collagen is known to be highly thrombogenic. As such, we have developed a sandwich molding technique to infuse recombinantly expressed elastin into collagen matrices. Triblock co-polymer elastin analogs, generated and characterized by our group and others, have shown the ability to undergo an inverse temperature phase

transition in aqueous solutions. Of specific mention is Lys-B10, the elastin analogue used in this study. The hydrophobic (Ile-Pro-Ala-Val-Gly) block, flank a central hydrophilic midblock (Val-Pro-Gly-Glu-Gly) that aids in co-ordination of water molecules in aqueous solutions. However, above the lower critical solution temperature, the hydrophobic endblocks co-accervate, yielding a hydrogel. We have shown the ability to not only modulate the mechanical behavior of recombinant elastin, but also introduce crosslinkable moieties into the elastin structure to promote intra/inter molecular crosslinking as well as crosslinking to other protein based materials or compatible substrates through the aid of labile lysine residues [238; 239]. Further, given the inverse transition temperature, we have been able to utilize elastin as a "glue" to adhere layers of collagen-elastin composites together. This further results in multi-ply composites, formed from single layer or multi-layer collagen lamellae infused with elastin. Consequently we created a series of thick composites that can be used for soft tissue repair and replacement and has potential utility in blood contacting applications.

Tunable ECM mimetics with enhanced mechanical properties. Depending on the application, tissue replacements require the ability to modulate material mechanical properties. The present study noted the effect of a variety of processing techniques (initial gel concentration, layering of collagen lamellae and initial collagen gel thickness) on 4 important mechanical properties – ultimate tensile strength, strain at failure, Young's Modulus (stiffness) and thickness of matrices. As expected, increasing collagen concentration resulted in increased strength and stiffness for gels cast at the same thickness (4 mm). This is a direct result of greater amounts of protein present in mats.

Further, lower concentration lamellae potentially have micro-inhomogenieties or flaws which are masked when absolute protein amount increases, which, however, did not have an effect on strain to failure. Increasing the number of layers of collagen resulted in an increase in the strength (UTS) of collagen matrices. This is a surprising discovery as UTS is the force normalized to the cross-sectional area. As such, the strength and stiffness is expected to remain constant. However, interestingly, there appears to be structural reinforcement of collagen matrices when they are layered. We hypothesize that there is integration of the layers with each other, which potentially results in buttressing of fibrillar microstructure. We observed that during mechanical testing, that failure of matrices occurred through transverse fracture in the direction perpendicular to axial stretch, without delamination of collagen layers. Additionally, layered structures were thinner than multiple single layers, further suggesting collagen fibrils between layers were integrating between mats, and potentially generating a compressed randomly interwoven structure. While there was an increase in strength, stiffness and strain to failure with layering of collagen mats, increased layering did not result in significant increases in the aforementioned mechanical properties. The final variable altered to modulate mechanical properties of collagen lamellae was initial gel thickness. Initial collagen gel thickness variation resulted in an increasing amount of strength of matrices. Again, although normalized by thickness, the expected strength and stiffness should remain the same. However, we observed that higher initial gel thicknesses resulted in stronger gels, that dried to stronger mats. We further showed that thicker gels have greater packing and compaction, exhibiting a non-linear increase in thickness with increased initial collagen gel thickness. Gels that are thicker, still, could potentially result

in stronger matrices. 8mm and thicker gels were not as stable and tended to shear parallel to the plane of casting when removed from the mold. We have developed a novel collagen based material with megapascal level strengths and stiffnesses in the 10's to 100's of megapascals. Thus, we have shown the ability to modulate mechanical strength as a function of initial gel concentration, layer of collagen mats, and initial collagen gel thickness; showing nonlinear improvement in strength, stiffness and strain at failure.

Optimization of a novel protein-based laser ablation strategy and preservation of native protein structure. Ultraviolet lasers have been used in a variety of applications in medicine: psoriasis treatment [247], ophthalmologic applications [248], arthroscopy [249], laser-assisted vascular plaque ablation [250], and development of tissue engineering scaffolds [251; 252; 253; 254; 255]. Perhaps one of the most renowned examples of excimer laser ablation is in laser-assisted in situ keratomileusis (LASIK) eye surgery. The primary advantage of excimer laser use is that ablation of tissue/ materials takes place with minimal damage to the surroundings. Unlike thermal ablation, which is the basis for CO_2 laser ablation, the benefit of excimer laser ablation is that it excites the molecular bonds sufficiently to dissociate them, ablate them, without thermal decomposition to elemental compounds. Further, the dissociated molecular products are cleared by an airstream which leaves a "clean" and non-denatured substrata that maintains native phenotype. Although non-thermal in nature, excimer laser ablation and other UV based optical ablation schemes generate small amounts of localized heat when maintained on a particular locus. Specific to tissue engineering, Nakayama and Matsuda used an excimer laser to improve compliance of polyurethane tubes by microablation of

holes of a variety of sizes improving compliance [255]. Engelmayr and colleagues used a similar approach to ablate adjacent (non-tangential, overlapping) holes in a polyglycerol sebacate scaffold. The resulting scaffold had a accordion-like honeycomb architecture with enhanced compliance and appreciable cellular alignment [253]. Further, Chollet et al report the use of excimer laser ablation to modulate cellular alignment. Specifically they report that 25 μm to 100 μm width RGD patterned substrates (separated by laser ablation) result in cellular alignment [252]. Of note is the fact that thermal energy build up is inevitable when a substrate is irradiated. As such, for our studies it was first crucial to determine the optimal conditions that result in collagen ablation without denaturation. Parameters such as fluence (spatial laser energy density) and rastering of the substrate, with multiple passes over the same region ensured collagen matrices were ablated with minimal thermal denaturation as demonstrated by ultrastructural analysis and differential scanning calirometry. Conventional laser ablation can be achieved in two primary modes – direct-write or rastering (over a mask). The former is typically more time intensive and involves "writing" a pattern of individual features on the substrate. The latter, however, involves moving a relatively larger laser spot across the substrate. When coupled with a mask that is laser opaque, features, as determined by the mask, are ablated. Although the theoretical resolution of excimer laser ablation is the wavelength of the beam (in our studies, 248nm), the practical resolution is typically 1 order of magnitude higher – 2-10 μm. We have thus generated metal and aluminum-on-quartz masks that attenuate UV light, but allow transmission in 10 μm or greater gaps (features). Consequently, we have been able to rapidly fabricate detailed patterns on protein based matrices with high fidelity as demonstrated in Figure 3.3. To establish the efficacy of excimer laser ablation

of collagen matrices, collagen gels at 2.5 mg/mL initial concentration, 4 mm initial thickness and layered 4 times, were constructed, and excimer ablated. Thermal denaturation was determined by analyzing thermal transitions of collagen, which showed no measurable denaturation, and analyzing collagen ultrastructure – noting the retention of bulk and ablation edge native D-periodicity, 67nm banding patterns, and fibrillar structure. These results are similar to those reported in clinical practice with excimer laser ablation strategies yielding small (0.1 - 0.3 μm) regions of damage [256].

Generation of mechanically compliant protein substrates through laser ablation. Tissue engineered substrates need to mechanically match native tissue. For adequate tissue integration, it is critical that tissue mimetic substrates and scaffolds exhibit matching deformation characteristics to native tissue, to ensure there aren't undue stresses on suture sites and to ensure the host tissue integrates favorably with grafts. One of the prime examples of this is compliance mismatch in synthetic vascular grafts and tissue engineered blood vessels. Several groups have reported the potential for early graft failure to occur at anastamotic sites due to mechanical mismatch [43; 257; 258]. We have shown the ability to generate a series of mechanically tunable collagen based constructs that have strengths and stiffnesses that exceed several soft tissues. To modulate the stiffness and compliance of these mechanically resilient and tissue mimetic substrates, we have designed and optimized a laser ablation scheme that does not adversely effect the native structure of collagen matrices – with retention of thermal properties and native ultrastructure. These ablated substrates were embedded in recombinantly expressed elastin and mechanically tested. The chosen ablation scheme, a triangular waveform

pattern with vertical strips resulted in highly compliant structures, wherein structures with approximating unity aspect ratios showed collagen strips extending and straightening prior to failure. We hypothesize that increased vertical strip thickness helps buttress collagen strips, keeping them anchored to the composite structure, aiding in in-plane extension. Conversely, thinner vertical strips could allow for twisting and out-of-plane bending of collagen waves which would consequently have a lower strain at failure, Design 2. As a consequence of large amounts of material removal, there was a decrease in ultimate tensile strength. However, tissue engineered microablated composites exhibited mechanical properties that mimic several tissues. The mechanical properties of unablated and microablated composites can be tuned comparing favorably to native tissue, ex. cartilage [259], ligament [259; 260], coronary artery [260], and carotid artery (1.76-2.64 MPa UTS),[261] Table 3.3. We have developed a novel method to ablate micro-features for the further modulation of collagen as well as collagen elastin substrates to mimic the mechanical response of native tissue. We next determined the ability for collagen based matrices to be cellularized, and the potential for alignment on ablated matrices.

Table 3.3: Mechanical properties of unablated and ablated collagen matrices

	Ultimate Tensile Strength (MPa)	Strain at Failure (%)	Young's Modulus (MPa)
Unablated matrices	13.3 ± 2.19	18.0 ± 3.73	93.7 ± 19.8
Ablated matrices	0.683 - 5.82	9.43 - 69.6	2.91 - 88.1
Arteries[#,$]	1.4-11.1	N.A	1.54 ± 0.33
Veins[$]	N.A	N.A	3.11 ± 0.65
Cartilage[∂]	3.7 - 10.5	N.A	0.7 - 15.3
Ligament[∂]	24 - 112	N.A	65 - 541

#: [260]

$: [261]

∂: [259]

Cell supportive matrices with conforming cell adhesion. Several studies have noted the importance of cells in recapitulation of native tissue structure and function. For example, SMC in the vascular media act to both maintain contractility during pulsatile blood flow, as well as vasoconstrict as a function of neuronal or chemokine action. Further, cells in the myocardium and several other muscle tissue align in the direction of physiologic stress to aid in bio-mechanical function and contractility. For tissue-engineered constructs, development of a cellular niche that complements cell adhesion, alignment and proliferation is quintessential to promotion of engrafted material healing and integration. The ability to align cells *in vitro* however has been attempted using a myriad of techniques. Notably, Zorlatuna et al have demonstrated that various nanopatterns on collagen membranes enhance vascular smooth muscle alignment as a function of channel dimension and length of cell interaction, needing up to 21 days for alignment [113]. A potential disadvantage of this technique is that micron level inhomogenieties in substrates, that result from large scale fabrication of constructs, may cause cells not to "see" the nanoscale features presented on surfaces. Engelmayr et al have demonstrated that cells seeded in micron sized pores created in polyglycerol sebacate result in localized cardiomyocyte alignment [253]. In contrast to their approach which uses geometric confinement to conform cells to specific material patterns, we propose a excimer–laser assisted ablation scheme that can potentially create ordered micro-ribbons that are intrinsically cell adhesive. Through the use of microfabrication technology and excimer laser ablation, we have developed cell adhesive substrates with precise micron-level patterns that ultimately demonstrate a facile method for the adhesion and conforming of cells as confluent cell layers on collagen matrices and are produced in

a matter of hours. Further, actin staining reveals that cellular cytoskeletal filament is indicative of the potential for cells to conform to the waveform pattern with potential anisotropic distribution. Further, cells appear to conform to the waveform pattern, allowing for rapid generation of large-scale cellularized tissue engineered substrates with structural, mechanical and rapid cellular adhesivity. Further studies could potentially enhance cellular adhesion and enhance preferential alignment of cells in the direction of collagen waves – providing a means to further tailor cellular anisotropy. We have generated a highly scalable and strong collagen that is cell adhesive, results in cellular conformation to scaffolds and provides significant mechanical strength similar to native tissue. Further, there is no additional need for cell binding additives, such as fibronectin/ vitronectin/ RGD, nano-/micro-patterning or buttressing of mechanical structure with nanoparticles/ non-biological polymers.

3.5 Conclusion:

Engineering of substrates for tissue repair and replacement have made several leaps over the past 20 years. Although a relatively old technology, the use of collagen-based technologies for tissue engineering is still a highly active area of research. The benefits of collagen are numerous, including its high species homology, ease of availability, intrinsic cell adhesiveness, strength, FDA approval, and ability for large scale fabrication and processing into constructs that are relevant for tissue engineering (as we have shown). This is the first report of a systematic study of the modulation of initial collagen gel concentration, gel thickness and layering of collagen lamellae to yield entirely collagen based materials suitable for tissue engineering. Further, we have shown an unexpected non-linear increase in strength and stiffness of matrices, due to buttressing and integration of multi-layer collagen constructs. Additionally, this is the first report of the use of excimer laser technology use for the ablation of biologically derived protein based matrices suitable for tissue engineering. Through the use of excimer laser technology, we have determined optimal parameters for the ablation of collagen matrices with high fidelity and preservation of native structure- determined using differential scanning calirometery and transmission electron microscopy. Further, with the addition of recombinantly expressed elastin mimetic peptides, nanofibrous composite extracellular mimetics have been created. Mechanical testing of ablated matrices show the ability to further modulate mechanical properties and improve compliance, stiffness and strength to better mimic a host of soft tissue. The critical dimensions we have chosen for ablation patterns, based on our and other's work, result in the coordinated adhesion of rMSCs.

CHAPTER 4

Design of Tissue-Mimetic Arterial Grafts

4.1 Introduction

The design of a tissue engineered vascular graft to supplant diseased arteries requires consideration of mechanical, biological and clinical factors that influence behavior *in vitro* and *in vivo* [31; 262; 263]. To date, tissue engineered products have yet to replace the current "gold standard" of an autologous artery or vein. Much progress has been made in determining the key factors that contribute to the eventual success of a vessel graft. Mechanical requirements include (i) sufficient burst pressure to prevent catastrophic failure of the vessel and long-term fatigue resistance, (ii) compliance that approximates that of native vessels to prevent mechanical mismatch, and (iii) suitable suture retention strength to permit implantation and tolerate hydrodynamic and mechanical forces at the anastomoses. Biological and clinical considerations include (i) generation of a non-fouling luminal surface to prevent thrombosis, (ii) mediation of the immune response due to surgical trauma and potential graft rejection and regeneration, and (iii) evaluation *in vivo* [3; 262].

Several groups have demonstrated the efficacies of various strategies that range from modifications of existing ePTFE/Dacron™ grafts to acellular / cellularized constructs to de novo engineering of tissue substitutes that mimic native vessels [264]. Tissue engineered blood vessels (TEBV) derived from cell-sheet tissue engineering and degradable synthetic polymer scaffolding has demonstrated early clinical success. Continued progress with several additional systems, suggest that these technologies will

continue to evolve [31; 45; 265]. Clinical success will be determined utilizing a "bottom-up" approach where recapitulation of the fundamental features of the vascular wall, incorporation of key elements that obviate thrombosis and acute graft failure, and potentially the addition of a cellular component to ameliorate the unavoidable inflammatory response towards healing [86; 266; 267]. The strategy we have developed does not rely on the time consuming process of seeded cells to produce ECM, or approaches that utilize biodegradable scaffolds and lengthy bioreactor conditioning [9; 73; 268]. It is postulated that this scheme will lead to shortened fabrication time, enhanced tissue integrity, and improved biological responses after *in vivo* implantation.

Our lab and others have recently synthesized and characterized a series of elastin-like protein polymers that consist of sequentially repeated amino acid blocks [269; 270; 271; 272]. With the ability to easily modify these protein polymers: modify peptide chain length, consensus repeat sequence, and introduction of additional oligopeptide units, protein polymers can be produced with enhanced biological, thermodynamic, and mechanical properties. We have designed a series of elastin-like polypeptides that can be fabricated as films or other geometrical constructs, have robust mechanical properties, a high degree of resilience, minimal thrombogenicity, and long-term stability *in vivo* [273; 274; 275; 276; 277; 278; 279; 280; 281].

Collagen, a vital component of the ECM milieu, is required for mechanical and biological support. Electrospinning, casting gels, and wet spinning have been the mainstay for large-scale production of collagen matrices for tissue engineering. Although much progress has been made in the field of electrospinning, the use of organic solvents leads to collagen denaturation [282]. Likewise, the lack of mechanical integrity of

collagen hydrogels precludes their use as a structural component. We have described a novel strategy incorporating collagen gels, dried to collagen lamellae to improve mechanical strength. Further, in developing collagen lamellae it was hypothesized that the inclusion of elastomeric protein components in collagen gels, forming interpenetrating networks, would yield modifiable mechanical and tissue-mimetic analogs for bioengineered vascular tissue fabrication. Consequently, composite structures were fabricated from recombinant elastin mimetics and collagen analogs with defined composition and microarchitecture, including collagen fiber orientation and packing density, without deleterious effects on the preservation of native collagen structure.

The incorporation of bone marrow mesenchymal stem cells (BM-MSCs) within tissue engineered and biodegradable scaffolds has been widely reported. Specific to vascular grafts, bone marrow derived mesenchymal stem cells have been shown to differentiate into endothelial progenitor like-cells [91; 92; 93; 94; 283] and other vascular wall cellular constituents, including fibroblasts [284] and smooth muscle cells [284; 285]. MSCs have also been shown to attenuate the inflammatory and immune responses associated with surgical trauma and implants. MSCs have the ability to direct macrophage polarization toward an M2 phenotype (healing/ resolution) over an M1 phenotype (inflammatory), decrease antigen presentation, and promote secretion of anti-inflammatory cytokines [97; 98; 101; 286; 287].

The work described details a novel approach that utilizes the aforementioned biopolymers in a combinatorial approach that yields protein based interpenetrating matrices with megapascal strengths and stiffness approximating native tissue. Mechanical characterization of non-crosslinked and crosslinked matrices show the potential to

modulate and tailor the mechanical strengths of these novel biologically derived polymers for a variety of vascular and other soft tissue engineering applications. Further, these novel materials show the potential for cellularization without the addition of dopants, and for blood contacting applications given their hemocompatibility and *in vivo* stability. This is the first report of the ultra-rapid fabrication of cellularized vascular grafts (synthesis within 4-24 h) compared to alternative techniques, which can take on the order of weeks to months.

4.2 Materials and Methods

Isolation and purification of monomeric Type I collagen. Monomeric Type I rat tail tendon collagen was obtained by acid extraction from Sprague-Dawley rats (Pel-Freez Biologicals, Rogers, AR) following a procedure adapted from Silver and Trelstad [202]. Briefly, rat tail tendons were extracted with the aid of autoclaved pliers and dissolved in 10 mM HCl for 4 h at 25°C to dissolve the proteinaceous components. Insoluble tissue and other contaminants were removed by centrifugation at 30,000g at 4˚C for 30 min with subsequent vacuum filtration through 20 μm, 0.45 μm and 0.2 μm filters. The sterile filtered collagen in HCl was precipitated from solution by adding NaCl to a final concentration of 0.7 M. The precipitated collagen was pelleted by centrifugation, redissolved in 10 mM HCl and dialyzed first against 20 mM phosphate buffer at room temperature, then at 4°C, second against 10 mM HCl at 4°C and finally against deionized water at 4°C. The collagen was then frozen and lyophilized until use.

Synthesis of a recombinant elastin-like protein polymer (ELP). Development and production of the ELP, LysB10, has been described elsewhere [239]. Briefly, a triblock amphiphilic copolymer was designed to contain hydrophobic endblocks and hydrophilic midblock. The 75kDa polypeptide comprised 33 repeats of the pentapeptide sequence $[IPAVG]_5$, and the 58 kDa midblock comprised 28 repeats of the sequence $[(VPGAG)_2VPGEG(VPGAG)_2]$. Flanking both the hydrophobic plastic endblocks and the hydrophilic elastic midblock were the crosslinkable amino acid sequences: [KAAK] which allow for amine-based crosslinking. Subsequent to expression in *E. coli,* protein

was extracted and purified using hot/cold centrifugation cycles and nucleic acid removal. Protein solutions were then dialyzed against water and lyophilized.

Production of dense collagen-elastin interpenetrating networks (CEMs). Monomeric rat tail tendon collagen and Lys-B10 were dissolved in 10 mM HCl, at concentrations ranging between 0.6125 mg/ml - 5.0 mg/ml and various collagen and elastin ratios. Mixtures were neutralized using a gelation buffer (4.14 mg/ml monobasic sodium phosphate, 12.1 mg/ml dibasic sodium phosphate, 6.86 mg/ml TES (N-tris (hydroxymethyl) methyl-2-aminoethane sulfonic acid sodium salt, 7.89 mg/ml sodium chloride, pH 8.0) at 4˚C and were poured immediately into rectangular molds (10 x 8 x 0.4 cm) for 24 h. Gels were subsequently placed in a fiber incubation buffer (7.89 mg/ml sodium chloride, 4.26 mg/ml dibasic sodium phosphate,10 mM Tris, pH 7.4) at 37°C for 48 h to promote collagen fibrillogenesis. Gels were then dried at room temperature under a steady air stream. Stacked CEM lamellae consisting of 2 to 4 layers were generated by serially drying additional gels on top of dried mats. Some specimens were crosslinked in genipin in 1X PBS at 37°C for 24 h.

Imaging of composite architecture. Optical microscopy, fluorescence microscopy, scanning electron microscopy (SEM), and transmission electron microscopy (TEM) were used to analyze the collagen structure pre and post embedment in elastin. For SEM studies, briefly, dry collagen lamellae were hydrated in water for 24 h and dehydrated in serial exchanges of ethanol-water mixtures from 30%-100%. The samples were then critical point dried (Auto Samdri 815 Series A, Tousimis, Rockville, MD), sputter coated

with 8 nm of gold (208HR Cressington, Watford, England) and imaged at an accelerating voltage of 10 keV using a field emission scanning electron microscope (Zeiss Supra 55 FE-SEM, Peabody, MA). To determine the ultrastructure and presence of D-periodicity in the fibrils, showing maintenance of native collagen structure, hydrated samples were prepared for TEM. Samples in PBS were washed in 0.1 M cacodylate buffer and fixed in glutaraldehyde. After washing in water, samples were partially dehydrated in ethanol and stained with uranyl acetate. Samples were then fully dehydrated in ethanol, embedded in resin and polymerized. Ultrathin (60 - 80 nm) samples were cut using a RMC MT-7000 ultramicrotome (Boeckeler, Tucson, AZ). Post-staining with uranyl acetate and lead citrate was followed by imaging using a JOEL JEM-1400 TEM (JOEL, Tokyo, Japan) at 90 kV.

Cellularization of CEM/ composite sheets with rat bone marrow derived mesenchymal stem cells (rMSCs). CEM lamellae were sterilized in 70% ethanol for 30 mins. Scaffolds were dried and washed multiple times in PBS and incubated in media prior to seeding with cells. rMSCs were cultured in T75 flasks (Corning LifeSciences, Corning, NY) for 3 - 5 days until near confluence. Cells were used between the 3rd and 5th passage. Cells were trypsinized and resuspended at concentrations of 50,000, 100,000, and 200,000 cells/cm^2 in full media. Cells were seeded on collagen constructs for 4 h, 12 h and 24 h. Live/Dead™ staining (Invitrogen, Carlsbad, CA) and subsequent confocal microscopy (Leica SP5XMP) was performed on constructs, to determine optimal seeding time for confluence of cells on scaffolds. A subset of small diameter grafts (0.9 mm ID) were seeded with MSCs and murine dermal microvascular endothelial cells by infusion in

the lumen or seeding of adventitia with cells. For cell coverage quantification, 10x magnification images at 2048 x 2048 pixel^2 resolution were obtained. A MATLAB script was written that decomposed red, green and blue layers from the images. Green images (live cells) were then thresholded based on script input and spatial coverage of cells per field determined.

Fabrication of acellular and cellularized collagen-elastin nanofibrous grafts. Lys-B10, dissolved in molecular grade water at 4˚C at a concentration of 100 mg/mL, was used to embed acellular or cellularized CEM matrices in a sandwich molding setup, Figure 4.1. The setup was warmed to 25˚C to allow the liquid elastin mimetic to gel. The CEM-elastin composites were then removed from the glass support and trimmed to appropriate dimensions for testing. Long sheets were rolled on 0.9 mm, 1.3 mm and 4 mm ID glass mandrels, kept at 4˚C for 5 min to allow the elastin to go into a liquid state, and warmed to 25˚C to gel the elastin into one contiguous layer.

Mechanical testing of planar composites. To simulate application in planar soft tissues, collagen sheets were cut into 20 mm x 5 mm strips and mounted onto a Dynamic Mechanical Thermal Analyzer V (DMTA V, Rheometric Scientific, Piscataway, NJ) with a gauge length of 10 mm, immersed in PBS at 37˚C. Samples were preconditioned 15 times to 66% of the average maximum failure strain of initial test samples, and then tested to failure at 5 mm/min. A total of 8 samples were tested for each group. Thickness of hydrated samples was measured using optical microscopy and then correlated to mechanical data to determine the ultimate tensile strength and strain at

failure. Young's modulus was determined by from the slope of the last 4% of the stress-strain curve, in addition to ultimate tensile strength (UTS), stain at failure and Young's modulus.

Mechanical testing of tubular constructs. Pressure diameter testing to determine compliance and burst pressure of constructs was performed similar to previous reports [183]. Briefly, tubular collagen-elastin composites were mounted vertically, via luer-lock connectors with a 5 g axial weight, in PBS at 37°C. Grafts were inflated at a rate of 10 mmHg/s, monitored using a pressure transducer (WIKA), and videographed for distention, using a CCD camera. An edge detection program was written in MATLAB to identify and quantify radial distension of grafts based on the outer diameter and correlated to pressure readings. Compliance was determined as the percent difference in outer diameter at systole and diastole, divided by the pressure difference and initial diameter. Grafts were assumed to be incompressible for the range of compliance measurements. The pressure at which the graft started to leak, burst pressure, was also determined, n = 4 for 4 mm grafts and n = 4 for 1.25 mm grafts. Suture retention strength of grafts was determined by cutting 4 mm x 4 mm square sections from planar sheets or longitudinal sections of the graft wall. A 4-0 FS-2 prolene suture (Ethicon) was thrown through the middle of the square segment and pulled in the longitudinal direction using a DMTA (Rheometric Scientific), n = 4 for each of 4 grafts. Wall thickness measurements were made on 3 representative cross-sections of each graft. Each graft section was photographed. Image analysis using Adobe Photoshop allowed for the measurement of inner diameter, outer diameter and wall thickness, n=3 for each of 4 grafts.

Implantation of grafts in rat aortic interposition model. All animal experiments were approved by the Institutional Animal Care and Use Committee (IACUC) at Beth Israel Deaconess Medical Center. Female Sprague-Dawley rats ~275-300g (Charles River Labs, Wilmington, MA) were anesthetized using isofluorane (2% for induction and 1% for maintenance), shaved, sterilely prepped, and placed on a heating lamella at 37˚C. A vertical midline abdominal incision was made to expose the infrarenal aorta. Rats received 100 U/kg of heparin prior to aorta clamping through the IVC. The proximal and distal aorta were clamped using microclamps and a segment measuring approximately 1 cm was resected and replaced with an acellular graft using eight to ten interrupted sutures (10-0 Prolene). The abdominal incision was closed with 3-0 Prolene for the fascia and muscular layers, and 4-0 Prolene subcuticular suture for the skin. Rat received clopidogrel 75mg/kg per day for the first 3 days post-op. Samples (n=8) were explanted at 7 days.

Histological analysis to evaluate graft performance. At experimental endpoints, 7 days, rats were anesthetized (2.5% isofluorane induction, 1.5% isofluorane maintenance) and the thoracic cavity was exposed. Whole body fixation was performed. Briefly, an 18 gauge needle was introduced into the left ventricle, and the animal was exsanguinated using 200mL of saline, and fixed using 200mL of 10% buffered formalin. Samples were processed for histology. Histology samples were paraffin embedded and sectioned at 5 μm thickness. Evaluation of remodeling of the ECM was determined using Masson's Trichrome.

Computed tomography angiography (CTA) to evaluate graft performance. CTA was performed for 3-dimensional reconstruction and evaluation of patency of the implanted grafts. For each terminal timepoint (1week) 4 rats were anesthetized (2.5% isofluorane induction, 1.5% isofluorane maintenance) sterilely prepped and a sternotomy performed to expose the thoracic cavity. To facilitate acquisition of images, whole body exsanguination and fixation were performed and a radiopaque agent (Omnipaque, GE Healthcare, Milwaukee, WI) administered. Vessels were then visualized using a NanoSPECT (Bioscan, Washington DC) and processed using InVivoScope (Bioscan, Washington DC).

Statistical Analysis. Means and S.D. were obtained for all measurements, image analyses and mechanical data. Comparisons will be made using the Student's *t* test for paired data, ANOVA for multiple comparisons, with Tukey post hoc analysis for parametric data. Nonparametric tests will be carried out using the Kruskal-Wallis ANOVA, with Dunn's post hoc analysis as indicated. Values of $P < 0.05$ were considered statistically significant.

4.3 Results

Rapid generation of acellular and cellularized vascular grafts. Acellular and cellularized vascular grafts, comprised of biologically derived collagen and biomimetic recombinantly expressed elastin have been rapidly produced. The overall schematic for the design, cellularization, and construction of the vascular grafts is outlined in Figure 4.1. A solution of collagen and recombinantly expressed elastin were gelled, seeded with cells as desired, embedded in recombinant elastin, and rolled into tubes. Following this process, protein-based tissue substitutes could be reliably fabricated within 60 min (acellular) and within 24 h (cellularized).

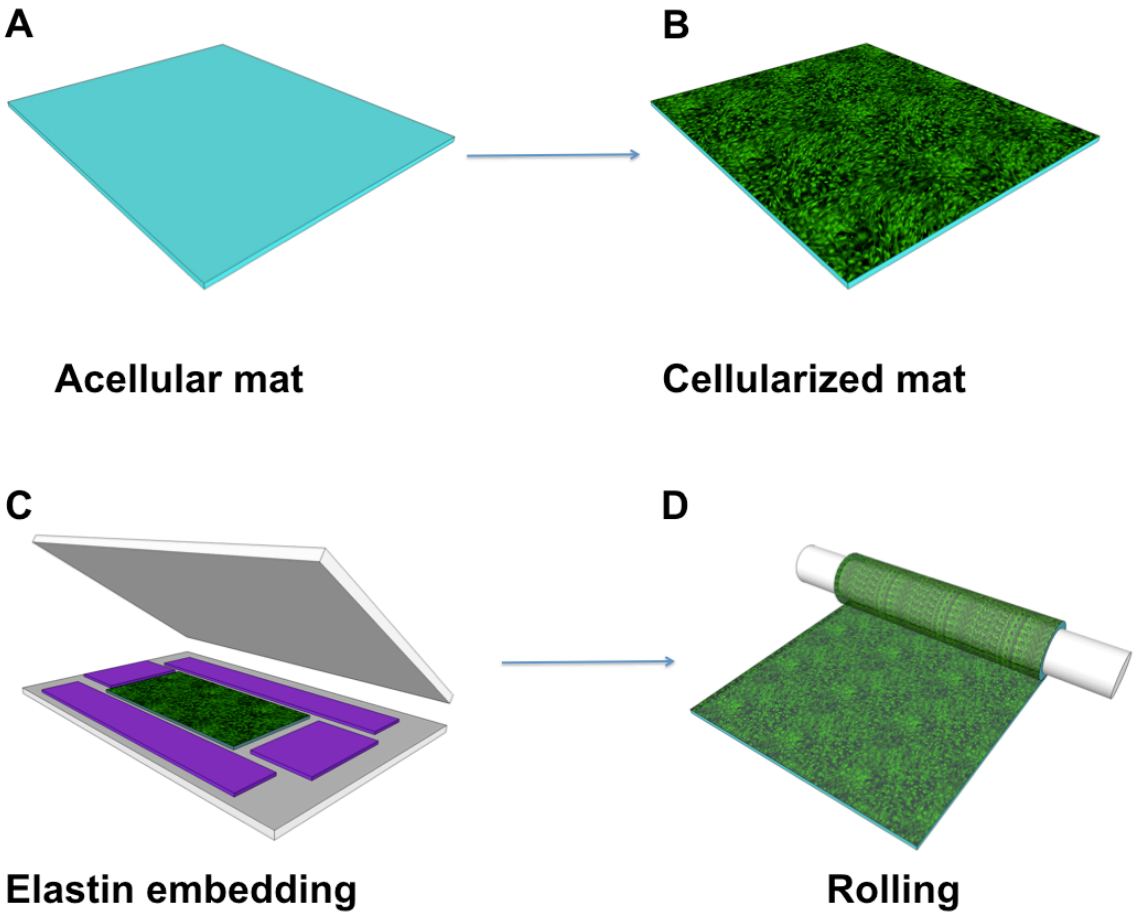

Figure 4.1. Schematic of fabrication scheme for acellular and cellularized grafts. (A) Collagen-elastin CEM lamellae are dried from collagen-elastin gels into defined thicknesses. (B) Lamellae can be cellularized with rMSCs at 100,000 cells/cm^2. (C) Acellular and cellularized lamellae are embedded in elastin at defined thicknesses dictated by plastic shims (purple). (D) Acellular and cellularized composite sheets are rolled on a mandrel to create vascular grafts.

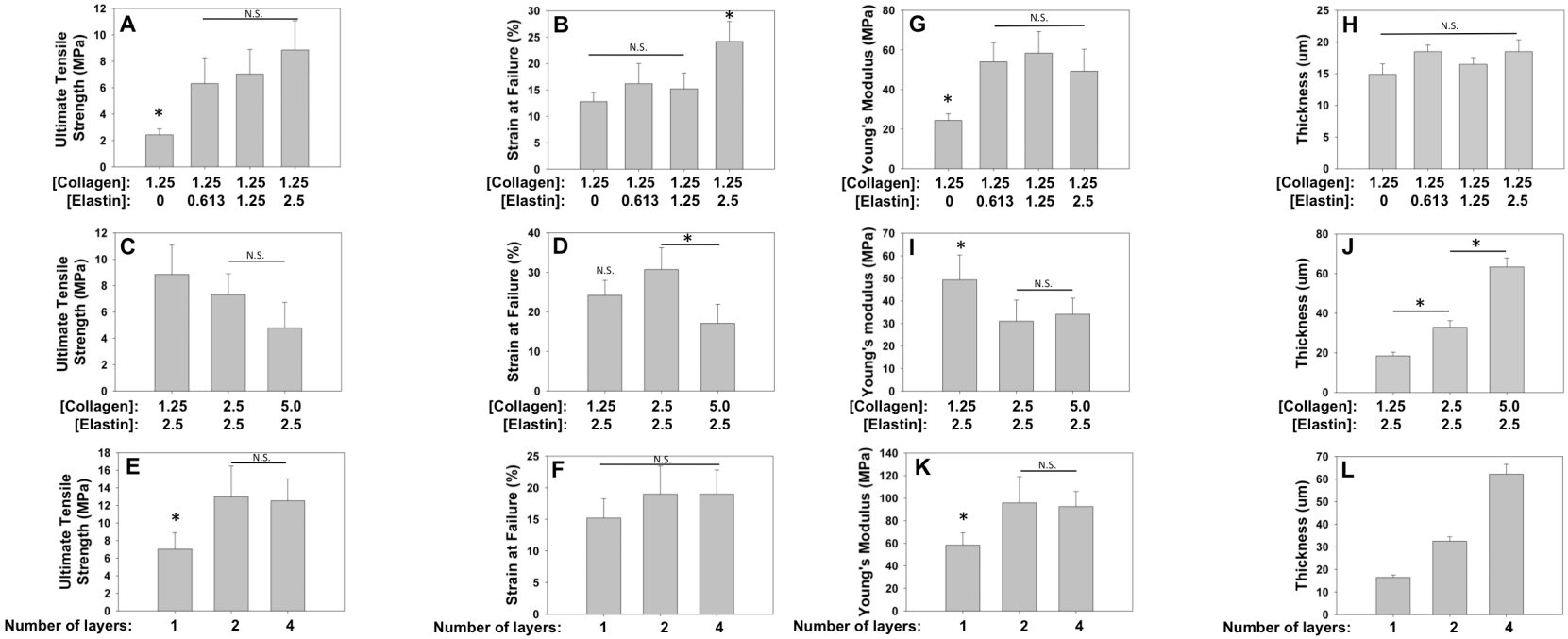

Figure 4.2: Mechanical properties of genipin crosslinked CEMs. Introducing elastin into collagen gels resulted in an improvement in strength and stiffness (A,B,G,H). Increasing collagen concentration while maintaining elastin concentration resulted in weaker matrices (C,D I,J). Increasing the number of layers of a 1.25 mg/ml collagen, 1.25 mg/ml elastin CEM shows an unexpected improvement in strength and stiffness, indicating interpenetration of matrices and reinforcement (E,F,K,L). (*$p<0.05$)

Generation of interpenetrating networks with tunable mechanics dependent on collagen/elastin mixing ratios and layering. Collagen-elastin composites exhibited strengths on the order of 10^6 - 10^7 pascals, comparing superiorly to traditional collagen hydrogels or elastin networks [288]. Higher initial elastin concentrations resulted in regional inhomogeneities during collagen gelation, and were, thus, not pursued. Elastin addition to collagen matrices during gelation resulted in a significant increase in strength and stiffness, Figure 4.2 A and G. Further, we noted that an elastin concentration of 2.5 mg/ml and collagen concentration of 1.25 mg/ml and 2.5 mg/ml showed significant increase in strain to failure, over lower collagen-elastin ratios and higher collagen concentrations, Figure 4.2 B and D. Increasing collagen concentration from 2.5 mg/ml to 5 mg/ml while maintaining elastin concentration at 2.5 mg/ml in initial gels, resulted in a decrease in UTS and a significant decrease in strain at failure, Figure 4.2 C and D.

Characterization of layered CEMs was performed on 1.25 mg/ml collagen and 1.25 mg/ml elastin matrices. Layered CEMs showed a significant increase in mechanical strength and stiffness from single layer matrices. UTS for single layer matrices (7.03 ± 1.86 MPa) rose significantly for 2 layer and 4 layer constructs (13.0 ± 3.49 MPa and 12.5 ± 2.49 MPa). Similarly Young's modulus rose from 1 layer to 2 and 4 layer constructs (58.4 ± 10.9 MPa, 95.7 ± 23.4 and 92.4 ± 13.5 MPa, respectively). This buttressing effect was limited to strength, and did not significantly decrease strain at failure (10 - 17 %) and stiffness (40 - 100 MPa), Figure 4.2 C, D & I. Thicknesses of matrices had a near linear relationship with initial collagen concentration, showing initial thicknesses of 14.9 ± 1.68

μm for 1.25 mg/ml collagen only and 115 ± 7.45 μm for 4 layered 1.25 mg/ml collagen, 2.5 mg/ml elastin matrices. We have thus created a series of tunable collagen-elastin CEM matrices with modulatable strengths (2.43 – 13.0 MPa), strains at failure (12.8 – 30.7%), stiffnesses (24.4 – 95.7 MPa) and thicknesses (14.9 - 115 μm).

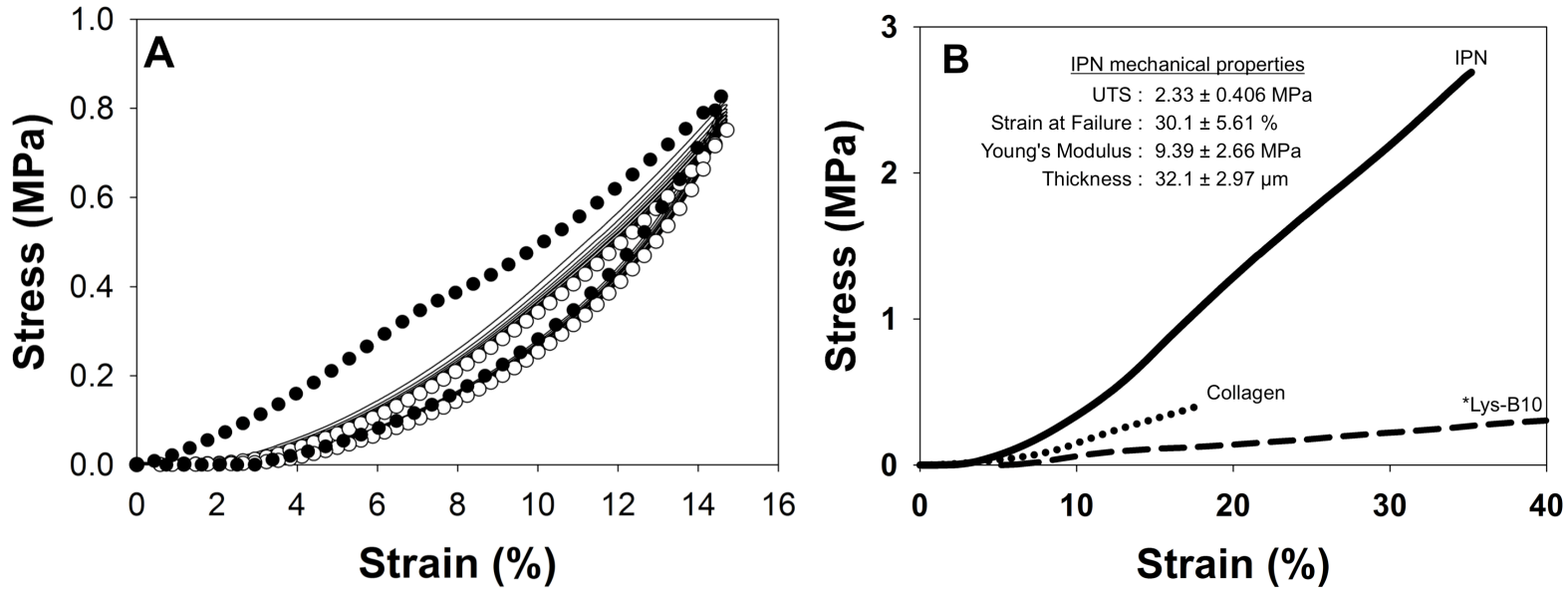

Figure 4.3. Representative stress-strain plots showing mechanical characterization of uncrosslinked 2.5 mg/ml collagen, 2.5 mg/ml elastin CEM. (A) Preconditioning curves of 2.5 mg/ml collagen - 2.5 mg/ml elastin CEM, ●: first cycle, ○: 15th cycle. (B) Characteristic mechanical response of CEM (—), LysB10 (**---**) and 2.5 mg/ml collagen only matrix (●●●), showing increase in stiffness and strain to failure with incorporation of elastin. *[239]

Development of composite biomaterials with soft tissue-matching properties.

Strong micron-thin crosslinked collagen-elastin CEMs result in the generation of mechanically tunable constructs, enabling mechanical matching of constructs to a variety of native tissue. However, given the UTS and stiffness of native vasculature (1.4 - 11.1 MPa and 1.54 ± 0.33 MPa, respectively) we developed a series of constructs that were better mechanically matched. Further, given the high extensibility of 2.5 mg/ml collagen-2.5 mg/ml elastin matrices (30.7 ± 5.54 %), this design was chosen for further study. Uncrosslinked CEMs of the aforementioned concentrations were constructed and mechanically tested. The addition of elastin during collagen gelation, increases matrix strength and stiffness, over collagen or elastin alone, and resulted in mechanical properties more closely matching native vascular tissue, Figure 4.3 B. UTS of uncrosslinked CEM matrices was 2.33 ± 0.406 MPa, strain to failure was 30.1 ± 5.61 % and stiffness was approximately 50% decreased compared to crosslinked matrices, 9.39 ± 2.66 MPa, Figure 4.3 B. Resilience, a measure of recovered energy during unloading of matrices, shows much of the energy is recovered during subsequent loading-unloading cycles, comparing favorably to tissue, with minimal energy loss during cyclic loading. The resilience of CEM matrices was 72.9 ± 5.91 %, Figure 4.3 A. CEM matrices showed enhanced mechanical properties compared to constitutive materials alone. 2.5 mg/ml collagen only matrices had a UTS of 0.474 ± 0.0711 MPa, a strain to failure of 21.1 ± 3.32 %, and a Young's Modulus of 2.15 ± 0.690 MPa. Based on previous studies from our group, LysB10-only constructs showed an UTS of 2.88 ± 0.910 MPa, a strain to failure of 430 ± 34.0 % and a Young's Modulus of 0.530 ± 0.0200 MPa.

Table 4.1: Mechanical characterization of uncrosslinked 2.5 mg/ml collagen, 2.5 mg/ml elastin CEM and grafts, compared to native tissue and prosthetic grafts.

	Wall thickness (μm)	Compliance (%/100mmHg)	Burst Pressure (mmHg)	Suture retention strength (gF)
Implant Graft 1.3 mm[#]	285 ± 30.4	2.36 ± 0.194	1354 ± 293	38.0 ± 3.46
Implant Graft 4.0 mm[#]	602 ± 38.2	2.04 ± 0.330	1237 ± 143	72.5 ± 3.59
Venous[%]	250*	0.7 - 2.6	1600 - 2500	180 - 250
Arterial [%]	350-710*	4.7 - 17.0	2200 - 4225	88 - 200
Synthetic grafts	200-600	0.2 - 1.9	2580 - 8270	250 - 1200

[#]Grafts were constructed from 2.5 mg/ml collagen, 2.5 mg/ml elastin CEM

[%][4]

*[34]

Biomimetic vascular grafts with mechanical matching to native vasculature. Three critical mechanical features that need to be maintained for success of vascular grafts are compliance, burst pressure and suture retention strength. Compliance of 1.3 mm graft and 4 mm grafts closely resembled that of native saphenous vein, 2.36 ± 0.194 %/100mmHg, 2.04 ± 0.330 %/100mmHg, and 0.7 - 2.6 %/100mmHg, respectively. Burst pressures of tissue engineered grafts were significantly higher than physiologic/pathophysiologic range, 1354 ± 293 mmHg for 1.3 mm grafts and 1237 ± 143 mmHg for 4 mm grafts. Suture retention strength was a function of number of layers within the graft wall. The 1.3 mm grafts had 4-5 layers of composite rolled, Figure 4.4, and 4.0 mm grafts had 8-9 layers. The suture retention strength increased from 38.0 ± 3.46 gF to 72.5 ± 3.59 for 1.3 mm grafts to 4 mm grafts. Further, we have shown the ability to modulate wall thickness as a function of layering/rolling of grafts. 1.3 mm grafts were constructed from a 20 mm composite sheet rolled on a 1.3 mm mandrel. Consequently grafts had a wall thickness of 285 ± 30.4 μm. Similarly, 4 mm grafts were constructed from 100 mm composite sheets rolled on a 4 mm mandrel, and thus had a thicker 602 ± 38.2 μm wall. The observed mechanical strengths approximate or supersede native vasculature and synthetic grafts, Table 4.1.

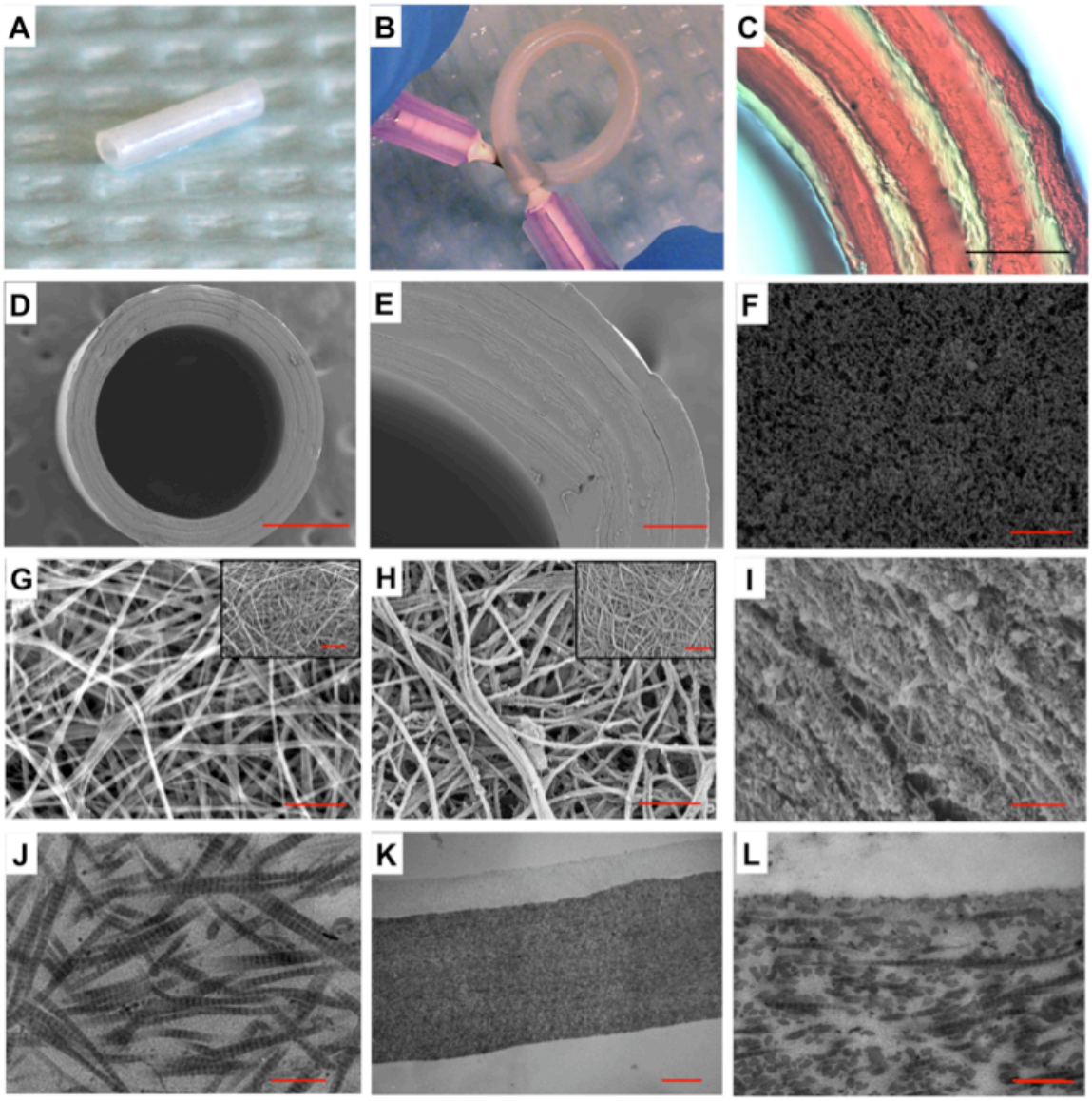

Figure 4.4. Meso- and Ultrastructure of CEM grafts. (A) Photo of unimplanted graft segment, (B) long graft segment showing kink resistance, (C) Van Geison stained cross-section of graft wall clearly delineating layers: collagen in CEM stained red, elastin yellow, scale bar 100 μm, (D) SEM of graft cross-section, scale bar 500 μm, (E) SEM of graft wall showing contiguous elastin layer and site of rolling initiation, scale bar 100 μm, (F) SEM of elastin structure on lumen of graft, scale bar 1 μm, (G) SEM of fibrous structure of 2.5 mg/ml collagen only lamella showing fibrillar collagen, 50 kX, scale bar 1 μm, 10 kX inset showing global nanofibrous morphology, scale bar 2 μm, (H) SEM of fibrous structure of 2.5 mg/ml collagen, 2.5 mg/ml elastin CEM lamella showing fibrillar collagen "decorated" with elastin, 50 kX, scale bar 1 μm, 10kX inset showing global nanofibrous morphology, scale bar 2 μm, (I) SEM of nanofibrous region of graft impregnated with elastin, scale bar 1 μm. (J) TEM of CEM lamella showing characteristic collagen banding, scale bar 1 μm. (K) and (L) TEM of cross-section of elastin (top) embedded CEM showing preservation of native structure, scale bar 10 μm and 0.5 μm respectively.

Graft structure and composition. Preliminary studies involving elastin coated on ePTFE have demonstrated the hemocompatiblity of certain recombinant elastin formulations [289; 290; 291]. Consequently, it is of critical importance that vascular grafts have a non-thrombogenic lumen, while ensuring mechanical integrity [292]. We have generated vascular grafts with a variety of inner diameters using CEMs embedded in an elastin matrix. Dry weight of elastin impregnated sheets shows a significant increase in elastin spatial concentration in constructs, 1620 ± 100 $\mu g/cm^2$, over CEMs alone, 1400 ± 89.8 $\mu g/cm^2$. Compared to collagen matrices alone, which have a spatial concentration of 772 ± 62.0 $\mu g/cm^2$, elastin impregnated CEMs, and resultant grafts are 47% collagen and 53% elastin by dry weight. *In vivo* studies detailed herein utilize a 1.3 mm ID graft, Figure 4.4 A and B. Van Geison staining of collagen, shows collagen (red) and elastin (yellow) localization in rolled graft, Figure 4.4 C. Since red staining is predominant in sections, elastin within CEM structures cannot be visualized optically. Van Geison stained sections show elastin (yellow) coats the lumen of grafts, Figure 4.4 C. Ultrastructure of rolled grafts was noted by SEM of critical point dried graft sections. 1.3 mm ID grafts had 4 - 5 rolled layers and 4 mm ID grafts had 8 - 9 rolled layers, Figure 4.4 D and E. The luminal surface has a uniform coating of elastin, including regions where rolling is initiated, Figure 4.4 E. Further, the uniform layer of elastin was confirmed by en face visualization of elastin on the luminal surface, which has a distinct fibrillar structure, Figure 4.4 F, compared to collagen or CEM matrices, Figures 4.4 G & H. We have, thus, demonstrated the ability to generate mechanically robust tubular collagen-elastin matrices with uniform luminal elastin which could potentially mediate acute thrombotic responses.

Preservation of fibrillar collagen micro- and ultra- structure. Native collagen microstructure and ultrastructure maintenance is essential to avoid premature degradation, immunogenic responses and loss of mechanical integrity. Collagen matrices alone show nanofibrous network formation with collagen fibrils measuring 83.1 ± 9.44 nm, Figure 4.4 G. However, when co-gelled with elastin, resulting in CEMs, fibrillar matrices still formed, with collagen fibrils "decorated" with elastin, Figure 4.4 H. Collagen fibril diameter increased to 88.1 ± 11.2 nm, but was not significantly different from matrices gelled without the addition of elastin. CEM matrices were then embedded in elastin, in a sandwich molding process that infused elastin into the fibrillar CEM network, filling the nano-porous matrix, Figure 4.4 I. Fibrillar collagen without native D-periodicity is insufficient in recapitulation of native matrices. We have shown the ability for collagen mats, Figure 4.4 G, to develop fibrillar matrices with native D-periodic banding patterns (unpublished). However, we have also demonstrated, with the aid of uranyl acetate staining of CEMs, the preservation of D-periodicity within the collagen component, Figure 4.4 J. Additionally, after embedding with elastin, fibrillar matrices and D-periodicity is maintained, Figures 4.4 K and L. It is apparent through elastin staining that infusion of collagen lamellae has occurred with a thin uniform layer of elastin asymmetrically exposed, Figures 4.4 K and L. We have thus shown ability to generate nanofibrous collagen-elastin interpenetrating networks with enhanced mechanical strength, fibrillar networks, and native collagen D-periodicity.

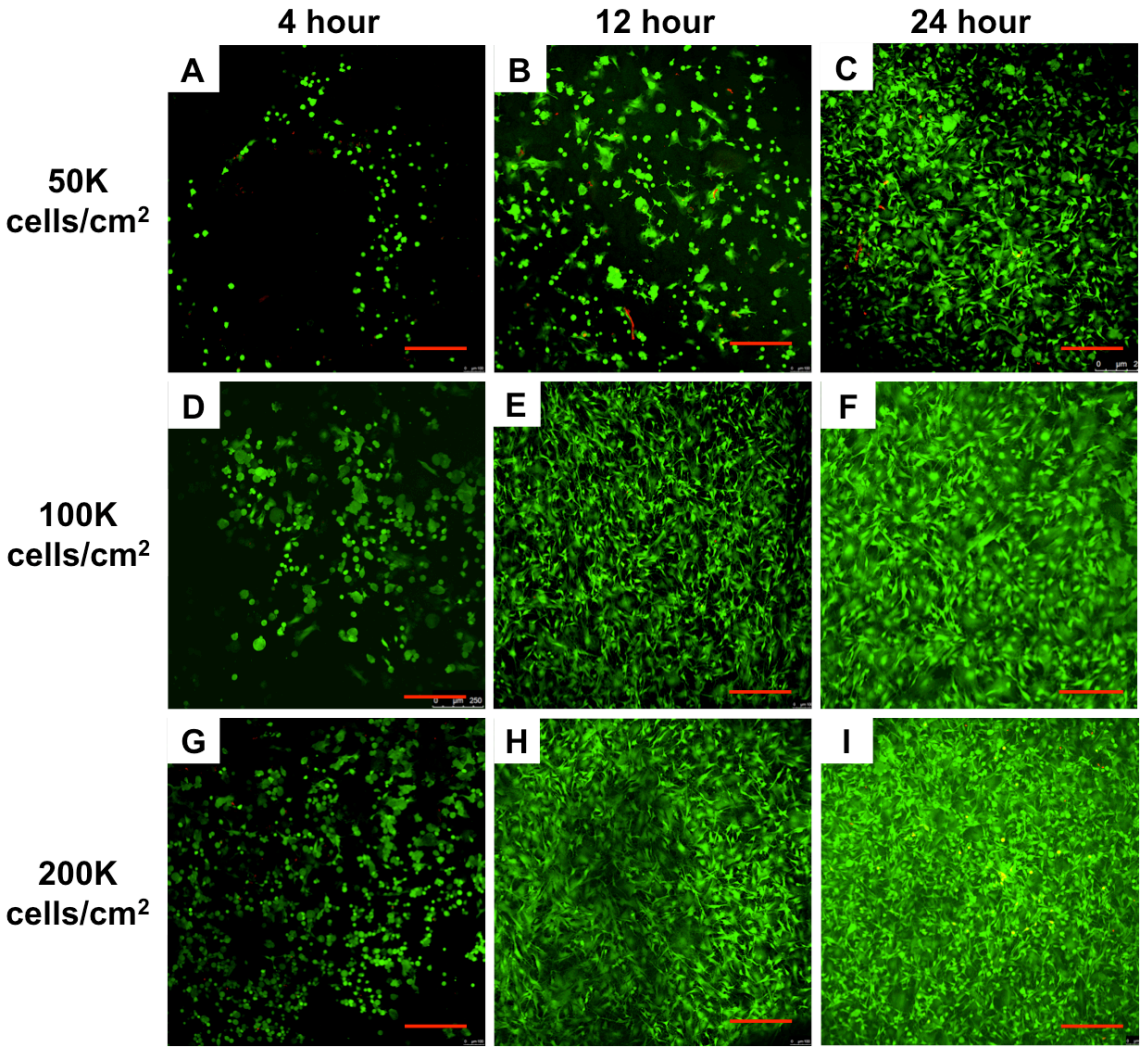

Figure 4.5. Cellularization of CEM. (A-I) Planar CEM seeded with rMSCs at 50 000, 100 000 and 200 000cells/cm^2, showing cell adhesion (4 h – 12 h) and spreading (12 h - 24 h).

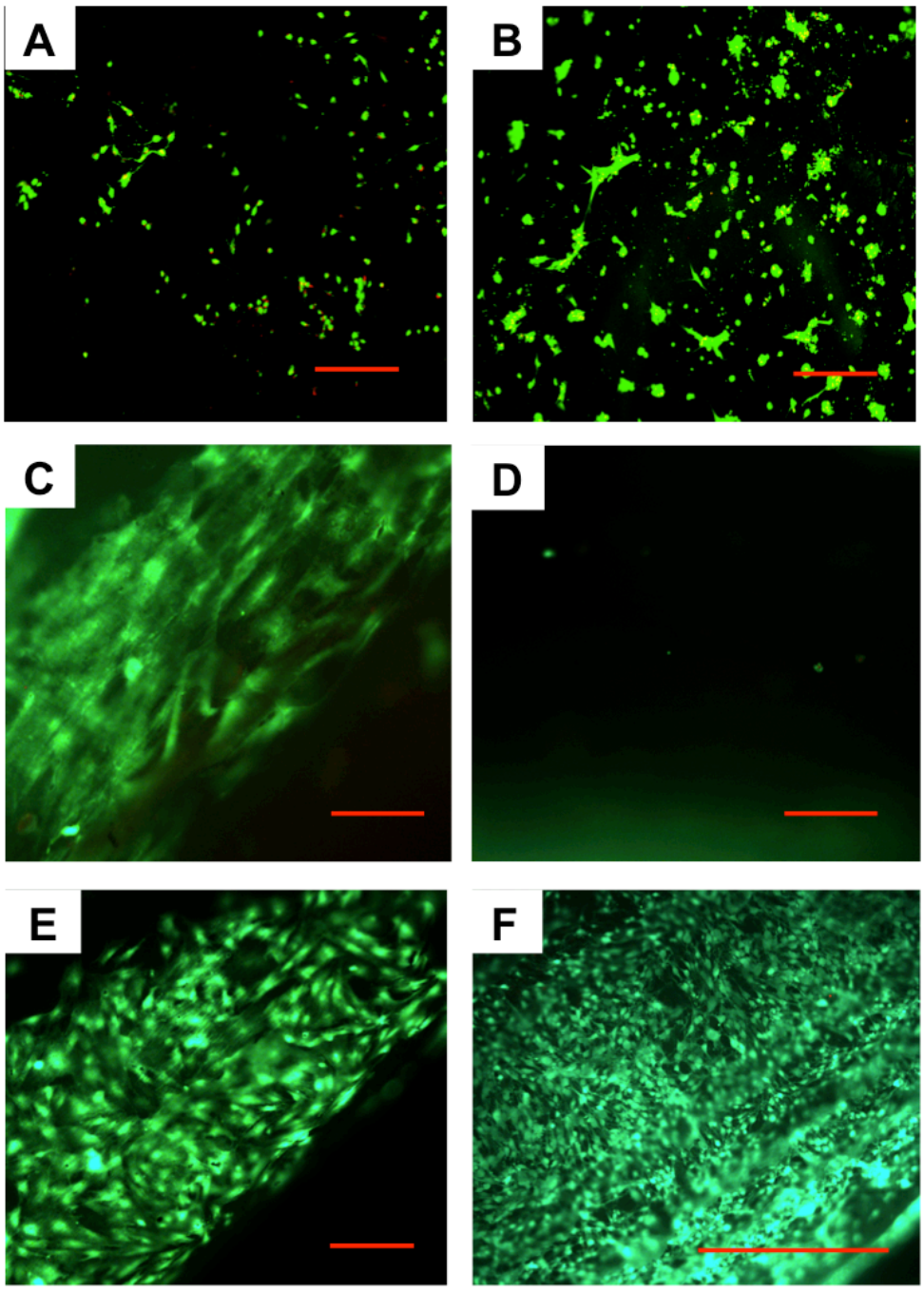

Figure 4.6. Live/Dead staining for cell viability on graft surfaces. (A) Planar CEM seeded with rMSCs at 100 000 cells/cm^2 for 24 h embedded in elastin. (B) Cellularized composite imaged after 3 days. A series of 0.9 mm grafts rolled either with infused superficial elastin facing the lumen or infused CEM facing the lumen (E-F) were constructed. (C) rMSCs were seeded on adventitial side (CEM exposed) of rolled grafts at 100 000 cells/cm^2 for 24 h. (D) No cells present on luminal elastin side. (E) rMSCs were seeded on luminal side (CEM exposed) of rolled grafts at 100 000 cells/cm^2 for 24 h, (F) murine dermal microvascular ECs were seeded on luminal side (CEM exposed) of rolled grafts at 100 000 cells/cm^2 for 24 h. Scale bar is 300 μm.

Rapid cellularization of CEMs result in generation of cellularized vascular media equivalents. Sterilized CEM matrices were seeded with rMSCs at various concentrations. Live/Dead™ staining showed low cell adhesion at 4 h with absence of filapodia and cell spreading for all concentrations, Figure 4.5 A, D and G. Quantification of cellularization at 4 h showed 6.93 ± 2.23 %, 16.2 ± 2.57 %, 28.1 ± 3.50 % confluence for respective spatial seeding densities of 50 000, 100 000 and 200 000 cells/cm^2. At 12 h, lower cell concentrations show moderate cell adhesion, but high cell concentrations show high cell attachment and spreading, Figure 4.5 B, E and H. Quantification of cellularization at 12 h showed 26.3 ± 3.64 %, 56.2 ± 4.20 %, 84.9 ± 6.28 % confluence for respective spatial seeding densities of 50 000, 100 000 and 200 000 cells/cm^2. At 24 h post seeding, cells seeded at 50 000 cells/cm^2 witnessed moderate adhesion with cell spreading, but cells seeded at 100 000 and 200 000 cells/cm^2 showed near confluence, Figure 4.5 C, F and I. Quantification of cellularization at 24 h showed 59.6 ± 12.1 %, 85.6 ± 6.06 %, 87.8 ± 6.35 % confluence for respective spatial seeding densities of 50 000, 100 000 and 200 000 cells/cm^2, respectively. We determined the minimal cell seeding concentration for confluence of CEMs with good cell adhesion and spreading within 24 h (100 000 cells/cm^2 over 200 000 cells/cm^2, $p=0.82$). Consequently, CEMs seeded at 100 000 cells/cm^2 for 24 h were carried forth to elastin embedding. Cellularized constructs were embedded in elastin using a sandwich molding process, which resulted in a reduction of cells. Imaging of cells immediately after embedding and after 3 days showed cell viability within composites and proliferation, Figure 4.6 A and B, respectively. Quantification of cellularization immediately after elastin embedding showed 12.0 ± 3.39

% confluence, compared to 3 days post embedding, 25.2 ± 5.47 %. In a similar approach, we seeded MSCs and ECs luminally and abluminally (MSCs only) and showed preferential adhesion and near confluence in 24 h of seeding, Figures 4.6 C-F. We have thus shown the ability to rapidly cellularize and embed CEM matrices with elastin. Cellularized matrices were produced in just over 24 h.

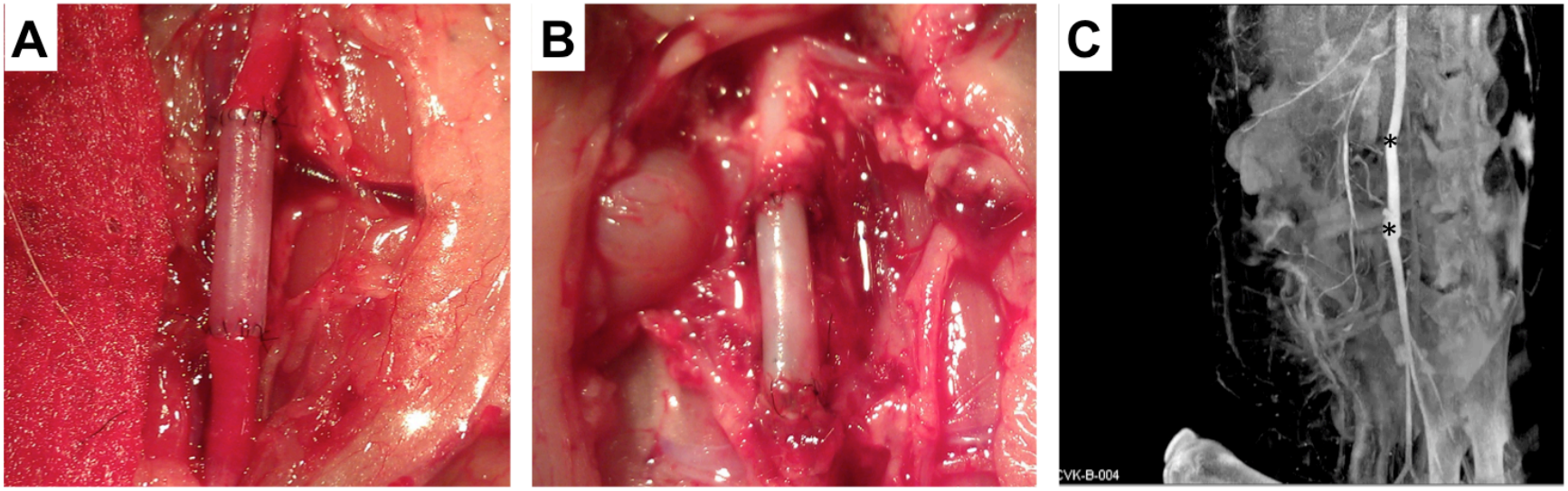

Figure 4.7 Implantation of a 1cm long 1.3mm ID aortic interposition graft in the infrarenal suprailiac position. Gross morphology of the graft was noted: (A) Photo of graft at implant showing reddish color of blood flow, (B) Photo of graft at explant after exsanguination and perfusion fixation. (C) Evaluation of patency of lumen using contrast based angiographic computed tomography, * delineate graft.

Patent small diameter vascular grafts *in vivo*. 1.3 mm ID vascular grafts were implanted for 1 week in a rat aortic interposition model. Rats were dosed with clopidogrel for 3 days post-op. Grafts could be easily trimmed to desired dimensions for implant (1 cm long), Figure 4.7 A. Grafts appeared to be fully perfused upon release of clamps and allowed for visualization of blood flow, Figure 4.7 A. Upon explant, grafts appeared patent with minimal adventitial adhesion to abluminal wall, Figure 4.7 B. CTA of perfusion fixed interposed grafts show maintenance of graft patency and lack of aneurysmal dilation, Figure 4.7 C. Visual observation of graft luminal surface showed no thrombus or visible intimal hyperplasia. Graft integrity was maintained with identifiable staining of ECM based graft components, Figure 4.8 A. There appears to be the development of a cellularized neointima which stained positive for collagen, mononuclear cells, and entrapped red blood cells, Figure 4.8 A, B and C. We have thus shown the ability for ECM mimetics to rapidly generate grafts that mimic the native environment, and allow for cell and tissue integration favorable for graft healing.

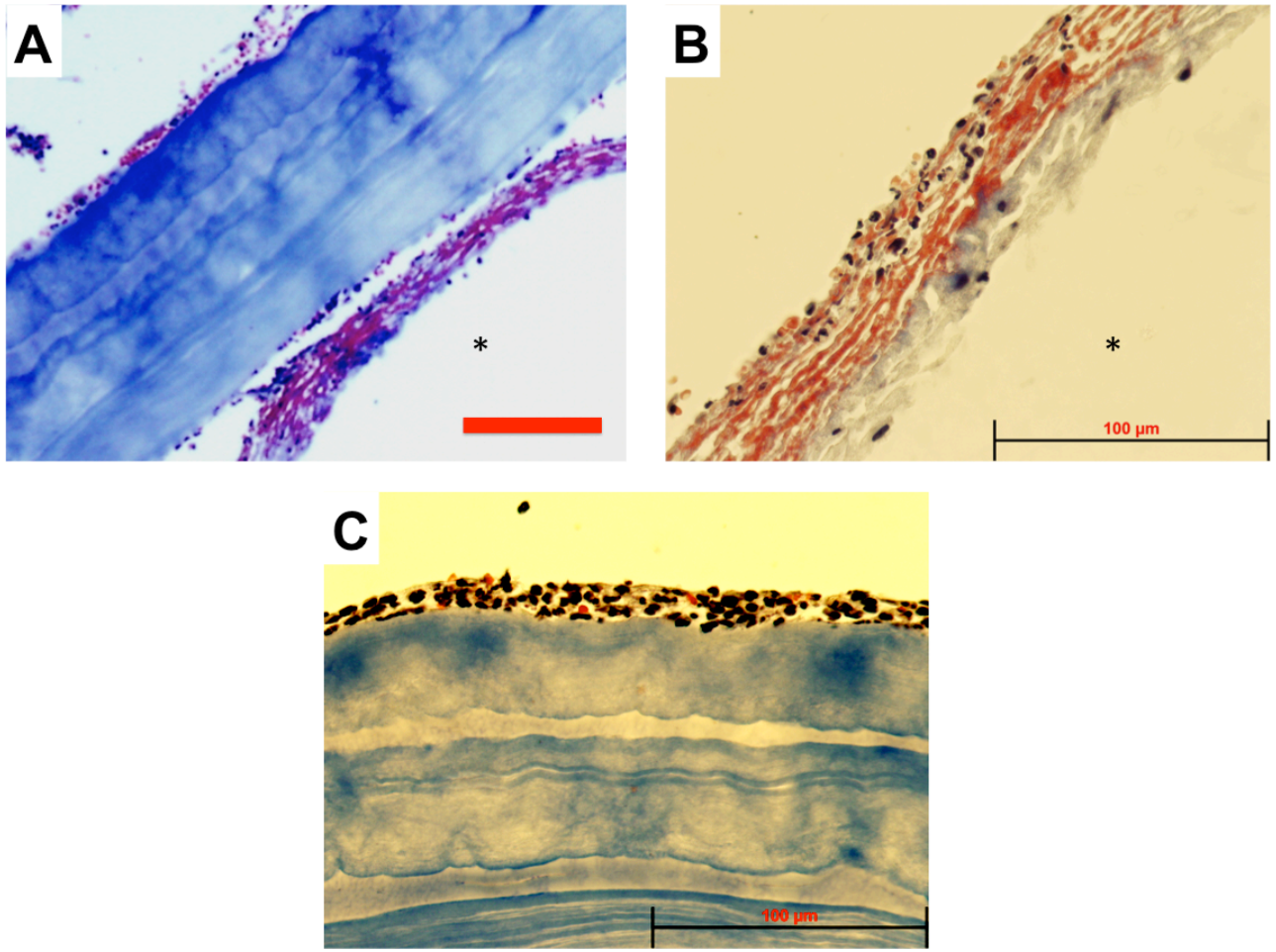

Figure 4.8 Evaluation of graft morphology and cellular infiltrate. (A) Masson's Trichrome staining of ECM of graft sections showing CEM layers in blue (Lys-B10 does not stain positively), and neointima, scale bar 100 μm, (B) magnified image showing trapped red blood cells and blue staining of neo-collagen matrix in neointima, (C) thin layer of mononuclear cells adherent on adventitial CEM surface. * indicates luminal side.

4.4 Discussion

Bioinspired matrices with tunable mechanical properties and tissue-mimetic microarchitecture. Collagen and elastin matrices have been used for several decades either independently, in combination or as composites with other materials for tissue engineering [8; 112; 293]. Although of great relevance and importance to tissue engineering and design of materials for implantation, mechanical failure of collagen gels has hampered efforts to fully utilize the properties of collagen. Several techniques have been developed to: aid the localized deposition of collagen on non-biologically derived matrices, recapitulate the ECM environment using synthetic polymers, or process collagen. The last of which often results in denatured variants that lack native structure. Moreover, the mechanical strength of traditional processing techniques for collagen matrices do not approximate native tissue. However, through the use of novel fabrication techniques, enhanced dehydration and compaction of collagen gels, and co-gelling with recombinantly expressed elastin, we have generated a series of mechanically tunable matrices that support cell adhesion and proliferation while exhibiting mechanical properties that are similar to vascular and other soft tissue. Mechanical strength and stiffness can be varied through the judicious selection of initial gel formulations, concentrations, gel thicknesses, layering of matrices and crosslinking. The addition of another matrix component during gelation (elastin-mimetic polypeptides), which decorates collagen fibrils, causes an increase in strain to failure and increased strength of matrices. Enhanced mechanical compliance due to the ability of elastin-mimetic polypetides to disrupt the inter-fibrillar structure of collagen, may result in decreased

collagen fibrillar branching and adhesions, allowing for enhanced fibril pullout and transition from brittle to ductile fracture. This further allows enhanced fibrillar slippage/pullout and withstanding additional force prior to formation of defects leading to failure as seen in many particulate reinforced composites [294]. Matrices of this type have been found in bone, that act as sacrificial bond forming matrices that allow for a "hidden length" of fibrils to be found, which may further explain the enhanced strain to failure of composite matrices over collagen only matrices [295]. Additionally, elastin-mimetic polypeptides may act as a "glue" to better adhere adjacent collagen fibrils, resulting in higher strengths [295]. Hydroxyl groups and sulphydryl groups in collagen and recombinant elastin matrices enable micro-crosslinks, both physical and chemical (Van der Waal's, ester, thioester) to form between monomers during gel dehydration. This has been shown to enhance mechanical strength of matrices [239; 296; 297; 298]. Through the modulation of macroscale crosslinks, due to the addition of genipin, we note further strengthening of uncrosslinked matrices when crosslinked. We show the ability to create mechanically resilient structures that exhibit high failure strain and enhanced compliance when used to form rolled tubes.

Mechanically matching biomimetic vascular grafts. For the long-term success of vascular grafts, 3 fundamental mechanical requirements exist: compliance matching native vascular tissue, burst pressures exceeding physiological/ pathophysiological ranges, and suturability. Compliance mismatch has been indicated in the failure of several small diameter vascular grafts [258; 299]. Further, it is seen that autologous tissue, when exposed to native flow regimes, remodels to acquire a phenotype and morphology similar

to native arteries [300; 301; 302]. Thus it is required that vascular grafts remodel while integrating into native tissue. To this end, several groups have investigated the use of porous biodegradable matrices that allow cellular infiltration (or are pre-seeded with cells) to allow and facilitate remodeling [230; 303; 304]. Given the long culture times, contamination risk, unclear cell source and cost, several of these strategies lack wide-scale clinical applicability [31]. The current trend in the field has been to recapitulate the native vascular environment *in vitro* using cell based approaches to secrete ECM. These scaffolds are then decellularized and the matrix they form used for engineered tissue [9]. While this approach has shown some clinical applicability, similar issues of long culture times, contamination, cell source and cost limit widespread use and utility in acute indications. The matrix formed, however, has been shown to be mechanically similar to native tissue and possesses strengths suitable for implantation [9; 45; 262]. We propose a novel approach that obviates some of the aforementioned limitations, by rapidly generating ECM-based vascular grafts, not secreted by cells. Grafts composed of purified Type I collagen, for strength and structural support [139; 183], and recombinantly expressed elastin, for thromboresistance [183; 289; 290; 291], demonstrate similar mechanics to native tissue. Compliance of tissue engineered grafts approximate that of native human saphenous vein (typically used for bypass surgery) and have burst pressures an order of magnitude higher than that ever reached in human vasculature. Grafts have sufficient suturability allowing for ease of implantation, with high durability (resistance to delamination of rolled layers).

Cellularized vascular grafts on demand. The design and fabrication of a cellularized

tissue mimetic composite within a clinically relevant timeframe for implantation has until now eluded the field of vascular tissue engineering. To date, the most successful cellularized construct implanted by L'Heureux et al in a variety of animal, non-human primate, and human models, take on the order of 3-6 months to generate [31]. While there is a market and scope for their technology, several limitations exist. Their method uses cells to secrete ECM, which is then rolled and allowed to adhere. In a similar approach, ECM matrices from cells seeded on biodegradable polymers presents a novel solution to potentially avoid delamination of rolled layers [45]. Dahl et al's strategy has shown efficacy in large animal models, but the time to produce grafts, limit utility for emergent indications. The advantage of the approach we propose is the rapidity with which cellularized constructs can be created. Herein, we describe a novel strategy that allows for the generation of cellularized vascular grafts within 24 h, while other techniques require week-month time frames. While the total time for the fabrication of acellular grafts is less than 60 min, cellularized CEM matrices is granted for 24 h to ensure cell adhesion, proliferation and near confluence. Cells are allowed to proliferate on collagen matrices prior to embedding with elastin, rolling on a 1.3 mm or 4 mm mandrel and re-gelling the elastin to form one contiguous layer. This novel technique allows for the rapid generation of cellularized vascular grafts that have sufficient mechanical strength and stability for implantation. MSCs provide a convenient source for the population of vascular grafts, given their ease of isolation from a variety of sources (bone marrow, peripheral blood, adipose tissue). Mesenchymal stem cells have been shown to differentiate into endothelial progenitor like-cells [91; 92; 93; 94; 283] and other vascular wall cellular constituents, including fibroblasts [284], and smooth muscle cells [284;

285]. This ability eliminates the need to isolate specific cell types for site specific repopulation engineered vascular constructs. A wide literature that suggests the ability of MSCs to attenuate the inflammatory and immune responses associated with surgical trauma and implants. Work from Badylak's group, and others, has shown the potential for the incorporation of bone marrow mesenchymal stem cells within tissue engineered and biodegradable scaffolds that modulate the inevitable host tissue inflammatory response. They have shown the ability for BM-MSCs to secrete a host of factors that ultimately direct the infiltrating macrophage response toward a M2 resolution (healing phenotype) over a M1 inflammatory phenotype. Further they have been shown to down-regulate MHC and costimulatory molecule expression, decrease inflammatory cytokine expression (TNF-α, IL-12, IFN-γ), increase anti-inflammatory cytokine expression (IL-10), promote T-reg proliferation, and interfere with lymphocyte replication [97; 98; 101; 286; 287]. Another interesting aspect of MSCs is their ability to modulate the thrombogenicity of blood contacting surfaces. Work done by Song Li's group and Chris Breuer's group has shown the anti-thrombogenic potential for MSCs on vascular grafts [86; 266; 267; 305]. While we have yet to test the efficacy of MSC immunomodulatory and anti-thrombogenic potential *in vivo*, we have constructed MSC based media equivalents, near confluent MSC or EC intima, and MSC seeded adventitia in a short, clinically relevant, one day time frame that can potentially revolutionize the current standard of care.

Non-thrombogenic vascular grafts. The 3 critical requirements for vascular grafts when implanted are: (i) durability to withstand continuous pulsatile blood flow; (ii) maintain

patency; and (iii) resist aneurysm formation. To assess the ability of tissue engineered vascular grafts to avoid catastrophic failure, resulting from (i)-(iii) mentioned above, it is critical to test grafts in a variety of animal models prior to implantation *in vivo*. While *in vitro* characteristics of mechanical robustness and fatigue resistance are critical, tissue engineered grafts are dynamic systems that integrate and function in a synergistic manner with host tissue. To this end, we developed small diameter vascular grafts for surgical implantation in a rat aortic interposition model. The advantage our model is: (1) the high blood flow and "harsh" biomechanical forces that are imposed on interposed vessels, and (2) there that are no major collateral vessels to compensate peripheral tissue perfusion, allowing definitive evaluation of graft performance. We strived to further create a challenging model to test efficacy of vascular grafts by limiting post-surgical dosing of anti-platelet medications to just 3 days post op, with no concomitant anti-thrombotic agent administration. Tissue engineered vascular grafts showed good success, without note of occlusive thrombi or neointimal hyperplasia at one week. We noted integration and healing of the anastamoses. CTA showed patency of grafts with no appreciable aneurysmal dilation. Histological evaluation showed no evident calcification, coverage of EC-like cells on the luminal surface, neo-collagen matrix synthesis, with minimal leukocyte infiltration and no occlusive thrombus presence. While 1 week timepoints are clinically relevant to establish short term efficacy of graft utility, longer timepoints (1 month, 3 month) will establish the full healing response and the ability for grafts to further integrate into the host vascular system.

4.5 Conclusion

We report the production of a novel series of modulatable biomaterials that show tissue mimetic responses based on isolated and purified Type I collagen and recombinantly expressed elastin. Materials show the ability to be mechanically tailored to match a variety of tissue based substrates by the variation of initial collagen and elastin concentrations. We show an unexpected increase in mechanical strength (UTS) and stiffness (Young's Modulus) as a function of network interpenetration and densification through matrix layering. To further modulate mechanics, genipin crosslinking was used. Through the use of CEMs embedded with recombinantly expressed elastin in a sandwich molding process, we demonstrated the ability to rapidly create rolled tubular constructs that exhibit mechanical properties similar to native tissue. We have demonstrated that the native ultrastructure of collagen is preserved with the addition of elastin in CEMs as well as the cellular adhesiveness. CEM matrices show rapid cellular adhesion, spreading and proliferation at modest cell densities (100 000 cells/cm^2). Since only 5 x 10^6 cells are required for a 4 mm ID graft, the potential for their use with a variety of cell types in clinical applications is conceivable. Embedding cell seeded constructs with elastin and subsequent rolling allows for the formation of tubular cellularized composites. This is the first report of MSC based media equivalents, which have the potential of modulating the inflammatory environment healing vascular grafts generated in 24 h. Implanted vascular grafts show excellent stability and lack of neointimal hyperplasia, aneurysmal dilation or luminal thrombosis/ stenosis. Given the ability to modulate mechanics, cellularized grafts and stability of implanted grafts *in vivo*, we believe this presents a paradigm in the development of extracellular matrix based materials and vascular grafts. Future studies

will involve the validation of acellular and cellularized grafts in rat (for longer time points, four weeks and three months) and higher animal models, the use of autologus MSCs cells from animals for seeded grafts, and potentially other cells types, such as induced pluripotent stem cells.

CHAPTER 5

Summary and Future directions:

5.1 Summary

Chapter 1 details the need, requirements and future of vascular grafts. Vascular disease results in the decreased utility and availability of autologous vascular tissue for small diameter (<6 mm) vessel replacements. While synthetic polymer alternatives to date have failed to meet the performance of autoglogus conduits, tissue engineered replacement vessels represent an ideal solution to this clinical problem. Ongoing progress requires combined approaches from biomaterials science, cell biology, and translational medicine to develop feasible solutions with the requisite mechanical support, non-fouling surface for blood flow, and tissue regeneration. Specific to mechanical considerations, grafts must have (i) sufficient burst pressure to prevent catastrophic failure of the vessel and long-term fatigue resistance, (ii) suitable compliance that approximates that of the native vessel to prevent mechanical mismatch, and (iii) sufficient suture retention strength to permit implantation and tolerate hydrodynamic and mechanical forces at the anastomosis. Biological and clinical considerations include (i) generation of a non-fouling luminal surface to prevent thrombosis, (ii) mediation of the immune response due to surgical trauma and potential graft rejection and regeneration, and (iii) demonstrated efficacy *in vivo*.

To this end, we have utilized a bottom-up approach to individually target the mechanical aspects, as described exclusively in Chapter 2 with collagen alignment, and parts of Chapter 3 and Chapter 4. While several different materials have been developed and characterized during the course of this investigation, select prototypes have aided in

intelligent design of next level constructs. For example dehydration strategies from Chapter 2 were employed in Chapter 3. Further, lessons learnt from composite mechanics and fabrication schemes in Chapter 3 were translated to developing interpenetrating networks and vascular grafts in Chapter 4. Given the wide range of materials and material properties elucidated during the course of this work, we postulate that these materials can be used for a variety of tissue engineering applications.

Collagen has been used widely as a biomaterial because of its strength, high species homology, known isolation and production protocols, and processability into higher order structures. However, prior processing techniques have resulted in a lack of ultrastructural control and mechanical strength as well as restricted construct size (nano/meso scales). This in turn prevented large-scale fabrication of tissue engineered constructs. More specifically, existing processes for making collagen constructs result in biomaterials that lack mechanical strength, integrity and structural support. The use of collagen based biomaterials has further been limited given its structural isotropy. The work described herein however outlines fabrication of micro-thin nanofibrous collagen matrices with (i) stretch induced anisotropy (Chapter 2), (ii) integration of layered structures to improve mechanical strength (Chapter 3), (iii) laser ablation schemes to create higher order structures mimicking native tissue structure, morphology and mechanics and alignment of cells on scaffold architecture (Chapter 3), (iv) development of composites for use as soft tissue replacements, and blood contacting surfaces (Chapter 3 and 4), and (v) potential for use in conjugating moieties that will allow for enhanced tissue repair, tissue regeneration, drug delivery and mechanical strengthening (future work). In all we have

created defined tissue mimetic architectures that guide cell and tissue morphology and hierarchical development of 3D tissue *in vitro* and *in vivo*.

In Chapter 2, we present a method for the fabrication of micro-thin nanofibrous collagen matrices with stretch-induced anisotropy. Monomeric rat tail tendon Type I collagen was neutralized in a phosphate buffer to yield large centimeter scale gels. PAGE analysis, microdifferential scanning calorimetry and transmission electron microscopy confirmed reconstitution of collagen and characteristic 67nm D-periodic banding. Collagen gels of varying concentration, 0.3125mg/mL-2.5mg/mL, were mounted on an automated stepper motor which stretched the gels to 0%, 10% and 20% strain, at rates of 3um/s and 300um/s. Fast Fourier Transforms (FFT's) of scanning electron micrographs showed collagen nanofibrils (~80nm) preferentially aligning in the direction of stretching, with dependence on stretch amount and rate. Further, structural anisotropy translated to mechanical anisotropy, yielding significantly higher ultimate tensile strengths and Young's moduli in the direction of alignment, compared to directions perpendicular to alignment or in unaligned matrices. In summary, we present the generation of a novel centimeter scale collagen based construct, with nanofibrous anisotropy; superior strength, alignment and construct size to previously published techniques; and potential utility in cardiovascular, dermal and other soft tissue engineering applications.

In Chapter 3, we showed that through the use of mechanical reinforcement of collagen matrices, and excimer laser ablation, mechanically compliant 3D tissue mimetic supports can be generated that support cellular adhesion, proliferation and alignment of cells, ultimately acting as scaffolds for soft tissue engineering. Collagen has been widely used

for the development of materials for repair, augmentation or replacement of damaged or diseased tissue. However, current processing techniques have limited its ability to be processed into large tissue constructs. Further, dense collagen films lack the mechanical compliance that is required to adequately mimic tissue. Conventional processing techniques for synthetic materials have resulted in the development of anisotropic matrices that can be mechanically tuned to by using mechanical, thermal or laser ablation schemes. Herein we describe a facile method for the large-scale fabrication of biologically derived materials through mechanical reinforcement and excimer laser ablation to create 3D tissue mimetic constructs that are mechanically tunable and support cellular adhesion and alignment. Collagen gels cast in a phosphate buffer were dried to form dense collagen mats. Subsequent gels were dried atop lamellae to create multilayer constructs. This series of novel collagen based substrates interestingly possessed a range of megapascal level strengths (1 - 15 MPa) and stiffnesses (2 – 100 MPa) which are a function of collagen concentration, collagen matrix thickness, crosslinking and a novel layering technique that results in matrix densification. To show potential utility in blood contacting applications, we developed a novel strategy to embed collagen matrices with recombinantly expressed elastin, resulting in composites with enhanced biological properties. Through the use of microfabrication technologies we have enhanced the strength and stiffness of collagen matrices, while significantly improving substrate extensibility. Excimer laser ablation of collagen matrices resulted in significantly higher compliance (9 % - 90 %) with no discernable denaturation, as determined by differential scanning calorimetry and transmission electron microscopy. Micro-ablated collagen matrices showed enhanced cellular rat bone marrow derived mesenchymal stem cell

alignment, as determined by actin staining. This chapter demonstrates how through the control of collagen gel hydration, global micro- and macro- structure, and laser ablation schemes, a series of strong (on the order of MPa) collagen sheets can be created. The result is constructs that have mechanical and biological properties mimicking native tissue coupled with cellular alignment and high compliance. Capitalizing on the natural abundance of collagen in native tissues, we have designed a bottom-up approach for the creation of bioartificial matrices. Through the development and utilization of layer-reinforced networks and novel microfabrication techniques, we have developed a natural biopolymer matrix with tunable mechanical properties suitable for a limitless variety of tissue engineering applications: biosynthetic blood vessels, tendon replacements, hernia patches, muscle tissue, nerve guidance conduits, artificial skin, and soft tissue applications.

In Chapter 4, we further target the development of materials for vascular tissue engineering based on prior studies outlined above. Cardiovascular disease (CVD) is the leading cause of morbidity and mortality in the United States and many other nations. One of the leading causes of CVD is arteriosclerosis, which often requires vessel bypass or replacement. Synthetic small diameter vascular grafts can rapidly fail and tissue engineered grafts require long fabrication times. Further, there have been only a limited number of reports detailing the use of tunable materials for the design of vascular grafts. Herein, we propose a hierarchical design of vascular grafts from extracellular matrix constituents to recapitulate native tissue structure and function. Through the use of novel processing and fabrication schemes for isolated and purified Type I collagen and

recombinantly expressed elastin, we have designed large (centimeter scale) interpenetrating networks that can be mechanically tailored to match a variety of tissue based substrates by the variation of initial collagen and elastin concentrations. Further, we show that matrix layering yields an unexpected increase in mechanical properties due to network interpenetration and densification. Matrices were tunable to yield a range of biologically derived materials that have ultimate tensile strengths ranging from 0.5 – 17 MPa, and stiffnesses ranging from 2.5 - 120 MPa. Further, we utilize microdomain solubilization of genetically engineered recombinant elastin to create viable blood contacting matrices. CEMs were embedded with recombinantly expressed elastin, in a sandwich molding process. Rolling of embedded matrices was the final step in demonstrating the ability to rapidly produce vascular grafts with maintenance of characteristic D-periodicity and native collagen structure. Given the native cellular adhesivity of collagen, seamless cellularization of CEM matrices could be performed with cell adhesion (4 – 12 hours), spreading (12-24 hours) and near confluence being reached in 24 hours at a variety of cellularization concentrations. These cellularized matrices were embedded in elastin in a rapid, 20 minute, process that resulted in the generation of cellularized vascular grafts. This is the first report of cellularized vascular grafts generated in 24 hours, with potential for utility in sub-acute care indications. Grafts were implanted in a rat aortic interposition model. Histological examination showed that implanted vascular grafts show good stability and lack of neointimal hyperplasia, aneurysmal dilation or luminal thrombosis/ stenosis. In summary, we have shown the ability to create mechanically tunable matrices with *in vivo* stability and rapid cellularization without the addition of foreign cell binding sequences. This work presents

a paradigm in the development of extracellular matrix based materials and vascular grafts.

5.2 Future Directions

Strengthening of collagen for greater utility. Collagen matrices can be embedded in a variety of polymeric matrices (either biological or synthetic) or co-cast as a gel with other matrices – resulting in improved (a) mechanical properties, (b) cytocompatibility, (c) biocompatibility and (d) drug delivery potential. The work presented shows how co-casting with elastin results in interpenetrating networks that have enhanced mechanical strength, stiffness and higher strain at failure. Using the large number of labile groups on collagen, there is the opportunity to enhance mechanical strength by crosslinking using homobifunctional, heterobifunctional or other crosslinking schemes that increase strength of matrices, of which genipin is shown in this study. This has potential utility in other tissue engineering applications [306]. Further, it has been suggested that generation of large collagen fibrils may enhance mechanical strength [307], and could potentially be investigated using different gelation systems, temperatures and mechanisms. For example, freeze dry to induce long crystal formation and structural anisotropy.

There is the opportunity to form matrices that have incorporated nano-/ micro-particles that can act to reinforce structure, dissipate stresses and blunt crack tip propagation (with respect to suture pullout). Although particles would be dispersed in a separate phase, there is the potential for matrix particle interaction that could further modulate mechanical strengths. Specifically, through the incorporation of calcites and other apatites, hardness of composites can be enhanced, and hard tissue engineering can be

envisioned. Co-casting with mineralized hydroxyapatite and calcium phosphates can result in materials with organization, strength, density and hardness mimicking hard tissues such as bone [308]. With respect to blood vessels and cartilage, co-casting with proteoglycans and glycoaminoglycans would allow for the generation of hydrophilic matrices that co-ordinate water molecules to mimic dampening in native tissue.

Enhancing hemocompatibility. Embedment of collagen only matrices or interpenetrating networks, depending on the porosity of gels or dried mats, allow for creation of composite materials that further enhance mechanical and biological suitability. Embedment with recombinantly expressed elastin results in the creation of matrices that are resistant to thrombosis (formation of blood clots) and minimal platelet adhesion (enhancing its utility of as a blood contacting device), as described in this study. However future studies could potentially include the functionalization of cell binding/ cell homing sequences to labile groups on collagen or elastin – for example lysine residues. Another example is the use of CD34 antibody (or a host of others) to home and conjugate circulating endothelial progenitor cells to graft surfaces [307]. Further, functionalization with a variety of other molecular moieties such as thrombomodulin can further obviate potential luminal thrombosis [309].

Use of novel ablation technology for 3D organ tissue fabrication. Given the practical spatial resolution of excimer lasers (1-10 μm) and the high fidelity of ablated matrices without deleterious effects on collagen scaffold properties, we plan to investigate ablation patterns for a variety of tissue engineering applications such as: hierarchical blood vessel

cultures, tissue engineered lung (diffusion barrier between alveoli and epithelial cells), blood brain barrier replacement, cardiac tissue engineering (as a soft tissue scaffold with cardiomyocyte growth *in vivo* or culture *in vitro*), localized seeding of cells for liver lobule, pancreas and kidney nephron functional unit regeneration, and others. Further, based on our initial results, we can create aligned muscle cells on collagen by ablation of linear lines on collagen. This will not only enable alignment of cells but potential muscle tissue replacement, design of artificial skin, tendon and heart valve leaflets with engineered anisotropy, with and without cells.

Collagen / collagen-composite drug delivery vehicles. Work by others in our group has shown the potential to conjugate/ trap drugs and small proteins in elastin matrices. There is the ability to create collagen/ CEM matrices that have several labile biologically relevant crosslinking groups, as detailed above. Thus, small molecules, drugs, or nano-/ micro-particles can potentially be physically embedded in the collagen/ CEM structure or tethered to collagen/ CEM matrix and used for graft-tissue response modulation or localized drug delivery.

Acellular and cellularized vascular graft testing. While the grafts tested in the study outlined herein were assessed for one week, we propose a series of longer timepoints with acellular and cellularized grafts. Specifically, we hope to implant 4 week, 3 month and potentially 1 year timepoints that will chronicle the long-term chronic response to the implanted vessels in the rat aortic interposition model.

For the next phase of *in vivo* testing we plan to implant small diameter grafts (4mm) in a pig model. While the pig model better simulates human tissue in size and host tissue response, farm breed pigs grow rapidly and "out grow" grafts, resulting in size mismatches which may not represent grafts implanted in adult humans. To circumvent this, we propose the use of minipig varieties that have a plateau growth curve that better simulates human growth [10]. Finally we plan to initiate platelet adhesion/ morphology, and hemocompatibility studies in baboon arteriovenous shunt models which will help establish large animal graft compatibility [290].

REFERENCES

[1]D. Lloyd-Jones, R.J. Adams, T.M. Brown, M. Carnethon, S. Dai, G. De Simone, T.B. Ferguson, E. Ford, K. Furie, C. Gillespie, A. Go, K. Greenlund, N. Haase, S. Hailpern, P.M. Ho, V. Howard, B. Kissela, S. Kittner, D. Lackland, L. Lisabeth, A. Marelli, M.M. McDermott, J. Meigs, D. Mozaffarian, M. Mussolino, G. Nichol, V.L. Roger, W. Rosamond, R. Sacco, P. Sorlie, T. Thom, S. Wasserthiel-Smoller, N.D. Wong, J. Wylie-Rosett, Heart disease and stroke statistics--2010 update: a report from the American Heart Association. Circulation 121 (2010) e46-e215.

[2]S. Ravi, Z. Qu, E.L. Chaikof, Polymeric materials for tissue engineering of arterial substitutes. Vascular 17 Suppl 1 (2009) S45-54.

[3]S.L. Mitchell, L.E. Niklason, Requirements for growing tissue-engineered vascular grafts. Cardiovasc Pathol 12 (2003) 59-64.

[4]V. Kumar, L. Brewster, J. Caves, E. Chaikof, Tissue Engineering of Blood Vessels: Functional Requirements, Progress, and Future Challenges. Cardiovascular Engineering and Technology 2 (2011) 137-148.

[5]L. Gui, A. Muto, S.A. Chan, C.K. Breuer, L.E. Niklason, Development of decellularized human umbilical arteries as small-diameter vascular grafts. Tissue Eng Part A 15 (2009) 2665-2676.

[6]D. Motlagh, J. Allen, R. Hoshi, J. Yang, K. Lui, G. Ameer, Hemocompatibility evaluation of poly(diol citrate) in vitro for vascular tissue engineering. J Biomed Mater Res A 82 (2007) 907-916.

[7]G.R. Campbell, J.H. Campbell, Development of tissue engineered vascular grafts. Curr Pharm Biotechnol 8 (2007) 43-50.

[8]W.J. Zhang, W. Liu, L. Cui, Y. Cao, Tissue engineering of blood vessel. J Cell Mol Med 11 (2007) 945-957.

[9]N. L'Heureux, S. Paquet, R. Labbe, L. Germain, F.A. Auger, A completely biological tissue-engineered human blood vessel. FASEB J 12 (1998) 47-56.

[10]L.E. Niklason, J. Gao, W.M. Abbott, K.K. Hirschi, S. Houser, R. Marini, R. Langer, Functional arteries grown in vitro. Science 284 (1999) 489-493.

[11]N. L'Heureux, T.N. McAllister, L.M. de la Fuente, Tissue-engineered blood vessel for adult arterial revascularization. N Engl J Med 357 (2007) 1451-1453.

[12]ANSI/AAMI/ISO, Cardiovascular implants - tubular vascular prostheses, in, 2001.

[13]P. Zilla, D. Bezuidenhout, P. Human, Prosthetic vascular grafts: wrong models, wrong questions and no healing. Biomaterials 28 (2007) 5009-5027.

[14]G. Konig, T.N. McAllister, N. Dusserre, S.A. Garrido, C. Iyican, A. Marini, A. Fiorillo, H. Avila, W. Wystrychowski, K. Zagalski, M. Maruszewski, A.L. Jones, L. Cierpka, L.M. de la Fuente, N. L'Heureux, Mechanical properties of completely autologous human tissue engineered blood vessels compared to human saphenous vein and mammary artery. Biomaterials 30 (2009) 1542-1550.

[15]D.N. Ku, D.P. Giddens, D.J. Phillips, D.E. Strandness, Jr., Hemodynamics of the normal human carotid bifurcation: in vitro and in vivo studies. Ultrasound Med Biol 11 (1985) 13-26.

[16]D.M. Wootton, D.N. Ku, Fluid mechanics of vascular systems, diseases, and thrombosis. Annu Rev Biomed Eng 1 (1999) 299-329.
[17]D.N. Ku, D.P. Giddens, C.K. Zarins, S. Glagov, Pulsatile flow and atherosclerosis in the human carotid bifurcation. Positive correlation between plaque location and low oscillating shear stress. Arteriosclerosis 5 (1985) 293-302.
[18]D.N. Ku, D.P. Giddens, Pulsatile flow in a model carotid bifurcation. Arteriosclerosis 3 (1983) 31-39.
[19]L.J. Goldstein, H.U. Khan, E.B. Sambol, K.C. Kent, P.L. Faries, A.G. Vouyouka, Carotid artery stenting is safe and associated with comparable outcomes in men and women. J Vasc Surg 49 (2009) 315-323; discussion 323-314.
[20]C.H. Timaran, E.B. Rosero, S.T. Smith, R.J. Valentine, J.G. Modrall, G.P. Clagett, Trends and outcomes of concurrent carotid revascularization and coronary bypass. J Vasc Surg 48 (2008) 355-360; discussion 360-351.
[21]A.H. Dorafshar, T.D. Reil, S.S. Ahn, W.J. Quinones-Baldrich, W.S. Moore, Interposition grafts for difficult carotid artery reconstruction: a 17-year experience. Ann Vasc Surg 22 (2008) 63-69.
[22]J. Byrne, P. Feustel, R.C. Darling, 3rd, Primary closure, routine patching, and eversion endarterectomy: what is the current state of the literature supporting use of these techniques? Semin Vasc Surg 20 (2007) 226-235.
[23]A. Solan, S.L. Dahl, L.E. Niklason, Effects of mechanical stretch on collagen and cross-linking in engineered blood vessels. Cell Transplant 18 (2009) 915-921.
[24]S. Sarkar, C. Hillery, A. Seifalian, G. Hamilton, Critical parameter of burst pressure measurement in development of bypass grafts is highly dependent on methodology used. J Vasc Surg 44 (2006) 846-852.
[25]B.C. Isenberg, R.T. Tranquillo, Long-term cyclic distention enhances the mechanical properties of collagen-based media-equivalents. Ann Biomed Eng 31 (2003) 937-949.
[26]T. Ziegler, R.M. Nerem, Tissue engineering a blood vessel: regulation of vascular biology by mechanical stresses. J Cell Biochem 56 (1994) 204-209.
[27]Z.H. Syedain, L.A. Meier, J.W. Bjork, A. Lee, R.T. Tranquillo, Implantable arterial grafts from human fibroblasts and fibrin using a multi-graft pulsed flow-stretch bioreactor with noninvasive strength monitoring. Biomaterials 32 714-722.
[28]J.E. Wagenseil, R.P. Mecham, Vascular extracellular matrix and arterial mechanics. Physiol Rev 89 (2009) 957-989.
[29]Y. Hong, S.H. Ye, A. Nieponice, L. Soletti, D.A. Vorp, W.R. Wagner, A small diameter, fibrous vascular conduit generated from a poly(ester urethane)urea and phospholipid polymer blend. Biomaterials 30 (2009) 2457-2467.
[30]A.R. Webb, B.D. Macrie, A.S. Ray, J.E. Russo, A.M. Siegel, M.R. Glucksberg, G.A. Ameer, In vitro characterization of a compliant biodegradable scaffold with a novel bioreactor system. Ann Biomed Eng 35 (2007) 1357-1367.
[31]N. L'Heureux, N. Dusserre, A. Marini, S. Garrido, L. de la Fuente, T. McAllister, Technology insight: the evolution of tissue-engineered vascular grafts--from research to clinical practice. Nat Clin Pract Cardiovasc Med 4 (2007) 389-395.
[32]L. Soletti, Y. Hong, J. Guan, J.J. Stankus, M.S. El-Kurdi, W.R. Wagner, D.A. Vorp, A bilayered elastomeric scaffold for tissue engineering of small diameter vascular grafts. Acta Biomater 6 110-122.

[33]M.T. Zaucha, J. Raykin, W. Wan, R. Gauvin, F.A. Auger, L. Germain, T.E. Michaels, R.L. Gleason, Jr., A novel cylindrical biaxial computer-controlled bioreactor and biomechanical testing device for vascular tissue engineering. Tissue Eng Part A 15 (2009) 3331-3340.
[34]N. L'Heureux, N. Dusserre, G. Konig, B. Victor, P. Keire, T.N. Wight, N.A. Chronos, A.E. Kyles, C.R. Gregory, G. Hoyt, R.C. Robbins, T.N. McAllister, Human tissue-engineered blood vessels for adult arterial revascularization. Nat Med 12 (2006) 361-365.
[35]S. Drilling, J. Gaumer, J. Lannutti, Fabrication of burst pressure competent vascular grafts via electrospinning: effects of microstructure. J Biomed Mater Res A 88 (2009) 923-934.
[36]S. Wang, Y. Zhang, H. Wang, G. Yin, Z. Dong, Fabrication and properties of the electrospun polylactide/silk fibroin-gelatin composite tubular scaffold. Biomacromolecules 10 (2009) 2240-2244.
[37]A. Nieponice, L. Soletti, J. Guan, B.M. Deasy, J. Huard, W.R. Wagner, D.A. Vorp, Development of a tissue-engineered vascular graft combining a biodegradable scaffold, muscle-derived stem cells and a rotational vacuum seeding technique. Biomaterials 29 (2008) 825-833.
[38]J.A. Shaw, B.A. Kingwell, A.S. Walton, J.D. Cameron, P. Pillay, C.D. Gatzka, A.M. Dart, Determinants of coronary artery compliance in subjects with and without angiographic coronary artery disease. J Am Coll Cardiol 39 (2002) 1637-1643.
[39]C.J. van Andel, P.V. Pistecky, C. Borst, Mechanical properties of porcine and human arteries: implications for coronary anastomotic connectors. Ann Thorac Surg 76 (2003) 58-64; discussion 64-55.
[40]R. Roeder, J. Wolfe, N. Lianakis, T. Hinson, L.A. Geddes, J. Obermiller, Compliance, elastic modulus, and burst pressure of small-intestine submucosa (SIS), small-diameter vascular grafts. J Biomed Mater Res 47 (1999) 65-70.
[41]S. Laurent, B. Caviezel, L. Beck, X. Girerd, E. Billaud, P. Boutouyrie, A. Hoeks, M. Safar, Carotid artery distensibility and distending pressure in hypertensive humans. Hypertension 23 (1994) 878-883.
[42]N.R. Tai, A. Giudiceandrea, H.J. Salacinski, A.M. Seifalian, G. Hamilton, In vivo femoropopliteal arterial wall compliance in subjects with and without lower limb vascular disease. J Vasc Surg 30 (1999) 936-945.
[43]S.E. Greenwald, C.L. Berry, Improving vascular grafts: the importance of mechanical and haemodynamic properties. J Pathol 190 (2000) 292-299.
[44]S.G. Wise, M.J. Byrom, A. Waterhouse, P.G. Bannon, A.S. Weiss, M.K. Ng, A multilayered synthetic human elastin/polycaprolactone hybrid vascular graft with tailored mechanical properties. Acta Biomater 7 (2011) 295-303.
[45]S.L. Dahl, A.P. Kypson, J.H. Lawson, J.L. Blum, J.T. Strader, Y. Li, R.J. Manson, W.E. Tente, L. DiBernardo, M.T. Hensley, R. Carter, T.P. Williams, H.L. Prichard, M.S. Dey, K.G. Begelman, L.E. Niklason, Readily available tissue-engineered vascular grafts. Sci Transl Med 3 (2011) 68ra69.
[46]S. Sarkar, H.J. Salacinski, G. Hamilton, A.M. Seifalian, The mechanical properties of infrainguinal vascular bypass grafts: their role in influencing patency. Eur J Vasc Endovasc Surg 31 (2006) 627-636.

[47]P.J. Schaner, N.D. Martin, T.N. Tulenko, I.M. Shapiro, N.A. Tarola, R.F. Leichter, R.A. Carabasi, P.J. Dimuzio, Decellularized vein as a potential scaffold for vascular tissue engineering. J Vasc Surg 40 (2004) 146-153.
[48]N.R. Tai, H.J. Salacinski, A. Edwards, G. Hamilton, A.M. Seifalian, Compliance properties of conduits used in vascular reconstruction. Br J Surg 87 (2000) 1516-1524.
[49]Y. Mine, H. Mitsui, Y. Oshima, Y. Noishiki, M. Nakai, S. Sano, Suture retention strength of expanded polytetrafluoroethylene (ePTFE) graft. Acta Med Okayama 64 (2010) 121-128.
[50]M. Isaka, T. Nishibe, Y. Okuda, M. Saito, T. Seno, K. Yamashita, Y. Izumisawa, T. Kotani, K. Yasuda, Experimental study on stability of a high-porosity expanded polytetrafluoroethylene graft in dogs. Ann Thorac Cardiovasc Surg 12 (2006) 37-41.
[51]M.D. ASTM Committee F-4 on Medical Surgical, Vascular graft update : safety and performance., ASTM, Philadelphia, Penn., 1986.
[52]C. Arrigoni, D. Camozzi, A. Remuzzi, Vascular tissue engineering. Cell Transplant 15 Suppl 1 (2006) S119-125.
[53]C. Fidkowski, M.R. Kaazempur-Mofrad, J. Borenstein, J.P. Vacanti, R. Langer, Y. Wang, Endothelialized microvasculature based on a biodegradable elastomer. Tissue Eng 11 (2005) 302-309.
[54]A. Kaushiva, V.M. Turzhitsky, M. Darmoc, V. Backman, G.A. Ameer, A biodegradable vascularizing membrane: a feasibility study. Acta Biomater 3 (2007) 631-642.
[55]E. Zetrenne, B.C. McIntosh, M.H. McRae, R. Gusberg, G.R. Evans, D. Narayan, Prosthetic vascular graft infection: a multi-center review of surgical management. Yale J Biol Med 80 (2007) 113-121.
[56]K. Torikai, H. Ichikawa, K. Hirakawa, G. Matsumiya, T. Kuratani, S. Iwai, A. Saito, N. Kawaguchi, N. Matsuura, Y. Sawa, A self-renewing, tissue-engineered vascular graft for arterial reconstruction. J Thorac Cardiovasc Surg 136 (2008) 37-45, 45 e31.
[57]C. Wang, Q. Zhang, S. Uchida, M. Kodama, A new vascular prosthesis coated with polyamino-acid urethane copolymer (PAU) to enhance endothelialization. J Biomed Mater Res 62 (2002) 315-322.
[58]K.H. Yow, J. Ingram, S.A. Korossis, E. Ingham, S. Homer-Vanniasinkam, Tissue engineering of vascular conduits. Br J Surg 93 (2006) 652-661.
[59]X.X. Yu, C.X. Wan, H.Q. Chen, Preparation and endothelialization of decellularised vascular scaffold for tissue-engineered blood vessel. J Mater Sci Mater Med 19 (2008) 319-326.
[60]C. Li, A. Hill, M. Imran, In vitro and in vivo studies of ePTFE vascular grafts treated with P15 peptide. J Biomater Sci Polym Ed 16 (2005) 875-891.
[61]W.W. Hancock, Delayed xenograft rejection. World J Surg 21 (1997) 917-923.
[62]S. Sarkar, K.M. Sales, G. Hamilton, A.M. Seifalian, Addressing thrombogenicity in vascular graft construction. J Biomed Mater Res B Appl Biomater 82 (2007) 100-108.
[63]R.N. Salom, J.A. Maguire, W.W. Hancock, Endothelial activation and cytokine expression in human acute cardiac allograft rejection. Pathology 30 (1998) 24-29.

[64]T. Quillard, S. Coupel, F. Coulon, J. Fitau, M. Chatelais, M.C. Cuturi, E. Chiffoleau, B. Charreau, Impaired Notch4 activity elicits endothelial cell activation and apoptosis: implication for transplant arteriosclerosis. Arterioscler Thromb Vasc Biol 28 (2008) 2258-2265.
[65]M. Poh, M. Boyer, A. Solan, S.L. Dahl, D. Pedrotty, S.S. Banik, J.A. McKee, R.Y. Klinger, C.M. Counter, L.E. Niklason, Blood vessels engineered from human cells. Lancet 365 (2005) 2122-2124.
[66]R.Y. Klinger, J.L. Blum, B. Hearn, B. Lebow, L.E. Niklason, Relevance and safety of telomerase for human tissue engineering. Proc Natl Acad Sci U S A 103 (2006) 2500-2505.
[67]M. Deutsch, J. Meinhart, P. Zilla, N. Howanietz, M. Gorlitzer, A. Froeschl, A. Stuempflen, D. Bezuidenhout, M. Grabenwoeger, Long-term experience in autologous in vitro endothelialization of infrainguinal ePTFE grafts. J Vasc Surg 49 (2009) 352-362; discussion 362.
[68]P. Zilla, M. Deutsch, J. Meinhart, Endothelial cell transplantation. Semin Vasc Surg 12 (1999) 52-63.
[69]J. Meinhart, M. Deutsch, P. Zilla, Eight years of clinical endothelial cell transplantation. Closing the gap between prosthetic grafts and vein grafts. ASAIO J 43 (1997) M515-521.
[70]J.M. Daniel, D.G. Sedding, Circulating smooth muscle progenitor cells in arterial remodeling. J Mol Cell Cardiol 50 (2011) 273-279.
[71]L.P. Neff, B.W. Tillman, S.K. Yazdani, M.A. Machingal, J.J. Yoo, S. Soker, B.W. Bernish, R.L. Geary, G.J. Christ, Vascular smooth muscle enhances functionality of tissue-engineered blood vessels in vivo. J Vasc Surg 53 (2011) 426-434.
[72]S.K. Yazdani, B. Watts, M. Machingal, Y.P. Jarajapu, M.E. Van Dyke, G.J. Christ, Smooth muscle cell seeding of decellularized scaffolds: the importance of bioreactor preconditioning to development of a more native architecture for tissue-engineered blood vessels. Tissue Eng Part A 15 (2009) 827-840.
[73]K. Iwasaki, K. Kojima, S. Kodama, A.C. Paz, M. Chambers, M. Umezu, C.A. Vacanti, Bioengineered three-layered robust and elastic artery using hemodynamically-equivalent pulsatile bioreactor. Circulation 118 (2008) S52-57.
[74]Q. Gan, T. Yoshida, J. Li, G.K. Owens, Smooth muscle cells and myofibroblasts use distinct transcriptional mechanisms for smooth muscle alpha-actin expression. Circ Res 101 (2007) 883-892.
[75]G.K. Owens, Regulation of differentiation of vascular smooth muscle cells. Physiol Rev 75 (1995) 487-517.
[76]G.K. Owens, Role of mechanical strain in regulation of differentiation of vascular smooth muscle cells. Circ Res 79 (1996) 1054-1055.
[77]G.K. Owens, Molecular control of vascular smooth muscle cell differentiation and phenotypic plasticity. Novartis Found Symp 283 (2007) 174-191; discussion 191-173, 238-141.
[78]M.B. Chan-Park, J.Y. Shen, Y. Cao, Y. Xiong, Y. Liu, S. Rayatpisheh, G.C. Kang, H.P. Greisler, Biomimetic control of vascular smooth muscle cell morphology and phenotype for functional tissue-engineered small-diameter blood vessels. J Biomed Mater Res A 88 (2009) 1104-1121.

[79]S.G. Ball, C.A. Shuttleworth, C.M. Kielty, Mesenchymal stem cells and neovascularization: role of platelet-derived growth factor receptors. J Cell Mol Med 11 (2007) 1012-1030.
[80]C.M. Kielty, S. Stephan, M.J. Sherratt, M. Williamson, C.A. Shuttleworth, Applying elastic fibre biology in vascular tissue engineering. Philos Trans R Soc Lond B Biol Sci 362 (2007) 1293-1312.
[81]Z. Gong, L.E. Niklason, Small-diameter human vessel wall engineered from bone marrow-derived mesenchymal stem cells (hMSCs). FASEB J 22 (2008) 1635-1648.
[82]L.E. Niklason, Techview: medical technology. Replacement arteries made to order. Science 286 (1999) 1493-1494.
[83]J.M. Caves, V.A. Kumar, A.W. Martinez, J. Kim, C.M. Ripberger, C.A. Haller, E.L. Chaikof, The use of microfiber composites of elastin-like protein matrix reinforced with synthetic collagen in the design of vascular grafts. Biomaterials 31 7175-7182.
[84]J.B. Allen, S. Khan, K.A. Lapidos, G.A. Ameer, Toward engineering a human neoendothelium with circulating progenitor cells. Stem Cells 28 318-328.
[85]J. Allen, S. Khan, M.C. Serrano, G. Ameer, Characterization of porcine circulating progenitor cells: toward a functional endothelium. Tissue Eng Part A 14 (2008) 183-194.
[86]C.K. Hashi, Y. Zhu, G.Y. Yang, W.L. Young, B.S. Hsiao, K. Wang, B. Chu, S. Li, Antithrombogenic property of bone marrow mesenchymal stem cells in nanofibrous vascular grafts. Proc Natl Acad Sci U S A 104 (2007) 11915-11920.
[87]J.D. Roh, R. Sawh-Martinez, M.P. Brennan, S.M. Jay, L. Devine, D.A. Rao, T. Yi, T.L. Mirensky, A. Nalbandian, B. Udelsman, N. Hibino, T. Shinoka, W.M. Saltzman, E. Snyder, T.R. Kyriakides, J.S. Pober, C.K. Breuer, Tissue-engineered vascular grafts transform into mature blood vessels via an inflammation-mediated process of vascular remodeling. Proc Natl Acad Sci U S A 107 4669-4674.
[88]D. Campoccia, J.A. Hunt, P.J. Doherty, S.P. Zhong, L. Callegaro, L. Benedetti, D.F. Williams, Human neutrophil chemokinesis and polarization induced by hyaluronic acid derivatives. Biomaterials 14 (1993) 1135-1139.
[89]M.B. Ariganello, D.T. Simionescu, R.S. Labow, J.M. Lee, Macrophage differentiation and polarization on a decellularized pericardial biomaterial. Biomaterials 32 439-449.
[90]M.B. Ariganello, R.S. Labow, J.M. Lee, In vitro response of monocyte-derived macrophages to a decellularized pericardial biomaterial. J Biomed Mater Res A 93 280-288.
[91]D.H. Walter, K. Rittig, F.H. Bahlmann, R. Kirchmair, M. Silver, T. Murayama, H. Nishimura, D.W. Losordo, T. Asahara, J.M. Isner, Statin therapy accelerates reendothelialization: A novel effect involving mobilization and incorporation of bone marrow-derived endothelial progenitor cells. Circulation 105 (2002) 3017-3024.
[92]A. Iwakura, C. Luedemann, S. Shastry, A. Hanley, M. Kearney, R. Aikawa, J.M. Isner, T. Asahara, D.W. Losordo, Estrogen-mediated, endothelial nitric oxide synthase-dependent mobilization of bone marrow-derived endothelial progenitor

cells contributes to reendothelialization after arterial injury. Circulation 108 (2003) 3115-3121.
[93]N. Werner, S. Junk, U. Laufs, A. Link, K. Walenta, M. Bohm, G. Nickenig, Intravenous transfusion of endothelial progenitor cells reduces neointima formation after vascular injury. Circulation research 93 (2003) e17-24.
[94]C. Urbich, S. Dimmeler, Endothelial progenitor cells: Characterization and role in vascular biology. Circulation research 95 (2004) 343-353.
[95]S.W. Cho, S.H. Lim, I.K. Kim, Y.S. Hong, S.S. Kim, K.J. Yoo, H.Y. Park, Y. Jang, B.C. Chang, C.Y. Choi, K.C. Hwang, B.S. Kim, Small-diameter blood vessels engineered with bone marrow-derived cells. Ann Surg 241 (2005) 506-515.
[96]Z. Gong, G. Calkins, E.C. Cheng, D. Krause, L.E. Niklason, Influence of culture medium on smooth muscle cell differentiation from human bone marrow-derived mesenchymal stem cells. Tissue Eng Part A 15 (2009) 319-330.
[97]Y. Shi, G. Hu, J. Su, W. Li, Q. Chen, P. Shou, C. Xu, X. Chen, Y. Huang, Z. Zhu, X. Huang, X. Han, N. Xie, G. Ren, Mesenchymal stem cells: a new strategy for immunosuppression and tissue repair. Cell Res 20 510-518.
[98]A. Uccelli, V. Pistoia, L. Moretta, Mesenchymal stem cells: a new strategy for immunosuppression? Trends Immunol 28 (2007) 219-226.
[99]C. Jorgensen, Mesenchymal stem cells immunosuppressive properties: is it specific to bone marrow-derived cells? Stem Cell Res Ther 1 15.
[100]H.K. Salem, C. Thiemermann, Mesenchymal stromal cells: current understanding and clinical status. Stem Cells 28 585-596.
[101]C. Gotherstrom, Immunomodulation by multipotent mesenchymal stromal cells. Transplantation 84 (2007) S35-37.
[102]D. Noel, F. Djouad, C. Bouffi, D. Mrugala, C. Jorgensen, Multipotent mesenchymal stromal cells and immune tolerance. Leuk Lymphoma 48 (2007) 1283-1289.
[103]X. Zhang, V. Thomas, Y.K. Vohra, In vitro biodegradation of designed tubular scaffolds of electrospun protein/polyglyconate blend fibers. J Biomed Mater Res B Appl Biomater 89 (2009) 135-147.
[104]F.M. Shaikh, A. Callanan, E.G. Kavanagh, P.E. Burke, P.A. Grace, T.M. McGloughlin, Fibrin: a natural biodegradable scaffold in vascular tissue engineering. Cells Tissues Organs 188 (2008) 333-346.
[105]K. Sutherland, J.R. Mahoney, 2nd, A.J. Coury, J.W. Eaton, Degradation of biomaterials by phagocyte-derived oxidants. J Clin Invest 92 (1993) 2360-2367.
[106]D. Motlagh, J. Yang, K.Y. Lui, A.R. Webb, G.A. Ameer, Hemocompatibility evaluation of poly(glycerol-sebacate) in vitro for vascular tissue engineering. Biomaterials 27 (2006) 4315-4324.
[107]L.P. Amarnath, A. Srinivas, A. Ramamurthi, In vitro hemocompatibility testing of UV-modified hyaluronan hydrogels. Biomaterials 27 (2006) 1416-1424.
[108]T.W. Chuang, K.S. Masters, Regulation of polyurethane hemocompatibility and endothelialization by tethered hyaluronic acid oligosaccharides. Biomaterials 30 (2009) 5341-5351.
[109]S.L. Goodman, Sheep, pig, and human platelet-material interactions with model cardiovascular biomaterials. J Biomed Mater Res 45 (1999) 240-250.
[110]J. Hjortnaes, D. Gottlieb, J.L. Figueiredo, J. Melero-Martin, R.H. Kohler, J. Bischoff, R. Weissleder, J. Mayer, E. Aikawa, Intravital Molecular Imaging of

Small-Diameter Tissue-Engineered Vascular Grafts: A Feasibility Study. Tissue Eng Part C Methods (2009).
[111]R.I. Lopez-Soler, M.P. Brennan, A. Goyal, Y. Wang, P. Fong, G. Tellides, A. Sinusas, A. Dardik, C. Breuer, Development of a mouse model for evaluation of small diameter vascular grafts. J Surg Res 139 (2007) 1-6.
[112]C.B. Weinberg, E. Bell, A blood vessel model constructed from collagen and cultured vascular cells. Science 231 (1986) 397-400.
[113]P. Zorlutuna, A. Elsheikh, V. Hasirci, Nanopatterning of collagen scaffolds improve the mechanical properties of tissue engineered vascular grafts. Biomacromolecules 10 (2009) 814-821.
[114]M. Chaouat, C. Le Visage, A. Autissier, F. Chaubet, D. Letourneur, The evaluation of a small-diameter polysaccharide-based arterial graft in rats. Biomaterials 27 (2006) 5546-5553.
[115]A.W. Lund, J.P. Stegemann, G.E. Plopper, Inhibition of ERK promotes collagen gel compaction and fibrillogenesis to amplify the osteogenesis of human mesenchymal stem cells in three-dimensional collagen I culture. Stem Cells Dev 18 (2009) 331-341.
[116]J. Qi, L. Chi, J. Wang, R. Sumanasinghe, M. Wall, M. Tsuzaki, A.J. Banes, Modulation of collagen gel compaction by extracellular ATP is MAPK and NF-kappaB pathways dependent. Exp Cell Res 315 (2009) 1990-2000.
[117]P. Fernandez, A.R. Bausch, The compaction of gels by cells: a case of collective mechanical activity. Integr Biol (Camb) 1 (2009) 252-259.
[118]Z. Jiang, M. Tao, K.A. Omalley, D. Wang, C.K. Ozaki, S.A. Berceli, Established neointimal hyperplasia in vein grafts expands via TGF-beta-mediated progressive fibrosis. Am J Physiol Heart Circ Physiol 297 (2009) H1200-1207.
[119]M. Zhou, C. Liu, Z. Wei, Z. Liu, X. Jiang, T. Qiao, F. Ran, [Constructing a small-diameter decellularized vascular graft pre-loaded with bFGF]. Zhongguo Xiu Fu Chong Jian Wai Ke Za Zhi 22 (2008) 370-375.
[120]D. Seliktar, R.A. Black, R.P. Vito, R.M. Nerem, Dynamic mechanical conditioning of collagen-gel blood vessel constructs induces remodeling in vitro. Ann Biomed Eng 28 (2000) 351-362.
[121]E.D. Grassl, T.R. Oegema, R.T. Tranquillo, Fibrin as an alternative biopolymer to type-I collagen for the fabrication of a media equivalent. J Biomed Mater Res 60 (2002) 607-612.
[122]C.L. Cummings, D. Gawlitta, R.M. Nerem, J.P. Stegemann, Properties of engineered vascular constructs made from collagen, fibrin, and collagen-fibrin mixtures. Biomaterials 25 (2004) 3699-3706.
[123]J.L. Long, R.T. Tranquillo, Elastic fiber production in cardiovascular tissue-equivalents. Matrix Biol 22 (2003) 339-350.
[124]D.D. Swartz, J.A. Russell, S.T. Andreadis, Engineering of fibrin-based functional and implantable small-diameter blood vessels. Am J Physiol Heart Circ Physiol 288 (2005) H1451-1460.
[125]J.Y. Liu, D.D. Swartz, H.F. Peng, S.F. Gugino, J.A. Russell, S.T. Andreadis, Functional tissue-engineered blood vessels from bone marrow progenitor cells. Cardiovasc Res 75 (2007) 618-628.

[126]M. Ehrbar, V.G. Djonov, C. Schnell, S.A. Tschanz, G. Martiny-Baron, U. Schenk, J. Wood, P.H. Burri, J.A. Hubbell, A.H. Zisch, Cell-demanded liberation of VEGF121 from fibrin implants induces local and controlled blood vessel growth. Circ Res 94 (2004) 1124-1132.
[127]L. Soletti, Y. Hong, J. Guan, J.J. Stankus, M.S. El-Kurdi, W.R. Wagner, D.A. Vorp, A bilayered elastomeric scaffold for tissue engineering of small diameter vascular grafts. Acta Biomater (2009).
[128]E. Pektok, B. Nottelet, J.C. Tille, R. Gurny, A. Kalangos, M. Moeller, B.H. Walpoth, Degradation and healing characteristics of small-diameter poly(epsilon-caprolactone) vascular grafts in the rat systemic arterial circulation. Circulation 118 (2008) 2563-2570.
[129]M. Stekelenburg, M.C. Rutten, L.H. Snoeckx, F.P. Baaijens, Dynamic straining combined with fibrin gel cell seeding improves strength of tissue-engineered small-diameter vascular grafts. Tissue Eng Part A 15 (2009) 1081-1089.
[130]L. Zhang, J. Zhou, Q. Lu, Y. Wei, S. Hu, A novel small-diameter vascular graft: in vivo behavior of biodegradable three-layered tubular scaffolds. Biotechnol Bioeng 99 (2008) 1007-1015.
[131]W. He, Z. Ma, W.E. Teo, Y.X. Dong, P.A. Robless, T.C. Lim, S. Ramakrishna, Tubular nanofiber scaffolds for tissue engineered small-diameter vascular grafts. J Biomed Mater Res A 90 (2009) 205-216.
[132]T. Shin'oka, G. Matsumura, N. Hibino, Y. Naito, M. Watanabe, T. Konuma, T. Sakamoto, M. Nagatsu, H. Kurosawa, Midterm clinical result of tissue-engineered vascular autografts seeded with autologous bone marrow cells. J Thorac Cardiovasc Surg 129 (2005) 1330-1338.
[133]G.A. Villalona, B. Udelsman, D.R. Duncan, E. McGillicuddy, R.F. Sawh-Martinez, N. Hibino, C. Painter, T. Mirensky, B. Erickson, T. Shinoka, C.K. Breuer, Cell-seeding techniques in vascular tissue engineering. Tissue Eng Part B Rev 16 341-350.
[134]M.R. Kibbe, J. Martinez, D.A. Popowich, M.R. Kapadia, S.S. Ahanchi, O.O. Aalami, Q. Jiang, A.R. Webb, J. Yang, T. Carroll, G.A. Ameer, Citric acid-based elastomers provide a biocompatible interface for vascular grafts. J Biomed Mater Res A 93 314-324.
[135]G.L. Bowlin, A. Meyer, C. Fields, A. Cassano, R.G. Makhoul, C. Allen, S.E. Rittgers, The persistence of electrostatically seeded endothelial cells lining a small diameter expanded polytetrafluoroethylene vascular graft. J Biomater Appl 16 (2001) 157-173.
[136]J.A. McKee, S.S. Banik, M.J. Boyer, N.M. Hamad, J.H. Lawson, L.E. Niklason, C.M. Counter, Human arteries engineered in vitro. EMBO Rep 4 (2003) 633-638.
[137]T.H. Petersen, T. Hitchcock, A. Muto, E.A. Calle, L. Zhao, Z. Gong, L. Gui, A. Dardik, D.E. Bowles, C.M. Counter, L.E. Niklason, Utility of telomerase-pot1 fusion protein in vascular tissue engineering. Cell Transplant 19 79-87.
[138]S.L. Dahl, C. Rhim, Y.C. Song, L.E. Niklason, Mechanical properties and compositions of tissue engineered and native arteries. Ann Biomed Eng 35 (2007) 348-355.
[139]S.L. Dahl, M.E. Vaughn, L.E. Niklason, An ultrastructural analysis of collagen in tissue engineered arteries. Ann Biomed Eng 35 (2007) 1749-1755.

[140]T. Shin'oka, Y. Imai, Y. Ikada, Transplantation of a tissue-engineered pulmonary artery. N Engl J Med 344 (2001) 532-533.
[141]T.L. Mirensky, G.N. Nelson, M.P. Brennan, J.D. Roh, N. Hibino, T. Yi, T. Shinoka, C.K. Breuer, Tissue-engineered arterial grafts: long-term results after implantation in a small animal model. J Pediatr Surg 44 (2009) 1127-1132; discussion 1132-1123.
[142]G. Matsumura, S. Miyagawa-Tomita, T. Shin'oka, Y. Ikada, H. Kurosawa, First evidence that bone marrow cells contribute to the construction of tissue-engineered vascular autografts in vivo. Circulation 108 (2003) 1729-1734.
[143]M.A. Sussman, Showing up isn't enough for vascularization: persistence is essential. Circ Res 103 (2008) 1200-1201.
[144]P.S. Wolfe, P. Madurantakam, K. Garg, S.A. Sell, M.J. Beckman, G.L. Bowlin, Evaluation of thrombogenic potential of electrospun bioresorbable vascular graft materials: acute monocyte tissue factor expression. J Biomed Mater Res A 92 (2010) 1321-1328.
[145]S.A. Sell, M.J. McClure, C.P. Barnes, D.C. Knapp, B.H. Walpoth, D.G. Simpson, G.L. Bowlin, Electrospun polydioxanone-elastin blends: potential for bioresorbable vascular grafts. Biomed Mater 1 (2006) 72-80.
[146]S.A. Sell, M.J. McClure, K. Garg, P.S. Wolfe, G.L. Bowlin, Electrospinning of collagen/biopolymers for regenerative medicine and cardiovascular tissue engineering. Adv Drug Deliv Rev 61 (2009) 1007-1019.
[147]F. Opitz, K. Schenke-Layland, T.U. Cohnert, B. Starcher, K.J. Halbhuber, D.P. Martin, U.A. Stock, Tissue engineering of aortic tissue: dire consequence of suboptimal elastic fiber synthesis in vivo. Cardiovasc Res 63 (2004) 719-730.
[148]G.R. Campbell, G. Turnbull, L. Xiang, M. Haines, S. Armstrong, B.E. Rolfe, J.H. Campbell, The peritoneal cavity as a bioreactor for tissue engineering visceral organs: bladder, uterus and vas deferens. J Tissue Eng Regen Med 2 (2008) 50-60.
[149]J.H. Campbell, J.L. Efendy, G.R. Campbell, Novel vascular graft grown within recipient's own peritoneal cavity. Circ Res 85 (1999) 1173-1178.
[150]A. Rachev, Z. Dominguez, R. Vito, System and method for investigating arterial remodeling. Journal of biomechanical engineering 131 (2009) 104501.
[151]N.P. Davis, H.C. Han, B. Wayman, R. Vito, Sustained axial loading lengthens arteries in organ culture. Ann Biomed Eng 33 (2005) 867-877.
[152]H.C. Han, D.N. Ku, R.P. Vito, Arterial wall adaptation under elevated longitudinal stretch in organ culture. Ann Biomed Eng 31 (2003) 403-411.
[153]B.H. Wayman, W.R. Taylor, A. Rachev, R.P. Vito, Arteries respond to independent control of circumferential and shear stress in organ culture. Ann Biomed Eng 36 (2008) 673-684.
[154]T.N. McAllister, M. Maruszewski, S.A. Garrido, W. Wystrychowski, N. Dusserre, A. Marini, K. Zagalski, A. Fiorillo, H. Avila, X. Manglano, J. Antonelli, A. Kocher, M. Zembala, L. Cierpka, L.M. de la Fuente, N. L'Heureux, Effectiveness of haemodialysis access with an autologous tissue-engineered vascular graft: a multicentre cohort study. Lancet 373 (2009) 1440-1446.

[155]R. Gauvin, T. Ahsan, D. Larouche, P. Levesque, J. Dube, F.A. Auger, R.M. Nerem, L. Germain, A novel single-step self-assembly approach for the fabrication of tissue-engineered vascular constructs. Tissue Eng Part A 16 1737-1747.
[156]M. Zhou, Z. Liu, Z. Wei, C. Liu, T. Qiao, F. Ran, Y. Bai, X. Jiang, Y. Ding, Development and validation of small-diameter vascular tissue from a decellularized scaffold coated with heparin and vascular endothelial growth factor. Artif Organs 33 (2009) 230-239.
[157]M. Zhou, Z. Liu, K. Li, W. Qiao, X. Jiang, F. Ran, T. Qiao, C. Liu, Beneficial effects of granulocyte-colony stimulating factor on small-diameter heparin immobilized decellularized vascular graft. J Biomed Mater Res A 95 (2010) 600-610.
[158]J.C. Fitzpatrick, P.M. Clark, F.M. Capaldi, Effect of decellularization protocol on the mechanical behavior of porcine descending aorta. Int J Biomater 2010 (2010).
[159]G.F. Liu, Z.J. He, D.P. Yang, X.F. Han, T.F. Guo, C.G. Hao, H. Ma, C.L. Nie, Decellularized aorta of fetal pigs as a potential scaffold for small diameter tissue engineered vascular graft. Chin Med J (Engl) 121 (2008) 1398-1406.
[160]C. Heidenhain, W. Weichert, G. Schmidmaier, B. Wildemann, M. Hein, P. Neuhaus, M. Heise, Polymer coating of porcine decellularized and cross-linked aortic grafts. J Biomed Mater Res B Appl Biomater 94 (2010) 256-263.
[161]C. Derham, H. Yow, J. Ingram, J. Fisher, E. Ingham, S.A. Korrosis, S. Homer-Vanniasinkam, Tissue engineering small-diameter vascular grafts: preparation of a biocompatible porcine ureteric scaffold. Tissue Eng Part A 14 (2008) 1871-1882.
[162]Y. Narita, H. Kagami, H. Matsunuma, Y. Murase, M. Ueda, Y. Ueda, Decellularized ureter for tissue-engineered small-caliber vascular graft. J Artif Organs 11 (2008) 91-99.
[163]G.E. Sandusky, G.C. Lantz, S.F. Badylak, Healing comparison of small intestine submucosa and ePTFE grafts in the canine carotid artery. J Surg Res 58 (1995) 415-420.
[164]S.F. Badylak, A.C. Coffey, G.C. Lantz, W.A. Tacker, L.A. Geddes, Comparison of the resistance to infection of intestinal submucosa arterial autografts versus polytetrafluoroethylene arterial prostheses in a dog model. J Vasc Surg 19 (1994) 465-472.
[165]D.R. Clarke, R.M. Lust, Y.S. Sun, K.S. Black, J.D. Ollerenshaw, Transformation of nonvascular acellular tissue matrices into durable vascular conduits. Ann Thorac Surg 71 (2001) S433-436.
[166]M.A. Sharp, D. Phillips, I. Roberts, L. Hands, A cautionary case: the SynerGraft vascular prosthesis. Eur J Vasc Endovasc Surg 27 (2004) 42-44.
[167]N. Das, M.J. Bratby, V. Shrivastava, A.J. Cornall, C.R. Darby, P. Boardman, S. Anthony, R. Uberoi, Results of a Seven-Year, Single-Centre Experience of the Long-Term Outcomes of Bovine Ureter Grafts Used as Novel Conduits for Haemodialysis Fistulas. Cardiovasc Intervent Radiol (2011).
[168]E.S. Chemla, M. Morsy, Randomized clinical trial comparing decellularized bovine ureter with expanded polytetrafluoroethylene for vascular access. Br J Surg 96 (2009) 34-39.

[169]J.I. Spark, S. Yeluri, C. Derham, Y.T. Wong, D. Leitch, Incomplete cellular depopulation may explain the high failure rate of bovine ureteric grafts. Br J Surg 95 (2008) 582-585.
[170]T.N. McAllister, N. Dusserre, M. Maruszewski, N. L'Heureux, Cell-based therapeutics from an economic perspective: primed for a commercial success or a research sinkhole? Regen Med 3 (2008) 925-937.
[171]M.H. Lee, J.A. Arcidiacono, A.M. Bilek, J.J. Wille, C.A. Hamill, K.M. Wonnacott, M.A. Wells, S.S. Oh, Considerations for tissue-engineered and regenerative medicine product development prior to clinical trials in the United States. Tissue Eng Part B Rev 16 (2010) 41-54.
[172]I.V. Yannas, D.S. Tzeranis, B.A. Harley, P.T. So, Biologically active collagen-based scaffolds: advances in processing and characterization. Philos Transact A Math Phys Eng Sci 368 (2010) 2123-2139.
[173]J. Glowacki, S. Mizuno, Collagen scaffolds for tissue engineering. Biopolymers 89 (2008) 338-344.
[174]K.E. Kadler, D.F. Holmes, J.A. Trotter, J.A. Chapman, Collagen fibril formation. Biochem J 316 (Pt 1) (1996) 1-11.
[175]K.E. Kadler, A. Hill, E.G. Canty-Laird, Collagen fibrillogenesis: fibronectin, integrins, and minor collagens as organizers and nucleators. Curr Opin Cell Biol 20 (2008) 495-501.
[176]E.G. Canty, K.E. Kadler, Procollagen trafficking, processing and fibrillogenesis. J Cell Sci 118 (2005) 1341-1353.
[177]A. Ratcliffe, Tissue engineering of vascular grafts. Matrix Biol 19 (2000) 353-357.
[178]H. Chajra, C.F. Rousseau, D. Cortial, M.C. Ronziere, D. Herbage, F. Mallein-Gerin, A.M. Freyria, Collagen-based biomaterials and cartilage engineering. Application to osteochondral defects. Biomed Mater Eng 18 (2008) S33-45.
[179]E.M. Engelhardt, E. Stegberg, R.A. Brown, J.A. Hubbell, F.M. Wurm, M. Adam, P. Frey, Compressed collagen gel: a novel scaffold for human bladder cells. J Tissue Eng Regen Med 4 (2010) 123-130.
[180]H.G. Sundararaghavan, G.A. Monteiro, N.A. Lapin, Y.J. Chabal, J.R. Miksan, D.I. Shreiber, Genipin-induced changes in collagen gels: correlation of mechanical properties to fluorescence. J Biomed Mater Res A 87 (2008) 308-320.
[181]M.G. Haugh, C.M. Murphy, R.C. McKiernan, C. Altenbuchner, F.J. O'Brien, Crosslinking and Mechanical Properties Significantly Influence Cell Attachment, Proliferation, and Migration Within Collagen Glycosaminoglycan Scaffolds. Tissue Eng Part A (2011).
[182]J.M. Caves, V.A. Kumar, W. Xu, N. Naik, M.G. Allen, E.L. Chaikof, Microcrimped collagen fiber-elastin composites. Adv Mater 22 (2010) 2041-2044.
[183]J.M. Caves, V.A. Kumar, A.W. Martinez, J. Kim, C.M. Ripberger, C.A. Haller, E.L. Chaikof, The use of microfiber composites of elastin-like protein matrix reinforced with synthetic collagen in the design of vascular grafts. Biomaterials 31 (2010) 7175-7182.
[184]X. Wang, X. Li, M.J. Yost, Microtensile testing of collagen fibril for cardiovascular tissue engineering. J Biomed Mater Res A 74 (2005) 263-268.

[185]J.M. Caves, V.A. Kumar, J. Wen, W. Cui, A. Martinez, R. Apkarian, J.E. Coats, K. Berland, E.L. Chaikof, Fibrillogenesis in continuously spun synthetic collagen fiber. J Biomed Mater Res B Appl Biomater 93 (2010) 24-38.
[186]A. Solan, V. Prabhakar, L. Niklason, Engineered vessels: importance of the extracellular matrix. Transplant Proc 33 (2001) 66-68.
[187]C. Guo, L.J. Kaufman, Flow and magnetic field induced collagen alignment. Biomaterials 28 (2007) 1105-1114.
[188]T.S. Girton, N. Dubey, R.T. Tranquillo, Magnetic-induced alignment of collagen fibrils in tissue equivalents. Methods Mol Med 18 (1999) 67-73.
[189]J. Torbet, M.C. Ronziere, Magnetic alignment of collagen during self-assembly. Biochem J 219 (1984) 1057-1059.
[190]T.K. Ohsumi, J.E. Flaherty, M.C. Evans, V.H. Barocas, Three-dimensional simulation of anisotropic cell-driven collagen gel compaction. Biomech Model Mechanobiol 7 (2008) 53-62.
[191]T.T. Tower, M.R. Neidert, R.T. Tranquillo, Fiber alignment imaging during mechanical testing of soft tissues. Ann Biomed Eng 30 (2002) 1221-1233.
[192]T.S. Girton, V.H. Barocas, R.T. Tranquillo, Confined compression of a tissue-equivalent: collagen fibril and cell alignment in response to anisotropic strain. J Biomech Eng 124 (2002) 568-575.
[193]S. Chen, N. Hirota, M. Okuda, M. Takeguchi, H. Kobayashi, N. Hanagata, T. Ikoma, Microstructures and rheological properties of tilapia fish-scale collagen hydrogels with aligned fibrils fabricated under magnetic fields. Acta Biomater 7 (2011) 644-652.
[194]R.B. Dickinson, S. Guido, R.T. Tranquillo, Biased cell migration of fibroblasts exhibiting contact guidance in oriented collagen gels. Ann Biomed Eng 22 (1994) 342-356.
[195]D. Ceballos, X. Navarro, N. Dubey, G. Wendelschafer-Crabb, W.R. Kennedy, R.T. Tranquillo, Magnetically aligned collagen gel filling a collagen nerve guide improves peripheral nerve regeneration. Exp Neurol 158 (1999) 290-300.
[196]S. Guido, R.T. Tranquillo, A methodology for the systematic and quantitative study of cell contact guidance in oriented collagen gels. Correlation of fibroblast orientation and gel birefringence. J Cell Sci 105 (Pt 2) (1993) 317-331.
[197]N. Dubey, P.C. Letourneau, R.T. Tranquillo, Guided neurite elongation and schwann cell invasion into magnetically aligned collagen in simulated peripheral nerve regeneration. Exp Neurol 158 (1999) 338-350.
[198]P. Lee, R. Lin, J. Moon, L.P. Lee, Microfluidic alignment of collagen fibers for in vitro cell culture. Biomed Microdevices 8 (2006) 35-41.
[199]X. Cheng, U.A. Gurkan, C.J. Dehen, M.P. Tate, H.W. Hillhouse, G.J. Simpson, O. Akkus, An electrochemical fabrication process for the assembly of anisotropically oriented collagen bundles. Biomaterials 29 (2008) 3278-3288.
[200]C.K. Sandra Deitch, Xiaofeng Cui, Thomas Boland, Delphine Dean, Collagen Matrix Alignment Using Inkjet Printer Technology. Materials Research Society symposia proceedings Syposium DD (2008).
[201]D. Vader, A. Kabla, D. Weitz, L. Mahadevan, Strain-induced alignment in collagen gels. PLoS One 4 (2009) e5902.

[202]F.H. Silver, R.L. Trelstad, Type I collagen in solution. Structure and properties of fibril fragments. J Biol Chem 255 (1980) 9427-9433.
[203]G.D. Pins, D.L. Christiansen, R. Patel, F.H. Silver, Self-assembly of collagen fibers. Influence of fibrillar alignment and decorin on mechanical properties. Biophys J 73 (1997) 2164-2172.
[204]G.C. Wood, M.K. Keech, The formation of fibrils from collagen solutions. 1. The effect of experimental conditions: kinetic and electron-microscope studies. Biochem J 75 (1960) 588-598.
[205]R. Reed, M.J. Wood, M.K. Keech, Helical nature of the collagen fibril. Nature 177 (1956) 697-699.
[206]J.D. San Antonio, A.D. Lander, M.J. Karnovsky, H.S. Slayter, Mapping the heparin-binding sites on type I collagen monomers and fibrils. J Cell Biol 125 (1994) 1179-1188.
[207]D. Stamov, M. Grimmer, K. Salchert, T. Pompe, C. Werner, Heparin intercalation into reconstituted collagen I fibrils: Impact on growth kinetics and morphology. Biomaterials 29 (2008) 1-14.
[208]J.E. Paderi, R. Sistiabudi, A. Ivanisevic, A. Panitch, Collagen-binding peptidoglycans: a biomimetic approach to modulate collagen fibrillogenesis for tissue engineering applications. Tissue Eng Part A 15 (2009) 2991-2999.
[209]G. Forgacs, S.A. Newman, B. Hinner, C.W. Maier, E. Sackmann, Assembly of collagen matrices as a phase transition revealed by structural and rheologic studies. Biophys J 84 (2003) 1272-1280.
[210]M. Djabourov, J.P. Lechaire, F. Gaill, Structure and rheology of gelatin and collagen gels. Biorheology 30 (1993) 191-205.
[211]M. Achilli, J. Lagueux, D. Mantovani, On the effects of UV-C and pH on the mechanical behavior, molecular conformation and cell viability of collagen-based scaffold for vascular tissue engineering. Macromol Biosci 10 (2010) 307-316.
[212]M. Raspanti, M. Viola, M. Sonaggere, M.E. Tira, R. Tenni, Collagen fibril structure is affected by collagen concentration and decorin. Biomacromolecules 8 (2007) 2087-2091.
[213]K. Stuart, A. Panitch, Characterization of gels composed of blends of collagen I, collagen III, and chondroitin sulfate. Biomacromolecules 10 (2009) 25-31.
[214]K. Stuart, A. Panitch, Influence of chondroitin sulfate on collagen gel structure and mechanical properties at physiologically relevant levels. Biopolymers 89 (2008) 841-851.
[215]L. Yang, K.O. van der Werf, B.F. Koopman, V. Subramaniam, M.L. Bennink, P.J. Dijkstra, J. Feijen, Micromechanical bending of single collagen fibrils using atomic force microscopy. J Biomed Mater Res A 82 (2007) 160-168.
[216]J.A. van der Rijt, K.O. van der Werf, M.L. Bennink, P.J. Dijkstra, J. Feijen, Micromechanical testing of individual collagen fibrils. Macromol Biosci 6 (2006) 697-702.
[217]K.G. Cornwell, P. Lei, S.T. Andreadis, G.D. Pins, Crosslinking of discrete self-assembled collagen threads: Effects on mechanical strength and cell-matrix interactions. J Biomed Mater Res A 80 (2007) 362-371.

[218]J. Jokinen, E. Dadu, P. Nykvist, J. Kapyla, D.J. White, J. Ivaska, P. Vehvilainen, H. Reunanen, H. Larjava, L. Hakkinen, J. Heino, Integrin-mediated cell adhesion to type I collagen fibrils. J Biol Chem 279 (2004) 31956-31963.
[219]J. Heino, M. Huhtala, J. Kapyla, M.S. Johnson, Evolution of collagen-based adhesion systems. Int J Biochem Cell Biol 41 (2009) 341-348.
[220]J. Heino, The collagen family members as cell adhesion proteins. Bioessays 29 (2007) 1001-1010.
[221]A. Bigi, G. Cojazzi, S. Panzavolta, N. Roveri, K. Rubini, Stabilization of gelatin films by crosslinking with genipin. Biomaterials 23 (2002) 4827-4832.
[222]H.W. Sung, R.N. Huang, L.L. Huang, C.C. Tsai, In vitro evaluation of cytotoxicity of a naturally occurring cross-linking reagent for biological tissue fixation. J Biomater Sci Polym Ed 10 (1999) 63-78.
[223]L.L. Huang, H.W. Sung, C.C. Tsai, D.M. Huang, Biocompatibility study of a biological tissue fixed with a naturally occurring crosslinking reagent. J Biomed Mater Res 42 (1998) 568-576.
[224]B. Lanfer, U. Freudenberg, R. Zimmermann, D. Stamov, V. Korber, C. Werner, Aligned fibrillar collagen matrices obtained by shear flow deposition. Biomaterials 29 (2008) 3888-3895.
[225]P. Zorlutuna, N. Hasirci, V. Hasirci, Nanopatterned collagen tubes for vascular tissue engineering. J Tissue Eng Regen Med 2 (2008) 373-377.
[226]B. Lanfer, F.P. Seib, U. Freudenberg, D. Stamov, T. Bley, M. Bornhauser, C. Werner, The growth and differentiation of mesenchymal stem and progenitor cells cultured on aligned collagen matrices. Biomaterials 30 (2009) 5950-5958.
[227]B. Lanfer, A. Hermann, M. Kirsch, U. Freudenberg, U. Reuner, C. Werner, A. Storch, Directed growth of adult human white matter stem cell-derived neurons on aligned fibrillar collagen. Tissue Eng Part A 16 (2010) 1103-1113.
[228]E.S. Place, N.D. Evans, M.M. Stevens, Complexity in biomaterials for tissue engineering. Nat Mater 8 (2009) 457-470.
[229]S.J. Hollister, Scaffold engineering: a bridge to where? Biofabrication 1 (2009) 012001.
[230]J. Yang, D. Motlagh, A.R. Webb, G.A. Ameer, Novel biphasic elastomeric scaffold for small-diameter blood vessel tissue engineering. Tissue Eng 11 (2005) 1876-1886.
[231]A. Salerno, M. Oliviero, E. Di Maio, S. Iannace, P.A. Netti, Design of porous polymeric scaffolds by gas foaming of heterogeneous blends. J Mater Sci Mater Med 20 (2009) 2043-2051.
[232]I. Gercek, R.S. Tigli, M. Gumusderelioglu, A novel scaffold based on formation and agglomeration of PCL microbeads by freeze-drying. J Biomed Mater Res A 86 (2008) 1012-1022.
[233]S.Y. Chew, Y. Wen, Y. Dzenis, K.W. Leong, The role of electrospinning in the emerging field of nanomedicine. Curr Pharm Des 12 (2006) 4751-4770.
[234]E. Sachlos, J.T. Czernuszka, Making tissue engineering scaffolds work. Review: the application of solid freeform fabrication technology to the production of tissue engineering scaffolds. Eur Cell Mater 5 (2003) 29-39; discussion 39-40.
[235]S.F. Badylak, R.M. Nerem, Progress in tissue engineering and regenerative medicine. Proc Natl Acad Sci U S A 107 (2010) 3285-3286.

[236]S.F. Badylak, D.O. Freytes, T.W. Gilbert, Extracellular matrix as a biological scaffold material: Structure and function. Acta Biomater 5 (2009) 1-13.
[237]S.F. Badylak, The extracellular matrix as a biologic scaffold material. Biomaterials 28 (2007) 3587-3593.
[238]R.E. Sallach, J. Leisen, J.M. Caves, E. Fotovich, R.P. Apkarian, V.P. Conticello, E.L. Chaikof, A permanent change in protein mechanical responses can be produced by thermally-induced microdomain mixing. J Biomater Sci Polym Ed 20 (2009) 1629-1644.
[239]R.E. Sallach, W. Cui, J. Wen, A. Martinez, V.P. Conticello, E.L. Chaikof, Elastin-mimetic protein polymers capable of physical and chemical crosslinking. Biomaterials 30 (2009) 409-422.
[240]H. Tang, M.J. Buehler, B. Moran, A constitutive model of soft tissue: from nanoscale collagen to tissue continuum. Ann Biomed Eng 37 (2009) 1117-1130.
[241]P.J. Elbischger, H. Bischof, G.A. Holzapfel, P. Regitnig, Computer vision analysis of collagen fiber bundles in the adventitia of human blood vessels. Stud Health Technol Inform 113 (2005) 97-129.
[242]J.M. Caves, W. Cui, J. Wen, V.A. Kumar, C.A. Haller, E.L. Chaikof, Elastin-like protein matrix reinforced with collagen microfibers for soft tissue repair. Biomaterials 32 (2011) 5371-5379.
[243]N. Bhardwaj, S.C. Kundu, Electrospinning: a fascinating fiber fabrication technique. Biotechnol Adv 28 (2010) 325-347.
[244]R.L. Dahlin, F.K. Kasper, A.G. Mikos, Polymeric Nanofibers in Tissue Engineering. Tissue Eng Part B Rev (2011).
[245]A.R. Webb, J. Yang, G.A. Ameer, Biodegradable polyester elastomers in tissue engineering. Expert Opin Biol Ther 4 (2004) 801-812.
[246]T. Hoshiba, H. Lu, N. Kawazoe, G. Chen, Decellularized matrices for tissue engineering. Expert Opin Biol Ther 10 (2010) 1717-1728.
[247]W. Lapolla, B.A. Yentzer, J. Bagel, C.R. Halvorson, S.R. Feldman, A review of phototherapy protocols for psoriasis treatment. J Am Acad Dermatol 64 (2011) 936-949.
[248]R.R. Krueger, Y.S. Rabinowitz, P.S. Binder, The 25th anniversary of excimer lasers in refractive surgery: historical review. J Refract Surg 26 (2010) 749-760.
[249]N.D. Glossop, R.W. Jackson, H.J. Koort, S.C. Reed, J.A. Randle, The excimer laser in orthopaedics. Clin Orthop Relat Res (1995) 72-81.
[250]F. Litvack, W.S. Grundfest, T. Papaioannou, F.W. Mohr, A.T. Jakubowski, J.S. Forrester, Role of laser and thermal ablation devices in the treatment of vascular diseases. Am J Cardiol 61 (1988) 81G-86G.
[251]N. Tandon, A. Marsano, R. Maidhof, K. Numata, C. Montouri-Sorrentino, C. Cannizzaro, J. Voldman, G. Vunjak-Novakovic, Surface-patterned electrode bioreactor for electrical stimulation. Lab Chip 10 (2010) 692-700.
[252]C. Chollet, S. Lazare, F. Guillemot, M.C. Durrieu, Impact of RGD micro-patterns on cell adhesion. Colloids Surf B Biointerfaces 75 (2010) 107-114.
[253]G.C. Engelmayr, Jr., M. Cheng, C.J. Bettinger, J.T. Borenstein, R. Langer, L.E. Freed, Accordion-like honeycombs for tissue engineering of cardiac anisotropy. Nat Mater 7 (2008) 1003-1010.

[254]T. Matsuda, D.J. Chung, Microfabricated surface designs for cell culture and diagnosis. ASAIO J 40 (1994) M594-597.
[255]Y. Nakayama, T. Matsuda, Microporous polymer surfaces prepared by an excimer laser ablation technique. ASAIO J 40 (1994) M590-593.
[256]C.A. Puliafito, R.F. Steinert, T.F. Deutsch, F. Hillenkamp, E.J. Dehm, C.M. Adler, Excimer laser ablation of the cornea and lens. Experimental studies. Ophthalmology 92 (1985) 741-748.
[257]L.J. Brossollet, Mechanical issues in vascular grafting: a review. Int J Artif Organs 15 (1992) 579-584.
[258]P.D. Ballyk, C. Walsh, J. Butany, M. Ojha, Compliance mismatch may promote graft-artery intimal hyperplasia by altering suture-line stresses. J Biomech 31 (1998) 229-237.
[259]S. Yang, K.F. Leong, Z. Du, C.K. Chua, The design of scaffolds for use in tissue engineering. Part I. Traditional factors. Tissue Eng 7 (2001) 679-689.
[260]R. Zhang, P.X. Ma, Synthetic nano-fibrillar extracellular matrices with predesigned macroporous architectures. J Biomed Mater Res 52 (2000) 430-438.
[261]A. Kurane, D.T. Simionescu, N.R. Vyavahare, In vivo cellular repopulation of tubular elastin scaffolds mediated by basic fibroblast growth factor. Biomaterials 28 (2007) 2830-2838.
[262]L. Bordenave, P. Menu, C. Baquey, Developments towards tissue-engineered, small-diameter arterial substitutes. Expert Rev Med Devices 5 (2008) 337-347.
[263]R.M. Nerem, Tissue engineering a blood vessel substitute: the role of biomechanics. Yonsei Med J 41 (2000) 735-739.
[264]M.R. Kapadia, D.A. Popowich, M.R. Kibbe, Modified prosthetic vascular conduits. Circulation 117 (2008) 1873-1882.
[265]L. Gui, L. Zhao, R.W. Spencer, A. Burghouwt, M.S. Taylor, S.W. Shalaby, L.E. Niklason, Development of Novel Biodegradable Polymer Scaffolds for Vascular Tissue Engineering. Tissue Eng Part A (2011).
[266]J.D. Roh, R. Sawh-Martinez, M.P. Brennan, S.M. Jay, L. Devine, D.A. Rao, T. Yi, T.L. Mirensky, A. Nalbandian, B. Udelsman, N. Hibino, T. Shinoka, W.M. Saltzman, E. Snyder, T.R. Kyriakides, J.S. Pober, C.K. Breuer, Tissue-engineered vascular grafts transform into mature blood vessels via an inflammation-mediated process of vascular remodeling. Proc Natl Acad Sci U S A 107 (2010) 4669-4674.
[267]C.K. Hashi, N. Derugin, R.R. Janairo, R. Lee, D. Schultz, J. Lotz, S. Li, Antithrombogenic modification of small-diameter microfibrous vascular grafts. Arterioscler Thromb Vasc Biol 30 (2010) 1621-1627.
[268]R. Gauvin, M. Guillemette, T. Galbraith, J.M. Bourget, D. Larouche, H. Marcoux, D. Aube, C. Hayward, F.A. Auger, L. Germain, Mechanical properties of tissue-engineered vascular constructs produced using arterial or venous cells. Tissue Eng Part A 17 (2011) 2049-2059.
[269]J. Cappello, Genetically engineered protein polymers, in: A.J. Domb, J. Kost, D.M. Wiseman, (Eds.), Handbook of Biodegradable Polymers, Harwood, Amsterdam, 1997, pp. 387-414.
[270]J. Cappello, J. Crissman, M. Dorman, M. Mikolajczak, G. Textor, M. Marquet, F. Ferrari, Genetic engineering of structural protein polymers. Biotechnology progress 6 (1990) 198-202.

[271]K. McGrath, D. Kaplan, Protein-Based Materials, Birkhaüser, Boston, 1997.
[272]K.P. McGrath, D.A. Tirrell, M. Kawai, T.L. Mason, M.J. Fournier, Chemical and biosynthetic approaches to the production of novel polypeptide materials. Biotechnology progress 6 (1990) 188-192.
[273]L. Huang, R.A. McMillan, R.P. Apkarian, R.P. Pourdeyhimi, V.P. Conticello, E.L. Chaikof, Generation of synthetic elastin-mimetic small diameter fibers and fiber networks. Macromolecules 33 (2000) 2989-2997.
[274]K. Nagapudi, L. Huang, R.A. McMillan, W. Brinkman, V.P. Conticello, E.L. Chaikof, Photomediated solid-state crosslinking of an elastin-mimetic recombinant protein polymer. Macromolecules 35 (2002) 1730-1737.
[275]K. Nagapudi, W.T. Brinkman, J. Leisen, B.S. Thomas, E.R. Wright, C. Haller, V.P. Conticello, E.L. Chaikof, Protein-based thermoplastic elastomers. Macromolecules 38 (2005) 345-354.
[276]K. Nagapudi, W.T. Brinkman, B.S. Thomas, J.O. Park, M. Srinivasarao, E. Wright, V.P. Conticello, E.L. Chaikof, Viscoelastic and mechanical behavior of recombinant protein elastomers. Biomaterials 26 (2005) 4695-4706.
[277]X. Wu, R. Sallach, C.A. Haller, J.A. Caves, K. Nagapudi, V.P. Conticello, M.E. Levenston, E.L. Chaikof, Alterations in physical cross-linking modulate mechanical properties of two-phase protein polymer networks. Biomacromolecules 6 (2005) 3037-3044.
[278]S.W. Jordan, C.A. Haller, R.E. Sallach, R.P. Apkarian, S.R. Hanson, E.L. Chaikof, A recombinant elastin-mimetic coating on an ePTFE prosthesis reduces acute thrombogenicity in a baboon arteriovenous shunt. . Biomaterials 28 (2007) 1191-1197.
[279]R.E. Sallach, A. Martinez, W. Cui, J. Wen, E.L. Chaikof, Elastin-mimetic protein polymers capable of physical and chemical crosslinking. Biomaterials 30 (2009) 409-422.
[280]R.E. Sallach, A. Martinez, W. Cui, J. Wen, E.L. Chaikof, In vivo biocompatibility and long-term stability of a recombinant elastin-mimetic block copolymer. Biomaterials In review (2009).
[281]X. Wu, R.E. Sallach, J.M. Caves, V.P. Conticello, E.L. Chaikof, Deformation responses of a physically cross-linked high molecular weight elastin-like protein polymer. Biomacromolecules 9 (2008) 1787-1794.
[282]D.I. Zeugolis, S.T. Khew, E.S. Yew, A.K. Ekaputra, Y.W. Tong, L.Y. Yung, D.W. Hutmacher, C. Sheppard, M. Raghunath, Electro-spinning of pure collagen nano-fibres - just an expensive way to make gelatin? Biomaterials 29 (2008) 2293-2305.
[283]S.A. Sorrentino, F.H. Bahlmann, C. Besler, M. Muller, S. Schulz, N. Kirchhoff, C. Doerries, T. Horvath, A. Limbourg, F. Limbourg, D. Fliser, H. Haller, H. Drexler, U. Landmesser, Oxidant stress impairs in vivo reendothelialization capacity of endothelial progenitor cells from patients with type 2 diabetes mellitus: Restoration by the peroxisome proliferator-activated receptor-gamma agonist rosiglitazone. Circulation 116 (2007) 163-173.
[284]W.M. Lester, A.A. Damji, I. Gedeon, M. Tanaka, Interstitial cells from the atrial and ventricular sides of the bovine mitral valve respond differently to denuding endocardial injury. In Vitro Cell Dev Biol 29A (1993) 41-50.

[285]D.A. Filip, A. Radu, M. Simionescu, Interstitial cells of the heart valves possess characteristics similar to smooth muscle cells. Circulation research 59 (1986) 310-320.
[286]K.H. Yoo, I.K. Jang, M.W. Lee, H.E. Kim, M.S. Yang, Y. Eom, J.E. Lee, Y.J. Kim, S.K. Yang, H.L. Jung, K.W. Sung, C.W. Kim, H.H. Koo, Comparison of immunomodulatory properties of mesenchymal stem cells derived from adult human tissues. Cell Immunol 259 (2009) 150-156.
[287]Z. Ye, Y. Wang, H.Y. Xie, S.S. Zheng, Immunosuppressive effects of rat mesenchymal stem cells: involvement of CD4+CD25+ regulatory T cells. Hepatobiliary Pancreat Dis Int 7 (2008) 608-614.
[288]K.M. Pryse, A. Nekouzadeh, G.M. Genin, E.L. Elson, G.I. Zahalak, Incremental mechanics of collagen gels: new experiments and a new viscoelastic model. Ann Biomed Eng 31 (2003) 1287-1296.
[289]A. Waterhouse, S.G. Wise, M.K. Ng, A.S. Weiss, Elastin as a nonthrombogenic biomaterial. Tissue Eng Part B Rev 17 (2011) 93-99.
[290]S.W. Jordan, C.A. Haller, R.E. Sallach, R.P. Apkarian, S.R. Hanson, E.L. Chaikof, The effect of a recombinant elastin-mimetic coating of an ePTFE prosthesis on acute thrombogenicity in a baboon arteriovenous shunt. Biomaterials 28 (2007) 1191-1197.
[291]S.W. Jordan, E.L. Chaikof, Novel thromboresistant materials. J Vasc Surg 45 Suppl A (2007) A104-115.
[292]S.W. Jordan, K.M. Faucher, J.M. Caves, R.P. Apkarian, S.S. Rele, X.L. Sun, S.R. Hanson, E.L. Chaikof, Fabrication of a phospholipid membrane-mimetic film on the luminal surface of an ePTFE vascular graft. Biomaterials 27 (2006) 3473-3481.
[293]J.P. Stegemann, S.N. Kaszuba, S.L. Rowe, Review: advances in vascular tissue engineering using protein-based biomaterials. Tissue Eng 13 (2007) 2601-2613.
[294]E.T. Thostenson, C. Li, T.-W. Chou, Nanocomposites in context. Composites Science and Technology 65 (2005) 491-516.
[295]G.E. Fantner, T. Hassenkam, J.H. Kindt, J.C. Weaver, H. Birkedal, L. Pechenik, J.A. Cutroni, G.A. Cidade, G.D. Stucky, D.E. Morse, P.K. Hansma, Sacrificial bonds and hidden length dissipate energy as mineralized fibrils separate during bone fracture. Nat Mater 4 (2005) 612-616.
[296]X. Wu, R.E. Sallach, J.M. Caves, V.P. Conticello, E.L. Chaikof, Deformation responses of a physically cross-linked high molecular weight elastin-like protein polymer. Biomacromolecules 9 (2008) 1787-1794.
[297]E.T. Thostenson, Z. Ren, T.-W. Chou, Advances in the science and technology of carbon nanotubes and their composites: a review. Composites Science and Technology 61 (2001) 1899-1912.
[298]H.D. Wagner, R.A. Vaia, Nanocomposites: issues at the interface. Materials Today 7 (2004) 38-42.
[299]M.W. Weston, K. Rhee, J.M. Tarbell, Compliance and diameter mismatch affect the wall shear rate distribution near an end-to-end anastomosis. J Biomech 29 (1996) 187-198.
[300]A. Mekontso-Dessap, M. Kirsch, C. Guignambert, P. Zadigue, S. Adnot, D. Loisance, S. Eddahibi, Vascular-wall remodeling of 3 human bypass vessels:

organ culture and smooth muscle cell properties. J Thorac Cardiovasc Surg 131 (2006) 651-658.
[301]K. Wallner, C. Li, M.C. Fishbein, P.K. Shah, B.G. Sharifi, Arterialization of human vein grafts is associated with tenascin-C expression. J Am Coll Cardiol 34 (1999) 871-875.
[302]J.W. Butany, T.E. David, M. Ojha, Histological and morphometric analyses of early and late aortocoronary vein grafts and distal anastomoses. Can J Cardiol 14 (1998) 671-677.
[303]J. Hu, X. Sun, H. Ma, C. Xie, Y.E. Chen, P.X. Ma, Porous nanofibrous PLLA scaffolds for vascular tissue engineering. Biomaterials 31 (2010) 7971-7977.
[304]N. Hibino, T. Shin'oka, G. Matsumura, Y. Ikada, H. Kurosawa, The tissue-engineered vascular graft using bone marrow without culture. J Thorac Cardiovasc Surg 129 (2005) 1064-1070.
[305]T.L. Mirensky, N. Hibino, R.F. Sawh-Martinez, T. Yi, G. Villalona, T. Shinoka, C.K. Breuer, Tissue-engineered vascular grafts: does cell seeding matter? J Pediatr Surg 45 (2010) 1299-1305.
[306]D.I. Zeugolis, G.R. Paul, G. Attenburrow, Cross-linking of extruded collagen fibers--a biomimetic three-dimensional scaffold for tissue engineering applications. J Biomed Mater Res A 89 (2009) 895-908.
[307]A. de Mel, G. Jell, M.M. Stevens, A.M. Seifalian, Biofunctionalization of biomaterials for accelerated in situ endothelialization: a review. Biomacromolecules 9 (2008) 2969-2979.
[308]T. Yoshida, M. Kikuchi, Y. Koyama, K. Takakuda, Osteogenic activity of MG63 cells on bone-like hydroxyapatite/collagen nanocomposite sponges. J Mater Sci Mater Med 21 (2010) 1263-1272.
[309]G. Wong, J.M. Li, G. Hendricks, M.H. Eslami, M.J. Rohrer, B.S. Cutler, Inhibition of experimental neointimal hyperplasia by recombinant human thrombomodulin coated ePTFE stent grafts. J Vasc Surg 47 (2008) 608-615.